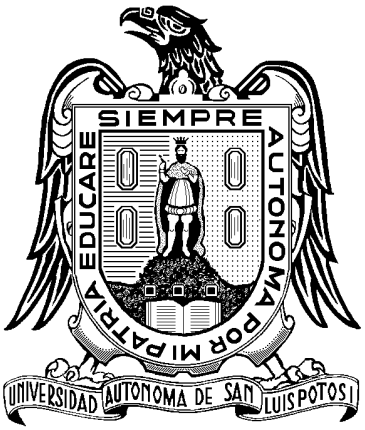

Measurement of Branching Ratios for Non-leptonic Cabibbo-suppressed Decays of the Charmed-Strange Baryon Ξ_c^+

TESIS PROFESIONAL

Para obtener el grado de:

DOCTOR EN CIENCIAS EN FÍSICA

QUE PRESENTA:

Eric Vázquez Jáuregui

ASESOR DE TESIS:

Dr. Jürgen Engelfried

Profesor Investigador

SAN LUIS POTOSÍ, S.L.P.

Agosto 2008

Abstract

We studied several Ξ_c^+ decay modes, most of them with a hyperon in the final state, and determined their branching ratios. The data used in this analysis come from the fixed target experiment SELEX, a multi-stage spectrometer with high acceptance for forward interactions, that took data during 1996 and 1997 at Fermilab with $600\,\mathrm{GeV}/c$ (mainly Σ^-, π^-) and $540\,\mathrm{GeV}/c$ (mainly p) beams incident on copper and carbon targets. The thesis mainly details the first observation of two Cabibbo-suppressed decay modes, $\Xi_c^+ \to \Sigma^+\pi^-\pi^+$ and $\Xi_c^+ \to \Sigma^-\pi^+\pi^+$. The branching ratios of the decays relative to the Cabibbo-favored $\Xi_c^+ \to \Xi^-\pi^+\pi^+$ are measured to be: $\Gamma(\Xi_c^+ \to \Sigma^+\pi^-\pi^+)/\Gamma(\Xi_c^+ \to \Xi^-\pi^+\pi^+) = 0.480 \pm 0.202$ and $\Gamma(\Xi_c^+ \to \Sigma^-\pi^+\pi^+)/\Gamma(\Xi_c^+ \to \Xi^-\pi^+\pi^+) = 0.184 \pm 0.086$. Systematic studies have been performed in order to check the stability of the measurements varying all cuts used in the selection of events over a wide interval and we do not observe evidence of any trend, so the systematic error is negligible in the final results because the quadrature sum of the total error is not affected.

The branching ratios for the same decay modes of the Λ_c^+ are measured to check the methodology of the analysis. The branching ratio of the decay mode $\Lambda_c^+ \to \Sigma^+\pi^-\pi^+$ is measured relative to $\Lambda_c^+ \to pK^-\pi^+$, while the one of the decay mode $\Lambda_c^+ \to \Sigma^-\pi^+\pi^+$ is relative to $\Lambda_c^+ \to \Sigma^+\pi^-\pi^+$, as they have been reported earlier. The results for the control modes are: $\Gamma(\Lambda_c^+ \to \Sigma^+\pi^-\pi^+)/\Gamma(\Lambda_c^+ \to pK^-\pi^+) = 0.716 \pm 0.144$ and $\Gamma(\Lambda_c^+ \to \Sigma^-\pi^+\pi^+)/\Gamma(\Lambda_c^+ \to \Sigma^+\pi^-\pi^+) = 0.382 \pm 0.104$. The branching ratio of the decay mode $\Xi_c^+ \to pK^-\pi^+$ relative to $\Xi_c^+ \to \Xi^-\pi^+\pi^+$ is considered as another control mode, the measured value is: $\Gamma(\Xi_c^+ \to pK^-\pi^+)/\Gamma(\Xi_c^+ \to \Xi^-\pi^+\pi^+) = 0.194 \pm 0.054$. Systematic studies have been also performed for the control modes and all systematic variations are also small compared to the statistical error.

We also report the first observation of two more decay modes, the Cabibbo-suppressed decay $\Xi_c^+ \to \Xi^-K^+\pi^+$ and the doubly Cabibbo-suppressed decay $\Xi_c^+ \to \Sigma^+K^+\pi^-$, but their branching ratios have not been measured up to now.

A mi madre y a mi padre
A mi alma gemela Elva
A mis hermanas Cristina y Elia
A mi hijo Julio y a mi sobrino Rubén

Agradecimientos

A mi asesor, el Doctor **Jürgen Engelfried**, por el apoyo que me brindó, por sus explicaciones amplias y claras llenas de paciencia, por sus observaciones y correcciones adecuadas, por sus consejos, por su conocimiento y el enorme esmero en sus enseñanzas, por las amenas charlas de Física llenas de sabiduría y anécdotas y por las tardes de futbol que compartimos.

Al **Consejo Nacional de Ciencia y Tecnología (CONACyT)** por brindarme el apoyo económico a través de la beca con número de registro 165806, que permitió realizar este trabajo. Este Proyecto fue realizado con financiamiento de la Secretaría de Educación Pública, de la Subsecretaría de Educación Superior e Investigación Científica y de la Dirección General de Educación Superior a través del *Convenio 2003-24-001-026*, también con Fondos Sectoriales SEP-CONACyT a través del Proyecto 54988 y con el Fondo de Apoyo a la Investigacion de la Universidad Autónoma de San Luis Potosí.

A mi **familia** por su infinito amor y su apoyo incondicional; a mi **madre** y a mi **padre** por su cariño y amor, a mis **hermanas Cristina y Elia**, y a mi sobrino **Rubén** por quererme a pesar de todo, a **Elva** que ha dado todo por estar a mi lado, a mi hijo **Julio** por su cariño y su fortaleza para soportarme y finalmente al *chiquilín* por su nobleza.

A la **Colaboración SELEX** por todo el trabajo que realizaron para que este experimento se llevara a cabo, especialmente a los doctores **Peter S. Cooper** y **James Russ** por su sabiduría y sus excelentes comentarios. También a los doctores **Vincent Smith** y **Soon Jun** por sus valiosas aportaciones.

A los **profesores** que contribuyeron en mi formación para tener la capacidad de realizar este trabajo, especialmente al **Dr. Pedro Villaseñor González** por sus oportunos consejos, al **Dr. Rubén Flores Mendieta** y a la **Dra. Mariana Kirchbach**, al **Fis. Alfonso Vargas Cisneros**, al **Ingeniero Andrés Mirón Herrera**, al **Ingeniero Miguel Alejandro Palacios** y al **Profesor Rodolfo Martínez Fernández**.

A mis amigos **Alejandro Blanco Covarrubias** y **Andrés García Castillo** por compartir grandes momentos y aceptarme a pesar de todo. A mis amigos **Mario López**, **Irving Vargas Cruz**, **José Ernesto Pavón**, **Adalberto Zamudio** y **Alejandro Ávila**.

A mis **compañeros del grupo de Altas Energías** Jorge Amaro, Alejandro Blanco, Ángel Flores, Guillermo Hinojosa, Miguel Olivo, Ibrahim Torres, José Luis Sánchez y a la "secretaria" del Laboratorio de Altas Energías Luz del Carmen Nuche.

Al **Laboratorio de Cálculo Numérico**, especialmente a **José Limón Castillo**, por su apoyo y ayuda al resolver los problemas de cómputo.

A todo el **personal del Instituto de Física**, especialmente a **Elsa Cabrera** y a **Don Toro**.

Al **Dr. Leopoldo Zúñiga** y al **Dr. Javier Moctezuma**.

A la familia **Hernández Medina**, con mucho cariño a **Iván**, **Adán** y a la maestra **Mireya**.

A todos mis **compañeros del Instituto de Física** y de la **Universidad Veracruzana**.

A los *Neutrinos* por compartir conmigo una cancha de futbol y soportarme dentro de ella.

Al *Club América* por las inmensas alegrías, especialmente por las tardes del 26 de mayo de 2002 y del 29 de mayo de 2005.

Contents

Introduction

The experimental study of charm baryons started in 1975 when an experiment at the Brookhaven National Laboratory reported on the production of a charmed-baryon by a neutrino beam, consistent with a Σ_c^{++} followed by its decay to a Λ_c^+ [1], and in 1976 when a photoproduction experiment at Fermilab reported a new anti-baryon state around $2.26 \pm 0.01\,\mathrm{GeV}/c^2$ [2]. Later on, the experimental study of charm-strange baryons began around 1983 when the experiment WA62 at CERN detected a particle made of c, s and u quarks [3]. This particle is called Ξ_c^+ (cascade charm) and some of its properties such as mass and mean life have been measured as well as several decay modes have been observed up to now.

This work mainly reports the first observation of the Cabibbo-suppressed decay modes $\Xi_c^+ \to \Sigma^+\pi^-\pi^+$ and $\Xi_c^+ \to \Sigma^-\pi^+\pi^+$ and measures their branching ratios relative to the Cabibbo-favored decay $\Xi_c^+ \to \Xi^-\pi^+\pi^+$, which has been seen by SELEX and some other experiments. The branching ratios of the same decay modes for the Λ_c^+, previously found by other experiments [4, 5, 6], and the branching ratio of the first Ξ_c^+ Cabibbo-suppressed decay observed, $\Xi_c^+ \to pK^-\pi^+$ relative to $\Xi_c^+ \to \Xi^-\pi^+\pi^+$, found by SELEX in 2000 [7], are also reported. The branching ratio of the decay mode $\Lambda_c^+ \to \Sigma^+\pi^-\pi^+$ is measured relative to $\Lambda_c^+ \to pK^-\pi^+$, while the one of the decay mode $\Lambda_c^+ \to \Sigma^-\pi^+\pi^+$ is relative to $\Lambda_c^+ \to \Sigma^+\pi^-\pi^+$, since these are the values previously reported and a comparison is expected in order to verify the methodology of the analysis performed.

As part of future activities in the study of the charm-strange baryon Ξ_c^+, two more modes are presented: $\Xi_c^+ \to \Xi^-K^+\pi^+$ (Cabibbo-suppressed) and $\Xi_c^+ \to \Sigma^+K^+\pi^-$ (this would be the first doubly Cabibbo-suppressed decay mode observed for the Ξ_c^+); these modes have a small statistical significance and the branching ratio was not measured; undoubtedly more studies are needed.

The Ξ_c^+ candidates were obtained by analyzing data from the SELEX experiment; a fixed target spectrometer at Fermilab, that took data during 1996 and 1997 with $600\,\mathrm{GeV}/c$ (mainly Σ^-, π^-) and $540\,\mathrm{GeV}/c$ (mainly p) beams that hit on copper and carbon targets.

This thesis has been designed in a self-consistent way, but chapters can be entirely skipped without losing the context.

First of all, in chapter 1, a brief introduction to the field of Particle Physics will be given, emphasizing out in the fundamental particles and their interactions.

In chapter 2, some general concepts used in this work will be explained, focusing on the strong and weak interactions and on particle decays.

In chapter 3 a detailed explanation of charm-strange baryons will be given, including history, structure, decay modes and branching ratios.

Later, in chapter 4, the SELEX experiment will be explained, emphasizing the detectors used in this analysis. The software used for the data analysis, that includes data and simulation treatment, will also be described.

In chapter 5 the data analysis, the methodology for the branching ratio determination and the error treatment will be explained. In addition, one example will be included to follow the analysis mechanism.

In chapter 6, the results found will be shown; the invariant mass distributions corresponding to the new Ξ_c^+ and the control decay modes will be presented, the branching ratio for the new decay modes as well as for the control modes will be included and the stability of the measurements as function of the most critical variables will also be checked.

Finally, in chapter 7, the conclusions of this work will be presented.

Motivation

Heavy flavor experiments at e^+e^- colliders and in the fixed target programs at CERN and Fermilab were aimed to collect large samples of charmed events in 1987; most of them would provide information about meson systems, but the expected number of charmed baryons was a small part of the sample. The most detailed study of the Ξ_c^+ came from a 20-day run in the CERN hyperon beam.

SELEX was proposed to make a systematic survey of charm baryon production and decay mechanism, it was expected to collect a large sample of charm baryons to give adequate statistics to study even highly suppressed modes. One physics aspect to answer was the evaluation of various mechanisms which influence the decay rates of charmed hadrons as well as to make detailed studies of their production mechanisms.

One reason to collect such data was "to understand if perturbative QCD can account for charm production under different circumstances and to establish which mechanisms dominate decay processes" as it can be read in the SELEX proposal [8]. More features have been added to the last sentence, 20 years later.

The importance of charm studies is based on some interesting general motivations:

- There is a vast array of theoretical technologies that are based on QCD and they require some additional assumptions. Since non-perturbative effects are larger in charm than in beauty physics, the theoretical methods can be applied with considerably validity in beauty physics and they can be tested there; while the transition from the non-perturbative to the perturbative domain can be tested in charm physics.

- A more detailed knowledge and understanding of charm physics is also essential for a better comprehension of beauty physics and for a more extensive exploitation of the discovery potential for New Physics there. This starts with the trivial observation that knowing charm branching ratios and decay sequences are important for interpreting beauty decays.

The attempts to measure absolute charm branching ratios date back to the very early stages of charm at accelerators. In principle, all decays of a

certain hadron have to be observed, and then to count how often a specific final state appears. In reality things are of course less straightforward.

In the charm baryon sector, the only measurements available for absolute branching ratios refer to the Λ_c^+ and no model-independent measurements exist. ARGUS [9] and CLEO [10] measured $B(\overline{B} \to \Lambda_c^+ X) \cdot B(\Lambda_c^+ \to pK^-\pi^+)$ and, assuming that the $\Lambda_c^+ X$ channel saturates the meson decays into baryons and that $\Lambda_c^+ X$ final states other than $\Lambda_c^+ \overline{N} X$ can be neglected, they also measure $B(\overline{B} \to \Lambda_c^+ X)$; hence $B(\Lambda_c^+ \to pK^-\pi^+)$ is extracted. ARGUS [11] and CLEO [12] also measured $\sigma(e^+e^- \to \Lambda_c^+ X) \cdot B(\Lambda_c^+ \to \Lambda l^+ \nu_l)$. The PDG group combines these measurements with $\sigma(e^+e^- \to \Lambda_c^+ X) \cdot B(\Lambda_c^+ \to pK^-\pi^+)$, estimating $B(\Lambda_c^+ \to pK^-\pi^+)$. The model-dependent systematic error estimated is of order 30%. A different approach is attempted, also by CLEO [13], measuring in a sample of two-jet continuum events containing both a charm tag ("D") as well as antiproton ($e^+e^- \to \overline{D}\overline{p}X$) with the antiproton in the opposite hemisphere to the $\overline{D}$. The hypothesis is that such selection criteria tag $e^+e^- \to \overline{D}\overline{p}\Lambda_c^+ X$ events; then $B(\Lambda_c^+ \to pK^-\pi^+)$ is determined by measuring the $pK^-\pi^+$ yield in the same hemisphere as the antiprotons in the $\overline{D}\overline{p}X$ sample. The value agrees with the PDG average from the older measurements described above. BESII experiment should vastly improve the absolute branching ratio measurement of the Λ_c^+. It should be noted that there are no absolute branching ratios for the other charmed baryons.

Absolute branching ratios for Λ_c^+ and Ξ_c^+ allow *charm counting* in B decays, besides knowing the relative importance of $\Lambda_c^+ \to \Lambda + X$ versus $\Lambda_c^+ \to N\overline{K} + X$ and $\Xi_c^+ \to \Xi + X$ versus $\Xi_c^+ \to \Lambda\overline{K} + X$ is of great help in identifying Λ_b and Ξ_b decays. The final states in Λ_c^+ and Ξ_c^+ decays can also shed new light on the spectroscopy of light flavor baryons, all of this can be described with quark models, QCD sum rules and lattice QCD, but evaluation of matrix elements of the relevant operators for baryons is even harder than that for mesons. Treatments based on the quark model and on QCD sum rules have not given any qualitatively new theoretical insights on the limits of factorization, neither on how to go beyond it nor on final state interaction.

The existence of charm hadrons and their basic properties has provided essential confirmation of the Standard Model, and at the same time it offers a unique angle to search for physics beyond the Standard Model because in contrast to s and b quarks, charm is an up-type quark; and unlike top, it hadronizes, moreover, the rarer the mode, the better the a priori chance to reveal the intervention of New Physics and Cabibbo-suppressed and doubly Cabibbo-suppressed channels would offer the best chance. Something has already been seen in mesons, since Close and Lipking started by pointing at the "anomalously high branching ratios" for Cabibbo-suppressed transitions

in D^+ decays compared to the corresponding Cabibbo-favored branching ratios [14].

The importance of studying charm-strange baryons lies in the small knowledge for the potential inside the hadron, which is difficult to calculate because it is a relativistic three-body potential where the spin-spin interaction needs to be taken into account as well as the different masses of the quarks.

Much less is known about the decays and branching ratios of charm baryons in comparison to charm mesons; even less about charm-strange baryons; besides there are only two Cabibbo-suppressed decays of charm-strange baryons reported up to now, both corresponding to the Ξ_c^+. The decay modes are: $\Xi_c^+ \to pK^-\pi^+$ (first observation of a Cabibbo-suppressed decay of the Ξ_c^+, reported by SELEX in 2000 [7]) and $\Xi_c^+ \to \Sigma^+K^-K^+$ (reported by FOCUS in 2003 [15]).

The accumulation of experimental data and measurement of branching ratios of Cabibbo-suppressed decay modes may help to test some theoretical models from Heavy Quark Expansion (HQE) [17, 18] and to validate some approximations.

More important features to study Cabibbo-suppressed decays of charm-strange baryons are:

- To obtain information of the weak interaction mechanism for nonleptonic decays.
- To provide useful information of the relative importance of decay mechanisms while measuring ratios of branching fractions; for example, comparing matrix elements for two decay modes.
- To give additional understanding of the role played by QCD (strong interaction) in the decay process.
- To get information on the role of W-exchange, internal W-emission, external W-emission and/or horizontal W-loop quarks diagrams.
- To help in understanding the discrepancy between the predicted and measured Ξ_c^+ lifetime [16].
- To quantify the effects of final state interactions due to quarks rearrangement in the different decays.

Finally, to find a numerical value of the ratio of the two partial widths ($\Gamma(\Xi_c^+ \to \Sigma^-\pi^+\pi^+)/\Gamma(\Xi_c^+ \to \Sigma^+\pi^-\pi^+)$, for example) can provide useful information of the relative importance of the two decay mechanisms and give additional understanding of the role played by the QCD strong interaction in this decay process.

Chapter 1

Introduction to Particle Physics

Particle Physics is one of the most fascinating areas in physics. It deals with the fundamental components of matter and the nature of its interactions. To begin with, introductory information related to Particle Physics will be included along this chapter.

1.1 The Fundamental Particles

By the end of the 19th century, it was known that all matter is composed of atoms; however the existence of 100 elements showing periodically recurring properties was a clear indication that atoms themselves have an internal structure, and are not indivisible.

The modern concept of the atom emerged at the beginning of the 20th century, particularly as a result of Rutherford's experiments; which stated that an atom is composed of a dense nucleus surrounded by an electron cloud. Following experiments showed that the nucleus itself can be decomposed into smaller particles; later after the discovery of the neutron in 1932, there was no longer a doubt that the building blocks of nuclei are protons and neutrons (called nucleons). The electron, neutron and proton were later joined by a fourth particle, the neutrino, which was postulated in 1930 in order to reconcile the description of β-decay with the fundamental laws of conservation of energy, momentum and angular momentum.

By the mid-thirties, these four particles could describe all the known phenomena of atomic and nuclear physics. Experiments at particle accelerators in the fifties and sixties showed that protons and neutrons are merely representatives of a large family of particles now called *hadrons*. Nowadays, more than 100 hadrons have thus far been detected, these ones, like atoms, can be classified in groups with similar properties. It was therefore assumed that they cannot be understood as fundamental constituent of matter. In the sixties, the quark model established an order: all known hadrons could be described as combinations of two or three quarks.

1.1.1 Leptons and quarks

The two fundamental types of building blocks are the *leptons*, which include the electron and the neutrino, plus the *quarks*. In scattering experiments, all of them are found to be smaller than $10^{-18}\,m$ (the experimental resolution up today), so they are possibly point-like particles. Leptons and quarks have spin 1/2, i.e. they are fermions. In contrast to atoms, nuclei, and hadrons, no excited states of quarks and leptons have been observed so far; thus they appear to be elementary particles.

Today, six leptons and six quarks as well as their antiparticles are known and they can be grouped into "generations" or " families", according to certain characteristics.

1.2 The Fundamental Interactions

Around the 19th century, four forces were considered to be basic: *gravitation*, electricity, magnetism and the barely comprehended forces between atoms and molecules. By the end of the 19th century, electricity and magnetism were understood to be manifestations of the same force: *electromagnetism*. When nuclear physics developed, two new short-ranged forces joined the ranks. These are the nuclear force, which acts between nucleons, and the *weak force*, which manifestes itself in nuclear β-decay. Today, it is known that the nuclear force is not fundamental but it is a result of the *strong force* binding quarks to form protons and neutrons. These strong and weak forces lead to the corresponding fundamental interactions between elementary particles.

The electromagnetic and weak interactions can be interpreted as two aspects of a single one: the *electroweak* interaction; developed by Glashow, Salam and Weinberg in the late sixties.

1.2.1 Intermediate bosons

The physical phenomena are based on four fundamental interactions which are: *gravitation*, *electromagnetism*, the *strong* and the *weak* interactions. Gravitation is of no significance in subatomic physics, it is only mentioned for completeness.

Interactions are mediated by the exchange of vector bosons, i.e. particles with spin 1. These are *photons* in electromagnetic interactions, *gluons* in strong interactions and the W^+, W^-, and Z^0 bosons in weak interactions.

Each of these three interactions is associated with a charge: electric charge, weak charge and strong charge, the latter one is also called *color charge*. It is known that a particle is subject to an interaction if and only if it carries the corresponding charge:

- Leptons and quarks carry weak charge.
- Quarks are electrically charged, so are some of the leptons.
- Color charge is only carried by quarks (not by leptons).

The W and Z bosons are very heavy particles ($M_W \approx 80\,\mathrm{GeV}/c^2$ and $M_Z \approx 91\,\mathrm{GeV}/c^2$). According to the Heisenberg uncertainty principle, at low energies, they can only be produced as virtual, intermediate particles in scattering processes for extremely short times (production of real W and Z bosons can occur with enough energy); therefore the weak interaction is of a very short range ($\sim 10^{-17}\,m$). The rest mass of the photon is zero; so the range of the electromagnetic interaction is infinite. The gluons, like photons, have zero rest mass, whereas photons have no electrical charge, gluons carry color charge; hence they can interact each other and this causes the strong interaction to be very short ranged ($\sim 1\,fm$).

Figure 1.1 summarizes the elementary particles mentioned above.

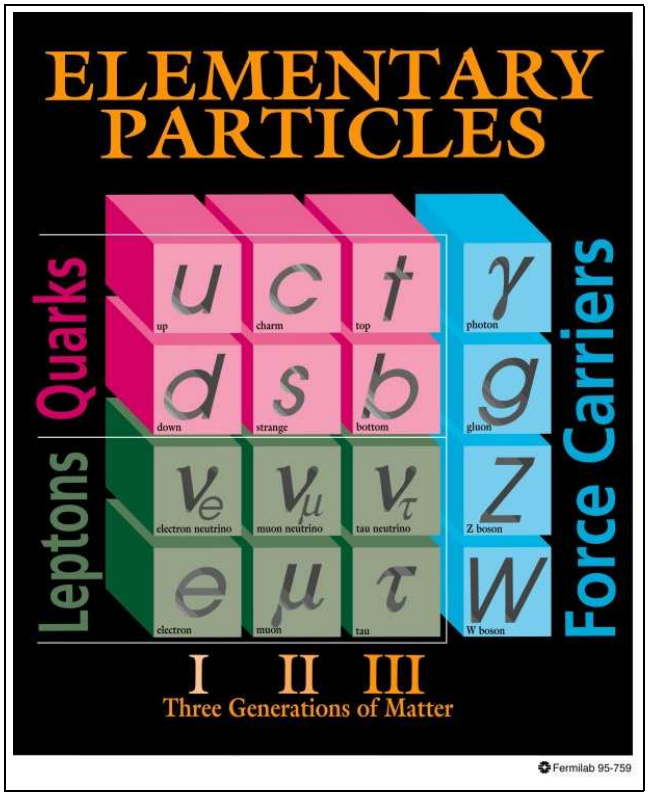

Figure 1.1: Elementary Particles table showing the three generations of matter and the force carriers.

1.3 Symmetries and some Conservation Laws

Symmetries are of great importance in Physics. The conservation laws of classical physics (energy, momentum and angular momentum) are a consequence of the fact that the interactions are invariant with respect to their canonically conjugate quantities (physical laws are independent of the time, location, and the orientation in space under which they take place).

An important symmetry in quantum mechanics is reflection symmetry; depending on whether the sign of the wave function changes under reflection or not, the system is said to have negative or positive *parity* (P), respectively. For those laws of nature with left-right symmetry, i.e., invariant under a reflection in space, the parity quantum number P of the system is conserved. *Parity* is conserved in electromagnetic and strong interactions it turns out to be violated in weak interactions.

Another important symmetry in quantum mechanics relates particles and antiparticles. An operator C is introduced which changes particles into antiparticles and vice versa, since the charge reverses its sign under this operation, it is called *charge conjugation*.

Finally, another important symmetry in quantum mechanics derives from the fact that certain groups ("multiplets") of particles behave practically identical in relation to the strong or weak interaction. Particles belonging to such a multiplet may be described as different states of the same particle. These states are characterized by a quantum number referred to as strong or weak *isospin*.

Summary

An introduction to the fundamental particles and their interactions was given in this chapter; but for the study performed in this work it is necessary to deeply understand the weak and strong interactions, as well as to know how the particle under study (Ξ_c^+) is included in the quark model; which will be detailed in the next chapter.

Chapter 2

General Theory

The useful concepts to know the physical ideas behind this work are presented in this chapter. First of all the quark model is detailed, then the theoretical concepts to comprehend the weak and strong interactions are explained in order to understand the decay mechanism that rules the Ξ_c^+ decay. Finally, the partial decay rate of a particle in a three body decay is analyzed with Fermi's Golden Rule.

2.1 Quark Model

The quark model was conceived in the mid-sixties in order to systematize the great diversity of hadrons which had been discovered up to then. Gell-Mann and Zweig made the step to postulate that a set of three particles corresponding to the fundamental representation of SU(3) should exist. These new particles were called *quarks* by Gell-Mann, where, as he described in his book *The Quark and the Jaguar*, the sound was first and the spelling was adopted later from the line "Three quarks for Muster Mark" in James Joyce's book *"Finnegan's Wake"*.

The SU(3) multiplet structure of the so called "elementary" particles was reminiscent of the grouping of chemical elements in Mendeleev's table.

As mentioned in Chapter 1, all hadrons are made up of a small variety of more basic entities, called quarks, bound together in different ways. Considering three quarks, the fundamental representation of SU(3), the multiplet from which all multiplets can be built, is a triplet. This basic quark multiplet is given in Figure 2.1. For the antiquark multiplet the signs of the additive quantum numbers must be reversed. A fourth quark such as charm (c) can be included by extending SU(3) to SU(4); however SU(4) flavor symmetry is badly broken owing to the much heavier c quark. The addition of a b quark extends the flavor symmetry to SU(5); but it would require four dimensions to draw the multiplets.

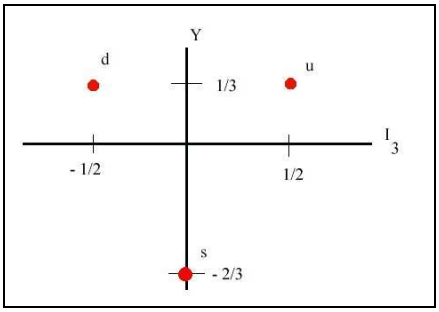

Figure 2.1: SU(3) quark multiplet, $I_3 = Isospin$, $Y = Hypercharge$.

Each quark is assigned spin 1/2 and baryon number $\mathfrak{B}$=1/3. Baryons are made of three quarks (qqq) and mesons of a quark-antiquark pair ($q\overline{q}$). In Figure 2.1, the additive quantum number shown as the "hypercharge" (Y) is:

$$Y = \mathfrak{B} + S + C + B + T \tag{2.1}$$

where $\mathfrak{B}$ is the baryon number, S the strangeness, C the charmness, B the bottomness and T the topness. The charge Q, is:

$$Q = I_3 + \frac{Y}{2} \tag{2.2}$$

where I_3 is the isospin.
The quantum numbers of the quarks are listed in Table 2.1.

Quark	Spin	$\mathfrak{B}$	Q	I_3	S	C	B	T	Y
d	$\frac{1}{2}$	$\frac{1}{3}$	$-\frac{1}{3}$	$-\frac{1}{2}$	0	0	0	0	$\frac{1}{3}$
u	$\frac{1}{2}$	$\frac{1}{3}$	$\frac{2}{3}$	$\frac{1}{2}$	0	0	0	0	$\frac{1}{3}$
s	$\frac{1}{2}$	$-\frac{1}{3}$	$-\frac{1}{3}$	0	-1	0	0	0	$-\frac{2}{3}$
c	$\frac{1}{2}$	$\frac{1}{3}$	$\frac{2}{3}$	0	0	+1	0	0	$\frac{4}{3}$
b	$\frac{1}{2}$	$-\frac{1}{3}$	$-\frac{1}{3}$	0	0	0	-1	0	$-\frac{2}{3}$
t	$\frac{1}{2}$	$\frac{1}{3}$	$\frac{2}{3}$	0	0	0	0	+1	$\frac{4}{3}$

Table 2.1: Quantum numbers of the quarks.

Baryon number conservation implies it is impossible to destroy or to make a single quark, but it is possible to annihilate or to create a quark-antiquark

pair; moreover quarks retain their identity under strong or electromagnetic transitions; that is, transmutations such as $s \to u$ + leptons, $s \to u + d\overline{u}$, etc. occur only under the influence of the weak interaction.

2.1.1 Quark-antiquark states: Mesons

In the quark model, mesons are made of a quark and an antiquark bound together. If only three flavors of quarks are considered, then there are nine possible combinations. Following SU(3), the nine $q\overline{q}$ combinations containing the light u, d and s quarks are grouped into an octet and a singlet of light quark mesons:

$$3 \otimes \overline{3} = 8 \oplus 1$$

Figure 2.2 shows an example of the SU(3) octet for mesons. In this case, a particular spin-parity J^P is selected ($J^P = 0^-$).

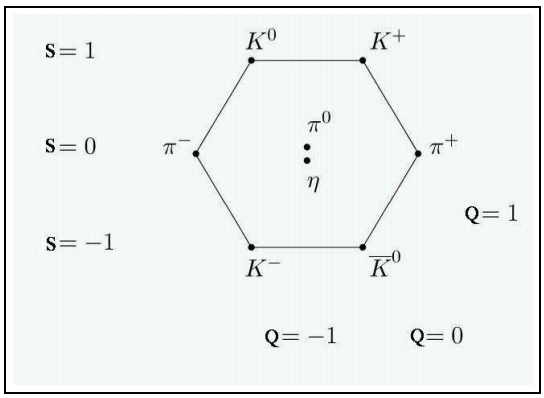

Figure 2.2: $J^P = 0^-$ octet for mesons.

If four flavors of quarks are considered, then the SU(4) symmetry is badly broken due to the much heavier c quark; however spin and parity can still be predicted. In an SU(4) classification the sixteen mesons are grouped into a 15-plet and a singlet:

$$4 \otimes \overline{4} = 15 \oplus 1$$

2.1.2 Three-Quark states: Baryons

The "ordinary" baryons are made up of u, d and s quarks (if three quarks are combined from the triplet $\{u,\ d,\ s\}$). The three flavors imply an approximate SU(3) flavor symmetry, which requires that baryons made of these quarks (27 possible qqq combinations) belong to the multiplets on the right side of:

$$3 \otimes 3 \otimes 3 = 10_S \oplus 8_M \oplus 8_M \oplus 1_A$$

where the subscripts have the meaning S=Symmetric, A=Antisymmetric and M=Mixed.

Figure 2.3 shows examples of the SU(3) multiplet for baryons. A $J^P = 1/2^+$ octet and a $J^P = 3/2^+$ decuplet, respectively.

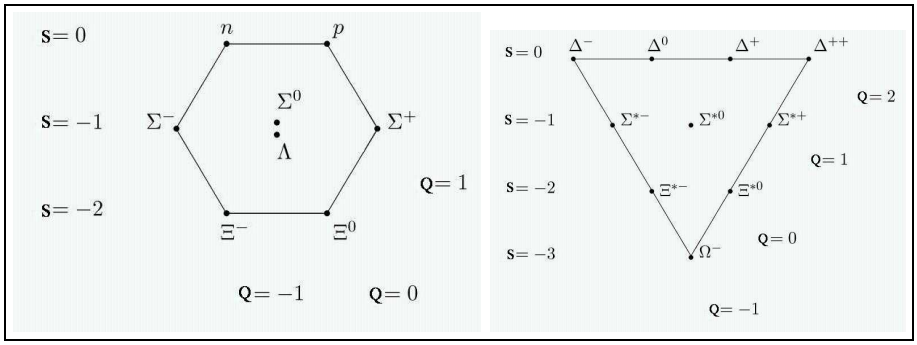

Figure 2.3: $J^P = 1/2^+$ octet and $J^P = 3/2^+$ decuplet for baryons, respectively.

At the time that the SU(3) quark model was developed, there was no experimental evidence for the bottom particle of the decuplet, the S=-3 particle (Ω^-), but its mass and quantum numbers were predicted using SU(3) relationships. Its subsequent discovery in 1964 at Brookhaven was an achievement for the model.

The addition of the c quark to the light quarks extends the flavor symmetry to SU(4) (see Chapter 3 about baryons with charm).

2.2 Color and Quantum Chromodynamics

In the quark model the particles of the baryon decuplet have a wavefunction fully symmetric in space, spin and flavor. This is most easily seen for the particles occupying the corner positions in the $J^P = 3/2^+$ states:

$$|\Delta^{++}; +3/2\rangle = |u\uparrow\rangle|u\uparrow\rangle|u\uparrow\rangle$$
$$|\Delta^{-}\ ; +3/2\rangle = |d\uparrow\rangle|d\uparrow\rangle|d\uparrow\rangle$$
$$|\Omega^{-}\ ; +3/2\rangle = |s\uparrow\rangle|s\uparrow\rangle|s\uparrow\rangle$$

If this were the whole story, the complete wavefunction would be totally symmetric for identical fermions, which is a blatant violation of the Pauli principle. A possible way out is to assume that the quarks carry an additional degree of freedom, *color*, that can take on three distinct values. Then the Pauli principle can be restored by assuming that the wavefunction is

completely antisymmetric in this new degree of freedom, which usually is labeled 'red', 'green' or 'blue'. The wave function can be written as:

$$|qqq\rangle_A = |color\rangle_A \times |space,\ spin,\ flavor\rangle_S$$

A baryon is thus described by a totally antisymmetric superposition of all arrangements of the three basic colors between the constituent quarks.

The name color is taken from the everyday experience that all ordinary colors can be composed from three basic colors. For ordinary colors, a superposition of equal amount of the basic colors red, green and blue yields white, and something similar also holds for the quarks' colors. Those colors exhibit an SU(3) color symmetry, so the color part of the baryon wavefunction can be shown to transform as an SU(3) singlet, that is, a baryon does not have any net color, it is 'white'. The mesons can also be understood as color singlets, made from a quark and an antiquark, where their color wavefunction is a superposition of color-anticolor states.

The measurements for the ratio of the cross sections:

$$\sigma(e^+e^- \to hadrons)/\sigma(e^+e^- \to \mu^+\mu^-)$$

and the lifetime of the τ-lepton in comparison to theoretical predictions are an impressive confirmation of the existence of exactly three colors.

2.2.1 Gluons

The interaction binding quarks into hadrons is the strong interaction, and according to Quantum Field Theory (QFT) it is always connected with a particle exchange. *Gluons* are the exchange particles that couple to the color charge. The experimental findings led to the development of the field theory called quantum chromodynamics (QCD). This is the gauge field theory which describes the strong interactions of colored quarks and gluons; it states that the interaction is mediated by exchange of a massless field particle with $J^P = 1^-$ (a vector boson). Gluons carry simultaneously color and anticolor, according to group theory, the 3×3 color combinations form two multiplets of states: a singlet and an octet. The octet states form a basis from which all other color states may be constructed, they correspond to an octet of gluons, and the way in which these eight states are constructed from color and anticolors is a matter of convention; one possible choice is:

$$r\overline{g}, \quad r\overline{b}, \quad g\overline{b}, \quad g\overline{r}, \quad b\overline{r}, \quad b\overline{g}, \quad \sqrt{1/2}(r\overline{r} - g\overline{g}), \quad \sqrt{1/6}(r\overline{r} + g\overline{g} - 2b\overline{b})$$

The color singlet:

$$\sqrt{1/3}(r\overline{r} + g\overline{g} + b\overline{b})$$

which is symmetrically constructed from the three colors and the three anticolors is invariant with respect to a re-definition of the color names (rotation in color space). It therefore has no effect in color space and cannot be exchanged between color charges.

By their exchange the eight gluons mediate the interaction between particles carrying color charge, not only for the quarks but also for the gluons themselves.

Emission and absorption of gluons can take place in QCD as do production and annihilation of quark-antiquark pairs; moreover three or four gluons can couple to each other in QCD.

Note that the SU(3) color symmetry is distinct from the SU(3) flavor symmetry discussed in the quark model section and it must not be confused; moreover the SU(3) color is an exact symmetry while the SU(3), SU(4) or SU(5) flavor symmetries are approximate.

2.2.2 The strong coupling constant

In quantum field theory, the coupling "constant" describing the interaction between two particles is an effective constant which is in fact dependent on Q^2 (the square of the four momentum transferred in the interaction). This dependence on Q^2 is very strong and the reason is that gluons as the field quanta of the strong interaction carry color themselves, and therefore can couple to other gluons. A first order perturbative calculation in QCD yields:

$$\alpha_s(Q^2) = \frac{12\pi}{(33 - 2n_f) \cdot \ln(Q^2/\Lambda^2)}$$

n_f denotes the number of quark flavors involved. Since a heavy virtual quark-antiquark pair has a very short lifetime and range, it can be resolved at very high Q^2. The Λ parameter is the only free parameter of QCD and it is determined, by comparing predictions with experimental data, to be $\Lambda \approx 250\,\mathrm{MeV/c}$. The application of perturbative expansion procedures in QCD is valid only if $\alpha_s \ll 1$. This is satisfied for $Q^2 \gg \Lambda^2 \approx 0.006\,(\mathrm{GeV/c})^2$.

The important physical properties of QCD are:

1. The gluons, which are the mediators of the strong interaction between quarks, are vector particles and carry color.

2. Asymptotic freedom, which implies that the effective coupling constant decreases logarithmically at short distances or high momentum transfer (at short distances the strong force decreases and quarks are quasi-free).

3. Confinement, which implies that the potential energy between color charges increases at large distances so that only color singlet states

exist (at large distances the strong force increases). As two quarks are pulled apart, the strong force that glues them together becomes ever more excited, forming powerful new force fields, "flux tubes," between the quarks.

2.3 Weak Interactions

The observed lifetimes of the pion and the muon are considerably longer than those of particles which decay either through strong or electromagnetic interactions. It is found that

$$\pi^- \to \mu^- \overline{\nu}_\mu \qquad \tau = 2.6 \times 10^{-8} sec. \tag{2.3}$$

$$\mu^- \to e^- \overline{\nu}_e \nu_\mu \qquad \tau = 2.2 \times 10^{-6} sec. \tag{2.4}$$

whereas particles decay by strong interactions in about 10^{-23} sec. and through electromagnetic interactions in about 10^{-20} sec. The lifetimes are inversely related to the coupling strength of these interactions. The pion and muon decays are evidence for another type of interaction with an even weaker coupling than electromagnetism.

Though all hadrons and leptons experience this weak interaction, and can undergo weak decays, which are often hidden by the much more rapid strong or electromagnetic decays. However the $\pi^\pm$ and the μ are special, and cannot decay via the latter two interactions. The π is the lightest hadron; whereas the neutral π can decay into photons, the charged pions cannot. As a result, the weak decay (2.3) is the dominant one. The reason why (2.4) is the dominant decay of the μ is interesting. In principle, the μ could decay electromagnetically via $\mu \to e\gamma$. The fact that the decay mode $\mu \to e\gamma$ is not seen (it is also appreciated that the μ is not an excited electron) and that the particular decay modes (2.3) and (2.4) occur are evidence for additive conserved lepton numbers: the electron number (L_e) and the muon number (L_μ) (it also exists the tau number (L_τ)). For example, the electron number assignments are:

$$L_e = +1 : \qquad e^-, \nu_e$$
$$L_e = -1 : \qquad e^+, \overline{\nu}_e$$
$$L_e = 0 \ : \textit{all other particles}$$

Similar arguments are made for L_μ and L_τ. Clearly, $L_\mu = 1$ and $L_e = 0$ for both the initial and final states of $\mu^- \to e^- \overline{\nu}_e \nu_\mu$, so this decay is consistent with the conservation of these quantum numbers; but $\mu^- \to e^- \gamma$ is not; actually known reactions conserve these three lepton numbers separately.

In scattering experiments weak interaction effects are difficult to observe.

Reactions of particles which are solely subject to the weak interaction (neutrinos) have extremely tiny cross sections. Most of the knowledge of the weak interaction has been obtained from particle decays; this one violates flavor conservation and the quarks and leptons are equally affected.

2.3.1 Types of Weak Interactions

The weak interaction can transform a charged lepton into its family's neutrino and it can produce a charged lepton (anti-lepton) and its anti-neutrino (neutrino) just the same manner quarks of one flavor can be transformed into quarks with another flavor in weak interactions. In all such reactions the identity of the quarks and leptons involved changes and the charge changes simultaneously by +1e or -1e. The term *charged current* was coined to describe such reactions. They are mediated by charged particles, the W^+ and W^-.

For a long time only this sort of weak interaction was known, nowadays it is known that the weak interaction may also proceed via the exchange of an additional electrically neutral particle, the Z_0 (as it is predicted by the electroweak theory). In this case the quarks and leptons are not changed. This is referred as *neutral currents*.

The $W^{\pm}$ and the Z^0 are vector bosons, i.e., they have spin one. Their masses are large: 80 GeV/c^2 and 91 GeV/c^2, respectively.

The charged currents can be divided up into three categories:

- Leptonic processes: the W boson only couples to leptons.

$$\ell + \overline{\nu}_\ell \longleftrightarrow \ell' + \overline{\nu}'_\ell$$

- Semileptonic processes: the exchanged W boson couples to both leptons and quarks.

$$q_1 + \overline{q}_2 \longleftrightarrow \ell + \overline{\nu}_\ell$$

- Non-leptonic processes: do not involve leptons at all.

$$q_1 + \overline{q}_2 \longleftrightarrow q_3 + \overline{q}_4$$

2.3.2 Coupling Strength of the Charged Current

The transition matrix element for a weak (charged current) process is proportional to the square of the *weak charge* g to which the W boson couples and to the propagator[1] of a massive spin-one particle:

[1] It has the general form $\frac{1}{Q^2+M^2c^2}$, where Q^2 is the square of the four-momentum transferred in the interaction and M is the mass of the exchange particle

$$\mathfrak{M}_{fi} \propto g \cdot \frac{1}{Q^2c^2 + M_W^2c^4} \cdot g \xrightarrow{Q^2 \to 0} \frac{g^2}{M_W^2c^4} = constant \tag{2.5}$$

The difference to an electromagnetic interaction is seen in the finite mass of the exchange particle. Instead of the photon propagator ($(Qc)^{-2}$), a propagator which is almost a constant for small enough momenta $Q^2 \ll M^2c^2$ is seen. The very large mass of the exchange boson means that at small Q^2 the weak interaction appears to be much weaker than the electromagnetic interaction. The mass also means that its range is also very limited ($\hbar/M_Wc \approx 2.5 \times 10^{-3}$ fm).

In the small four-momentum transfer approximation this interaction can be described as a point-like interaction of the four particles involved. This was in fact the original description of the weak interaction before the idea of the W and Z bosons was brought in. The coupling strength of this interaction is described by the *Fermi constant* G_F (proposed by E. Fermi in 1932), which is proportional to the square of the weak charge g, and they are related by:

$$\frac{G_F}{\sqrt{2}} = \frac{\pi\alpha}{2} \cdot \frac{g^2}{e^2} \cdot \frac{(\hbar c)^3}{M_W^2c^4} \tag{2.6}$$

with $\alpha = e^2/(4\pi\epsilon_0\hbar c)$ being the electromagnetic coupling constant.

2.3.3 CKM Quark Mixing Matrix

In weak interactions with charged currents quarks cannot just be transformed into their "partners" in the same doublet of the weak isospin:

$$\begin{pmatrix} u \\ d \end{pmatrix} \qquad \begin{pmatrix} c \\ s \end{pmatrix} \qquad \begin{pmatrix} t \\ b \end{pmatrix}$$

Quark transitions are not only observed within a family but, to a lesser degree, from one family to another. If two families of quarks are considered, then for charged currents, the "partner" of the flavor eigenstate $|u\rangle$ is therefore not the flavor eigenstate $|d\rangle$, but a linear combination of $|d\rangle$ and $|s\rangle$. This linear combination is called $|d'\rangle$. Similarly, the partner of the c-quark is a linear combination of $|s\rangle$ and $|d\rangle$, orthogonal to $|d'\rangle$ which is called $|s'\rangle$.

The coefficients of these linear combinations can be written as the cosine and sine of an angle called the *Cabibbo angle* θ_C. The quark eigenstates $|d'\rangle$ and $|s'\rangle$ of W exchange are related to the eigenstates $|d\rangle$ and $|s\rangle$ of the strong interaction, by a rotation through θ_C:

$$|d'\rangle = \cos\theta_C\,|d\rangle + \sin\theta_C\,|s\rangle \tag{2.7}$$

$$|s'\rangle = \cos\theta_C\,|s\rangle - \sin\theta_C\,|d\rangle \tag{2.8}$$

which may be written as a matrix:

$$\begin{pmatrix} |d'\rangle \\ |s'\rangle \end{pmatrix} = \begin{pmatrix} \cos\theta_C & \sin\theta_C \\ -\sin\theta_C & \cos\theta_C \end{pmatrix} \cdot \begin{pmatrix} |d\rangle \\ |s\rangle \end{pmatrix} \tag{2.9}$$

Whether the state vectors $|d\rangle$ and $|s\rangle$ or the state vectors $|u\rangle$ and $|c\rangle$ are rotated, or indeed both pairs simultaneously, is a matter of convention alone. Only the difference in the rotation angle is of physical importance. Usually the vectors of the charge -1/3 quarks are rotated while those of the charge +2/3 quarks are left untouched.

Experimentally, θ_C is determined by comparing the lifetimes and branching ratios of the semileptonic and hadronic decays of various particles. This yields:

$$\sin\theta_C \approx 0.22 \qquad \cos\theta_C \approx 0.98 \tag{2.10}$$

The transitions $c \longleftrightarrow d$ and $s \longleftrightarrow u$, as compared to $c \longleftrightarrow s$ and $d \longleftrightarrow u$ are suppressed by a factor of:

$$\sin^2\theta_C : \cos^2\theta_C \approx 1 : 20 \tag{2.11}$$

Adding the third generation of quarks, the 2×2 matrix is replaced by a 3×3 matrix, that is called: the *Cabibbo-Kobayashi-Maskawa matrix* (CKM matrix):

$$\begin{pmatrix} |d'\rangle \\ |s'\rangle \\ |b'\rangle \end{pmatrix} = \begin{pmatrix} V_{ud} & V_{us} & V_{ub} \\ V_{cd} & V_{cs} & V_{cb} \\ V_{td} & V_{ts} & V_{tb} \end{pmatrix} \cdot \begin{pmatrix} |d\rangle \\ |s\rangle \\ |b\rangle \end{pmatrix} \tag{2.12}$$

The matrix elements are correlated since the matrix is unitary. The total number of independent parameters is four: three real angles and an imaginary phase. The phase affects weak processes of higher order via the interference terms. *CP violation* is attributed to the existence of this imaginary phase [20].

The probability for a transition from a quark q to a quark q' is proportional to $|V_{qq'}|^2$, the square of the magnitude of the matrix element [19]. Transitions between quarks of the same family are called Cabibbo-favored decays, while quarks transitions from one family to another are called Cabibbo-suppressed decays. Two quark transitions in a single decay, both from one family to another, leads to a doubly Cabibbo-suppressed decay.

In this work, branching ratio measurements for non-leptonic weak decays of the charm-strange baryon Ξ_c^+ are performed; the analysis involves not only Cabibbo-favored decay modes but also Cabibbo-suppressed ones, so this will give information about $|V_{cd}|^2$ and $|V_{cs}|^2$; to be more specific: $|V_{cd}|^2/|V_{cs}|^2$.

2.4 Particle Decay

According to the Fermi's Golden Rule, the partial decay rate of a particle of mass M into n bodies in its rest frame is given in terms of the Lorentz-invariant matrix element $\mathfrak{M}$ by:

$$d\Gamma = \frac{(2\pi)^4}{2M}|\mathfrak{M}|^2 d\Phi_n(P; p_1, ..., p_n) \tag{2.13}$$

where $d\Phi_n$ is an element of n-body phase space given by:

$$d\Phi_n(P; p_1, ..., p_n) = \delta^4(P - \sum_{i=1}^{n} p_i) \prod_{i=1}^{n} \frac{d^3 p_i}{(2\pi)^3 2E_i} \tag{2.14}$$

The total decay rate, Γ, is the sum of the rates for all the decay channels. Clearly, the rate

$$\Gamma = -\frac{dN}{dt}/N \tag{2.15}$$

which leads to the exponential decay law for the number of particles (N)

$$N(t) = N(0)e^{-\Gamma t} \tag{2.16}$$

It is said that Γ^{-1} is the lifetime of the particle.

2.4.1 Three-Body Decays

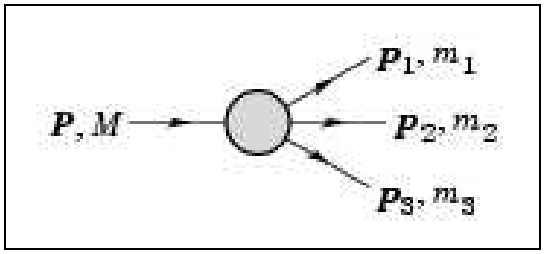

Figure 2.4: Three-body decay: A particle with momentum P and mass M decays to three particles having momenta p_1, p_2 and p_3 and masses m_1, m_2 and m_3, respectively.

For a three-body decay (Figure 2.4), it is defined:
$p_{ij} = p_i + p_j$ and $m_{ij}^2 = p_{ij}^2$, then $m_{12}^2 + m_{23}^2 + m_{13}^2 = M^2 + m_1^2 + m_2^2 + m_3^2$ and $m_{12}^2 = (P - p_3)^2 = M^2 + m_3^2 - 2ME_3$, where E_3 is the energy of particle 3 in the rest frame of M. In that frame, the momenta of the three decay particles lie in a plane. The relative orientation of these three momenta is fixed if their energies are known. The momenta can therefore be specified

in space by giving three Euler angles (α, β, γ) that specify the orientation of the final system relative to the initial particle. Then

$$d\Gamma = \frac{1}{(2\pi)^5}\frac{1}{16M}\,|\mathfrak{M}|^2\; dE_1\; dE_2\; d\alpha\; d(\cos\beta)\; d\gamma \tag{2.17}$$

Alternatively

$$d\Gamma = \frac{1}{(2\pi)^5}\frac{1}{16M}\,|\mathfrak{M}|^2\; |\mathbf{p_1}^*|\; |\mathbf{p_3}|\; dm_{12}\; d\Omega_1^*\; d\Omega_3 \tag{2.18}$$

where $(\mathbf{p_1}^*, \Omega_1^*)$ is the momentum of particle 1 in the rest frame of 1 and 2, and Ω_3 is the angle of particle 3 in the rest frame of the decaying particle. $|\mathbf{p_1}^*|$ and $|\mathbf{p_3}|$ are given by

$$|\mathbf{p_1}^*| = \frac{[(m_{12}^2 - (m_1+m_2)^2)(m_{12}^2 - (m_1-m_2)^2)]^{1/2}}{2m_{12}} \tag{2.19}$$

and

$$|\mathbf{p_3}| = \frac{[(M^2 - (m_{12}+m_3)^2)(M^2 - (m_{12}-m_3)^2)]^{1/2}}{2M} \tag{2.20}$$

If the decaying particle is a scalar or its spin states are averaged, then integration over the angles in Equation 2.17 gives:

$$d\Gamma = \frac{1}{(2\pi)^3}\frac{1}{8M}\,\overline{|\mathfrak{M}|^2}\; dE_1\; dE_2 = \frac{1}{(2\pi)^3}\frac{1}{32M^3}\,\overline{|\mathfrak{M}|^2}\; dm_{12}^2\; dm_{23}^2 \tag{2.21}$$

This is the standard form for the Dalitz plot.

2.4.1.1 Dalitz plot

For a given value of m_{12}^2, the range of m_{23}^2 is determined by its values when $\mathbf{p}_2$ is parallel or anti parallel to $\mathbf{p}_3$:

$$(m_{23}^2)_{max} = (E_2^* + E_3^*)^2 - \left(\sqrt{E_2^{*2} - m_2^2} - \sqrt{E_3^{*2} - m_3^2}\right)^2 \tag{2.22}$$

$$(m_{23}^2)_{min} = (E_2^* + E_3^*)^2 - \left(\sqrt{E_2^{*2} - m_2^2} + \sqrt{E_3^{*2} - m_3^2}\right)^2 \tag{2.23}$$

Here $E_2^* = (m_{12}^2 - m_1^2 + m_2^2)/2m_{12}$ and $E_3^* = (M^2 - m_1^2 - m_3^2)/2m_{12}$ are the energies of particles 2 and 3 in the m_{12} rest frame. The scatter plot in m_{12}^2 and m_{23}^2 is called a Dalitz plot. If $\overline{|\mathfrak{M}|^2}$ is constant, the allowed region of the plot will be uniformly populated with events. A nonuniformity in the

plot gives immediate information on $|\mathfrak{M}|^2$ [67]. Summarizing, it can be seen that the Dalitz plot is a way to represent the entire phase space (all essential kinematical variables) of any three-body final state in a scatter plot or two-dimensional histogram.

In a three-body decay the maximum of $|\mathbf{p_3}|$, is achieved when $m_{12} = m_1 + m_2$, *i. e.*, particles 1 and 2 have the same vector velocity in the rest frame of the decaying particle. If, in addition, $m_3 > m_1, m_2$, then, $|\mathbf{p_3}|_{max} > |\mathbf{p_1}|_{max}, |\mathbf{p_2}|_{max}$.

Summary

Now that the properties of the weak and strong interactions as well as the decay rate of particles have been revisited, it is possible to understand the decay mechanism in charm-strange baryons. The flavor symmetry for these hadrons is SU(4) (as mentioned before, badly broken owing to the much heavier c quark). The Ξ_c^+ weak decays under study in this work are non-leptonic (both Cabibbo-favored and Cabibbo-suppressed) and their study will provide information about the weak interaction mechanism. The role played by the QCD strong interaction in the decay processes can also be understood while studying the Ξ_c^+ modes: $\Sigma^-\pi^+\pi^+$ and $\Sigma^+\pi^-\pi^+$.

Chapter 3

Charm-Strange Baryons

To begin with, a brief introduction to the discovery of the quark charm, and the Ξ_c^+ and Λ_c^+ particles will be given in order to know a little history behind this work; then what charm baryons should exist will be explained with the quark model (an approximate SU(4) flavor symmetry) and finally, a description of Ξ_c^+ and Λ_c^+ decay modes and branching ratios to be measured later will be detailed. This is important because at this time the three-body decays of charm baryons are prohibitively difficult to calculate due to the complexity of associated final state interactions, and this work will shed some light into the theoretical calculations.

The experimental story of the c-quark began in 1974 [23, 24] and years later, the discovery of the Ξ_c^+ [25] in 1983 opened a new window in the study of charm baryons. The main particle under study in this work is the Ξ_c^+, whose mass is $2467.9 \pm 0.4\,\mathrm{MeV}/c^2$ and its mean lifetime is $(442 \pm 26) \times 10^{-15}\,sec$ [67].

3.1 History

Glashow, Iliopoulos and Maiani proposed the existence of a fourth quark some years before its discovery [26]. It was the first quark flavor predicted, and even the features of charm were specified:

- It possesses the same coupling as the u quark.
- Its mass is much heavier than the mass of the u quark, namely about $2\,\mathrm{GeV}/c^2$.
- It forms charged and neutral hadrons, where three mesons and four baryons only decay weakly, with lifetimes of very roughly $10^{-13}\,sec$.
- Its decay produces direct leptons and preferentially strange hadrons.

Glashow reiterated these properties in a talk at the 1974 Conference on Experimental Meson Spectroscopy (EMS-74) and concluded [27]:

"What to expect at EMS-76: there are just three possibilities:

1. Charm is not found, and I eat my hat.
2. Charm is found by hadron spectroscopers, and we celebrate.
3. Charm is found by outlanders, and you eat your hats".

A candidate event for the decay of a charm hadron was first seen in 1971 in an emulsion exposed to cosmic rays [28]. It showed a transition $X^{\pm} \to h^{\pm}\pi^0$ with $h^{\pm}$ denoting a charged hadron that could be a meson or a baryon. It was recognized that as the decaying object $X^{\pm}$ was found in a jet shower, it had to be a hadron and with an estimated lifetime around a few $\times 10^{-14}\, sec$ it had to be a weak decay. Assuming $h^{\pm}$ to be a meson, the mass of $X^{\pm}$ was about $1.8\,\mathrm{GeV}/c^2$.

3.1.1 Discovery of the Quark Charm

Although the *s*-quark was known from hadron spectroscopy, it was a surprise when in 1974 an extremely narrow resonance whose width was only 88 KeV was discovered at a center of mass energy of 3097 MeV. This particle was discovered nearly simultaneously in two differently conceived experiments (pp collisions, actually a fixed target p+Be, and e^+e^- annihilation). One collaboration called it J [23], the other called it ψ [24], so it was named J/ψ.

One of the experiments was held at Brookhaven with 30 GeV protons over a fixed target, led by Samuel C.C. Ting, and the other one at SLAC's SPEAR e^+e^- collider led by B. Richter. In 1974 Ting's group observed a sharp enhancement at $M(e^+e^-) = 3.1\,\mathrm{GeV}$. They did not announce the result waiting some months to confirm it; finally they went together with Richter's SLAC-LBL experiment, which observed a sharp resonant peak at the same energy in the interaction $e^+e^- \to \mu^+\mu^-, e^+e^-$. The ADONE e^+e^- collider at Frascati found itself in the unfortunate circumstance of having been designed for a maximum center-of-mass energy of 3.0 GeV. Immediately after the news of the J/ψ observation was received, currents in ADONE magnets were boosted beyond design limits and a scan in the $3.08 - 3.12\,\mathrm{GeV}$ was carried on and the new resonance was found and confirmed.

The resonance was attributed to the production of a new heavy quark. There were already theoretical suggestions that such a c quark ("charmed" quark as it was called) existed (the *bottom* quark was discovered at Fermilab in 1977 and the *top* quark in 1995, also at Fermilab).

Three papers [23, 24, 29], announcing the J/ψ discovery appeared in early

December 1974 in Physical Review Letters; afterwards B. Richter and Samuel C.C. Ting were awarded with the 1976 Nobel Prize in Physics.

3.1.2 Discovery of Charm Baryons

The discovery of the J/ψ indicated the existence of a new flavor beyond strangeness. Using the mass of this state De Rújula, Georgi and Glashow [30] predicted that the lowest baryon state with charm should have a mass close to $2200\,\mathrm{MeV}/c^2$ with the next higher state being more massive by about $160\,\mathrm{MeV}/c^2$. The first evidence of such charmed baryon production arose from the study of a neutrino interaction in the Brookhaven National Laboratory 7-ft bubble chamber. One event fit the reaction $\nu p \to \mu^- \Lambda^0 \pi^+ \pi^+ \pi^+ \pi^-$, which violated the $\Delta S = \Delta Q$ rule indicating the production and decay of a charmed baryon state; so the event had a clear charm signature and was consistent with the production of Σ_c^{++} (with mass $(2426 \pm 12)\,\mathrm{MeV}/c^2$) followed by the decay to Λ_c^+ (with mass $(2260 \pm 10)\,\mathrm{MeV}/c^2$) [1]. The subsequent observations of $\overline{\Lambda_c}(2260)$ in a photoproduction experiment confirmed both the interpretation and the mass [2].

In 1983, an experiment at CERN observed a narrow state at $2.46\,\mathrm{GeV}/c^2$ in the reaction $\Sigma^- + Be \to (\Lambda K^- \pi^+ \pi^+) + X$. The invariant mass distribution showed an excess of 82 events above a background estimated to be 147 (the statistical significance was more than 6 standard deviations) [25]. The positive charge of the observed state, which had strangeness -2, suggested the interpretation as a Cabibbo-favored decay of the charm-strange baryon A^+, a name used for the Ξ_c^+ at that time. The experiment also measured the lifetime of this particle and published it in 1985 [31].

3.2 Charm Baryons

Baryons made from u, d, s, and c quarks belong to SU(4) multiplets and the multiplet numerology is $4 \otimes 4 \otimes 4 = 20_S \oplus 20_M \oplus 20_M \oplus 4_A$ (where the subscripts have the meaning S=Symmetric, A=Antisymmetric and M=Mixed). Figure 3.1 shows the 20-plet (symmetric) for $J^P = 3/2^+$ with an $SU(3)$ decuplet on the lowest level and the 20-plet (mixed) for $J^P = 1/2^+$ with an $SU(3)$ octet on the lowest level. One level up in each multiplet are the baryons with one c quark. All the baryons in a given multiplet have the same spin and parity.

The members of an SU(2) isospin multiplet have the same mass to within $5\,\mathrm{MeV}/c^2$; however the SU(3) flavor symmetry is broken by mass differences of the order of $100\,\mathrm{MeV}/c^2$, and SU(4) flavor symmetry by considerably greater than $1\,\mathrm{GeV}/c^2$.

SU(4) and SU(5) are still useful for classification, even the flavor symmetries are very badly broken due to the larger mass of the c-quark compared

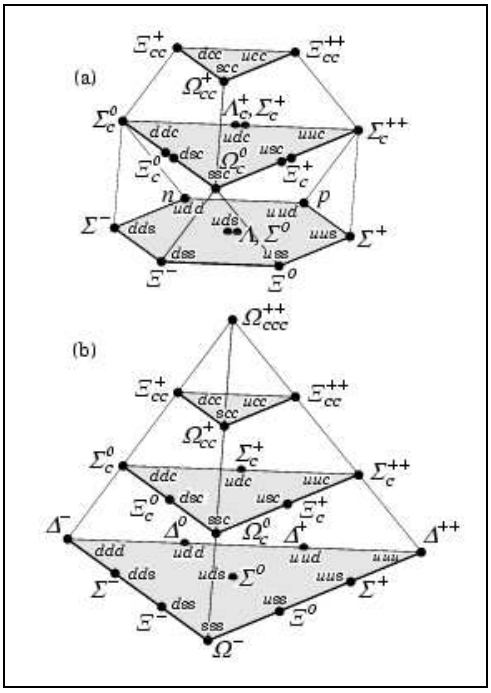

Figure 3.1: $SU(4)$ multiplets of baryons made of u, d, s and c quarks, with (a) $J^P = 1/2^+$ and (b) $J^P = 3/2^+$.

to u, d and s quarks.

As it can be seen in the framework of SU(4), nine ground state **cqq** $J^P = 1/2^+$ baryons and six **cqq** $J^P = 3/2^+$ baryons are expected; and all of them have been detected. Up to now, only a few excited state baryons have been observed.

If the middle level of the 20-plet (mixed) for $J^P = 1/2^+$ ((a) in Figure 3.1) is analyzed, it can be seen that it splits apart into two $SU(3)$ multiplets, a $\overline{3}$ and a 6. The states of the $\overline{3}$ are antisymmetric under the interchange of the two light quarks, whereas the states of the 6 are symmetric under this interchange. A prime is used to distinguish the Ξ_c in the 6 from the one in the $\overline{3}$ as it is illustrated in Figure 3.2. The particle under study in this work, Ξ_c^+, lies in the antisymmetric $\overline{3}$ multiplet (the name A^+ used in 1983 came from antisymmetric).

More than 70 decay modes have been measured for the Λ_c^+ [67]; for the doubly charged and neutral Σ_c states, they decay strongly with a pion to the Λ_c^+ ground state and several experiments have been measured their masses; for the Ξ_c^+ some Cabibbo-favored decay modes have been reported and only two Cabibbo-suppressed decay modes have been observed, as it can be seen in Table 3.1; finally for the Ξ_c^0 and Ω_c^0 some observations have been reported.

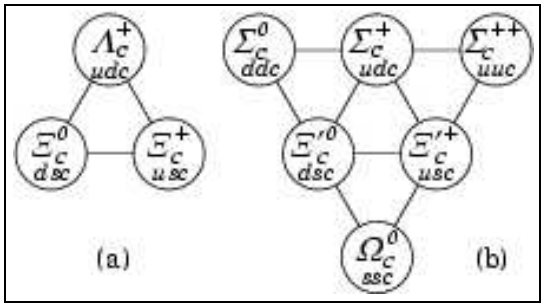

Figure 3.2: $SU(3)$ multiplets on second level of the $SU(4)$ multiplet for $J^P = 1/2^+$.

3.3 Branching Ratio

When a particle decays, it often does it in several ways. The probability that it decays to a particular mode is known as its branching fraction for that decay mode.

Most Ξ_c^+ branching fractions are measured relative to the decay mode $\Xi_c^+ \to \Xi^-\pi^+\pi^+$. There are no measurements of the absolute branching fraction for $\Xi_c^+ \to \Xi^-\pi^+\pi^+$, so it is defined as 1 in the Particle Data Group (PDG) [67] because it is a well known and established decay mode reported by several collaborations [32, 33, 34, 35, 36], and of course by SELEX [7].

Table 3.1 shows the Ξ_c^+ Cabibbo-favored decay modes reported up to now, while Table 3.2 shows the Ξ_c^+ Cabibbo-suppressed decay modes.

The main goal of this work is to provide information about the branching ratio of two never reported Ξ_c^+ Cabibbo-suppressed decay modes ($\Sigma^+\pi^-\pi^+$ and $\Sigma^-\pi^+\pi^+$). These very interesting branching ratios are to be measured relative to the $\Xi^-\pi^+\pi^+$ decay mode, as it was explained above. The branching ratios to be measured are:

$$BR_1 = \frac{\Gamma(\Xi_c^+ \to \Sigma^+\pi^-\pi^+)}{\Gamma(\Xi_c^+ \to \Xi^-\pi^+\pi^+)} \tag{3.1}$$

and

$$BR_2 = \frac{\Gamma(\Xi_c^+ \to \Sigma^-\pi^+\pi^+)}{\Gamma(\Xi_c^+ \to \Xi^-\pi^+\pi^+)} \tag{3.2}$$

The relative branching ratio between the new modes is also measured:

$$BR_3 = \frac{\Gamma(\Xi_c^+ \to \Sigma^-\pi^+\pi^+)}{\Gamma(\Xi_c^+ \to \Sigma^+\pi^-\pi^+)} \tag{3.3}$$

In order to check the methodology of the data analysis some control modes (reported before by SELEX and other collaborations) will be measured. The control modes are measured not only for the Ξ_c^+ particle but also for the Λ_c^+ particle. The control modes are:

Cabibbo-favored Decay Mode	Branching Ratio (relative to $\Xi^-\pi^+\pi^+$)
$pK_S^0K_S^0$	0.087 ± 0.022
$\Lambda\overline{K}^0\pi^+$	–
$\quad\Sigma(1385)^+\overline{K}^0$	1.0 ± 0.5
$\Lambda K^-\pi^+\pi^+$	0.323 ± 0.033
$\quad\Lambda\overline{K}^*(892)^0\pi^+\pi^+$	< 0.2 (90% C.L.)
$\quad\Sigma(1385)^+K^-\pi^+$	< 0.3 (90% C.L.)
$\Sigma^+K^-\pi^+$	0.94 ± 0.11
$\quad\Sigma^+\overline{K}^*(892)^0$	0.81 ± 0.15
$\Sigma^0K^-\pi^+\pi^+$	0.29 ± 0.16
$\Xi^0\pi^+$	0.55 ± 0.16
$\Xi^-\pi^+\pi^+$	DEFINED AS 1
$\quad\Xi(1530)^0\pi^+$	< 0.1 (90% C.L.)
$\Xi^0\pi^+\pi^0$	2.34 ± 0.68
$\Xi^0\pi^+\pi^+\pi^-$	1.74 ± 0.50
$\Xi^0e^+\nu_e$	$2.3^{+0.7}_{-0.9}$
$\Omega^-K^+\pi^+$	0.07 ± 0.04

Table 3.1: Branching Ratio of Ξ_c^+ Cabibbo-favored Decay Modes.

Cabibbo-suppressed Decay Mode	Branching Ratio
$pK^-\pi^+$	0.21 ± 0.03
$\quad p\overline{K}^*(892)^0$	0.12 ± 0.02
$\Sigma^+K^+K^-$	0.15 ± 0.07
$\quad\Sigma^+\phi$	< 0.11 (90% C.L.)
$\quad\Xi(1690)^0K^+$, $\Xi(1690)^0 \to \Sigma^+K^-$	< 0.05 (90% C.L.)

Table 3.2: Branching Ratio of Ξ_c^+ Cabibbo-suppressed Decay Modes.

$$BR_4 = \frac{\Gamma(\Xi_c^+ \to pK^-\pi^+)}{\Gamma(\Xi_c^+ \to \Xi^-\pi^+\pi^+)} \tag{3.4}$$

$$BR_5 = \frac{\Gamma(\Lambda_c^+ \to \Sigma^+\pi^-\pi^+)}{\Gamma(\Lambda_c^+ \to pK^-\pi^+)} \tag{3.5}$$

$$BR_6 = \frac{\Gamma(\Lambda_c^+ \to \Sigma^-\pi^+\pi^+)}{\Gamma(\Lambda_c^+ \to \Sigma^+\pi^-\pi^+)} \tag{3.6}$$

To perform some comparisons, it is also measured:

$$BR_7 = \frac{\Gamma(\Lambda_c^+ \to \Sigma^-\pi^+\pi^+)}{\Gamma(\Lambda_c^+ \to pK^-\pi^+)} \tag{3.7}$$

The control mode (3.4) was the first Cabibbo-suppressed decay mode found of the Ξ_c^+ and it was reported by SELEX [7]. The control modes (3.5) and (3.6) are very important to measure because they are previously reported modes of the Λ_c^+ [4, 6] having the same decay channels than those of the new Ξ_c^+ decay modes found in this work, so they will be used to test the analysis method.

3.4 Ξ_c^+ and Λ_c^+ Decay Modes

The Ξ_c^+ and Λ_c^+ decay modes reported in this work are summarized in the next table, along with the Q (free energy, calculated as $M_{\Xi_c^+} - \sum M_D$)[2] available for the decay:

[2] $M_{\Xi_c^+}$ is the mass of the Ξ_c^+ (mother) particle and $\sum M_D$ is the sum of the masses of the daughter particles

	Ξ_c^+	PDG	Q (MeV)
Cabibbo Favored	$\Xi^-\pi^+\pi^+$	Reported (Reference Mode)	868
Cabibbo Suppressed	$p^+K^-\pi^+$	Reported	896
	$\Sigma^+\pi^-\pi^+$	Found in this work	999
	$\Sigma^-\pi^+\pi^+$	Found in this work	991
	$\Xi^-K^+\pi^+$	Observed in this work (for future activities)	513
Doubly Cabibbo Suppressed	$\Sigma^+K^+\pi^-$	Observed in this work (for future activities)	645
	Λ_c^+	PDG	Q (MeV)
Cabibbo Favored	$pK^-\pi^+$	Reported	715
	$\Sigma^+\pi^-\pi^+$	Reported	818
	$\Sigma^-\pi^+\pi^+$	Reported	810

Table 3.3: Ξ_c^+ and Λ_c^+ Decay Modes.

The spectator diagram with external W emission for the Cabibbo-favored $\Xi_c^+ \to \Xi^-\pi^+\pi^+$ decay is shown in Figure 3.3. A quark pair from the vacuum ($d\bar{d}$) is recombined with a valence quark of the Ξ_c^+ and with the strange quark coming from the weak decay of the charm quark. It is seen that the branching fraction is proportional to the $|V_{cs}|^2$ element of the CKM matrix (plus phase space and ignoring other effects).

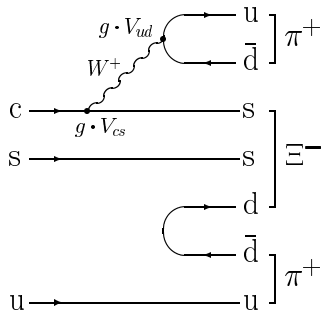

Figure 3.3: Spectator diagram for $\Xi_c^+ \to \Xi^-\pi^+\pi^+$.

The spectator diagram with external W emission for the Cabibbo-suppressed $\Xi_c^+ \to pK^-\pi^+$ (reported by SELEX in 2000 [7]) is also shown (Figure 3.4); in this case, the decay rate is proportional to the $|V_{cd}|^2$ element of the CKM matrix (plus phase space and ignoring other effects).

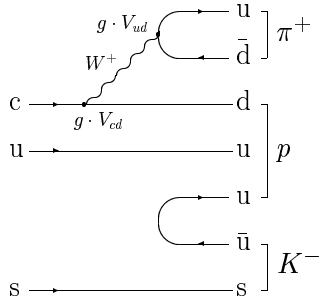

Figure 3.4: Spectator diagram for $\Xi_c^+ \to pK^-\pi^+$.

Finally, the spectator diagrams for the two Cabibbo-suppressed Ξ_c^+ decays found in this work are shown in Figure 3.5. It is important to note that one difference between these two modes is the production of $u\bar{u}$ and $d\bar{d}$ pairs from the vacuum. They have a very similar phase space since the difference in mass between the Σ^- and the Σ^+ is just around $8\,\mathrm{MeV}/c^2$.

Another difference is that in the case of the $\Sigma^+\pi^-\pi^+$ channel, the Σ^+ hyperon is produced due to the arrangement among two valence quarks (u and s) and the u quark coming from the vacuum; while in the case of the $\Sigma^-\pi^+\pi^+$ channel, the Σ^- hyperon is produced due to the arrangement among

only one valence quark (s), the d quark coming from the vacuum and the d quark coming from the Cabibbo-suppressed decay of the c quark.

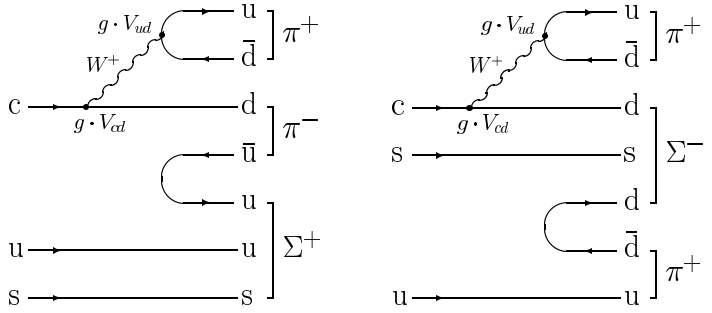

Figure 3.5: Spectator diagrams for $\Xi_c^+ \to \Sigma^+\pi^-\pi^+$ and $\Xi_c^+ \to \Sigma^-\pi^+\pi^+$.

The same diagrams for Λ_c^+ decay modes are also shown in Figure 3.6. The biggest difference is that the decay modes for the Λ_c^+ are Cabibbo-favored.

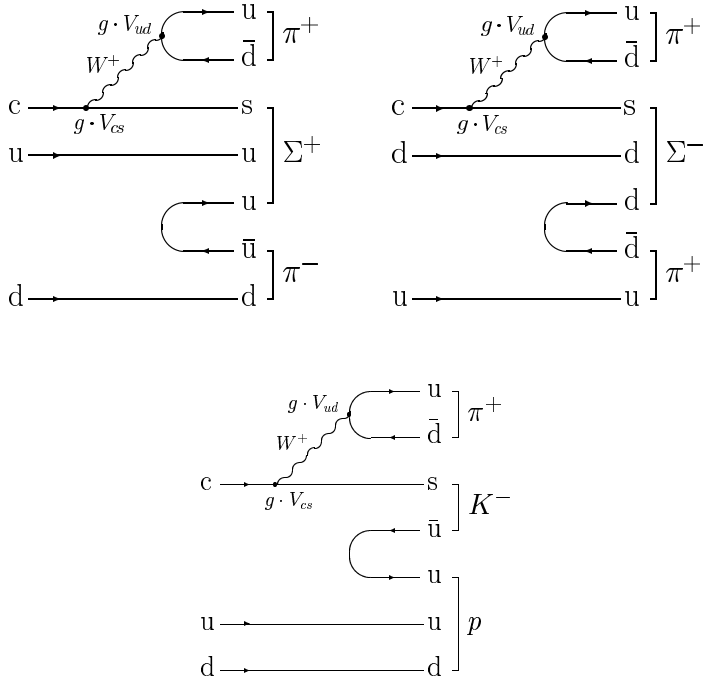

Figure 3.6: Spectator diagrams for $\Lambda_c^+ \to \Sigma^+\pi^-\pi^+$, $\Lambda_c^+ \to \Sigma^-\pi^+\pi^+$ and $\Lambda_c^+ \to pK^-\pi^+$.

It is appreciated that the W-internal and W-exchange diagrams have not been included since they are similar to the ones described above.

Two more modes are presented in this thesis as part of future activities related to the study of the Ξ_c^+. The spectator diagrams are shown in Figure 3.7 and the results will be presented in Chapter 6. The first one, $\Xi_c^+ \to \Xi^- K^+\pi^+$,

is a Cabibbo-suppressed decay, and the second one, $\Xi_c^+ \to \Sigma^+ K^+ \pi^-$, is a doubly Cabibbo-suppressed decay. Both spectator diagrams have a $W^+ \to u\bar{s}$ contribution in common, where the Cabibbo-suppressed decay takes place; besides, there is another diagram contribution for the $\Xi^- K^+ \pi^+$ decay which requires a $s\bar{s}$ from the sea.

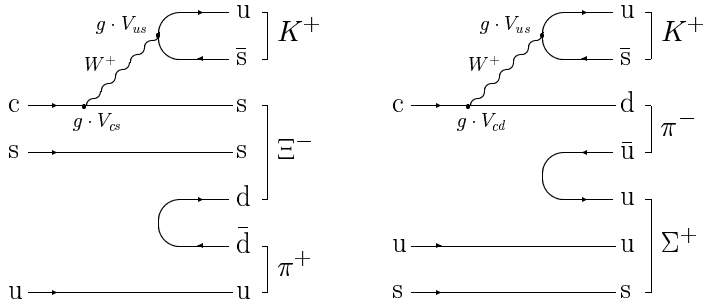

Figure 3.7: Spectator diagrams for $\Xi_c^+ \to \Xi^- K^+ \pi^+$(left) and $\Xi_c^+ \to \Sigma^+ K^+ \pi^-$(right).

3.4.1 α^2-parameter

To quantify the effects of final state quark rearrangements in the different decays via the relevant relative matrix elements, a parameter named α is calculated. The α^2-parameter is defined as the branching ratio corrected for phase space differences and, in the case of comparing Cabibbo-favored and Cabibbo-suppressed modes, for the ratio of the CKM matrix elements ($V_{cd}/V_{cs} = 0.233 \pm 0.001$ [67]).

The branching ratio for a Cabibbo-suppressed decay can be expressed as:

$$BR = \alpha^2 \cdot \left| \frac{V_{cd}}{V_{cs}} \right|^2 \cdot \rho \tag{3.8}$$

where ρ is the relative phase space contribution. This parameter will be calculated for all the branching ratio measurements.

3.5 Charm Models to Calculate Decay Rates

Theoretical tools for treating charm have made very significant progress in formalizing ideas into definite frameworks that allow further refinements:

- Corrections of higher orders in α_s have been computed for cross sections, structure and fragmentation functions.
- Different parameterizations have been explored.

- Heavy quark expansions have been developed to describe weak decays of charm hadrons.

- Efforts have been made to treat charm hadrons on the lattice.

Nonleptonic weak decays have a much difficult challenge to a theoretical description than semileptonic ones: there are more colour sources and sinks in the form of quarks and antiquarks, and there are more different combinations for colour flux tubes to form. The only classes of nonleptonic decays where a reasonable hope of some success can be expected are in channels with a two-body final state because the phase space is trivial and the number of form factors quite limited; on the other side, several further complications arise on the Cabibbo-suppressed level because there are two transition operators before QCD corrections are included, namely for $c \to s\overline{s}u$ and $c \to d\overline{d}u$ [37].

Beyond two hadrons in the final state, the degrees of freedom and the complexities of phase space increase in a way that it is not possible to have them under control, so the three-body decays of charm baryons are prohibitively difficult to calculate because of the complexity of associated final state interactions. The decays under study in this work are three-body and Cabibbo-suppressed.

Summary

As it was observed the SU(4) flavor symmetry is never nearly as successful as the SU(3) flavor symmetry in making quantitative predictions. The reason is that the c-quark is much more massive than u, d and s quarks, whereas making use of group theoretical symmetry implies that the various members of a multiplet are essentially identical except for the few quantum numbers that distinguish them. It was noted that the decay modes of the Ξ_c^+ baryon under study in this work (the ones not reported on PDG, and for the first observed, $\Xi_c^+ \to \Sigma^-\pi^+\pi^+$ and $\Xi_c^+ \to \Sigma^+\pi^-\pi^+$, as they will be shown in Chapter 6) are very similar; as it was seen on the spectator diagrams, there is an insignificant difference in the phase space, so a measurement of its relative branching ratio will provide information about the quark arrangement in the decay process (a QCD strong interaction mechanism) and it is expected that the results presented will help in theoretical calculations.

Chapter 4

SELEX Experiment

The observation of the Ξ_c^+ and Λ_c^+ decay modes was performed using data from SELEX experiment; so a detail description of the experiment is presented in this chapter. The code (software) used for the data analysis is also explained.

4.1 SELEX Overview

The SELEX (Segmented Large x_F Baryon Spectrometer) experiment (also called E781) was a multi-stage spectrometer with high acceptance for forward interactions. It was a fixed target experiment that took data during 1996 and 1997 at Fermilab, with 600 GeV/c (mainly Σ^-, π^-) and 540 GeV/c (mainly p) beams incident on copper and carbon targets. The main goal of SELEX was to obtain a large sample of charm baryon decays using a variety of incident beam particles and targets. There were some physics (charm and non-charm) goals such as:

- Charm hadroproduction with different beams and targets.
- Precision measurements of charm lifetimes.
- Study of new decay modes and their branching ratios.
- Detection of charm excited states.
- Measurement of total cross sections.
- Measurement of hadronic charge radii.
- Production polarization of hyperons.
- Primakoff production of excited states.
- Pion polarizability.

- Search for exotic states.

One of the most powerful detectors of the experiment was the vertex Silicon Strip Detector (SSD), capable of $4\,\mu m$ transverse position resolution at 600 GeV. The vertex separation L was measured with precision $\sigma \simeq 0.5\,mm$; having a small error on vertex separation is important because the significance L/σ is the most powerful cut to separate the charm signal from the background.

The SELEX experiment had an extensive particle identification system. Beam particles ($\Sigma^-/\pi^-, p/\pi^+$) were tagged with the Beam Transition Radiation Detector (BTRD). The 3000 phototube Ring Imaging Cherenkov Counter (RICH) was used to identify the secondary particles: electrons, muons, pions, protons, kaons and even hyperons; the RICH was capable of K/π separation up to 165 GeV/c. The Electron Transition Radiation Detectors (ETRD) were used to separate electrons from hadrons, which is important for the study of semileptonic decays. Three lead glass detectors were used to identify and measure the energy of photons and electrons.

SELEX had also a precise tracking system and 3 analyzing magnets to measure particle momenta. Eight Beam SSD planes with hit resolution $\sigma \sim 6\,\mu m$ were used to measure track parameters. The downstream tracking system included 26 Proportional Wire Chambers (PWC) planes with hit spatial resolution $\sigma \sim 0.6 - 1mm$. It also included three Vector Drift Chambers (VDC) each having 8 sensitive planes with hit resolution $\sigma \sim 100\,\mu m$. Finally, there were 18 large SSD with hit resolution $\sigma \sim 14\,\mu m$ to measure tracks with very high momentum. The SSD system had 74000 strips. This gave around 100,000 electronic channels. One of the innovations of SELEX was the Online Filter which decreased the background by a factor of 8 and was about 50 % efficient for a typical charm signal.

Figure 4.1 shows a schematic view of the SELEX apparatus where the vertex region has been enhanced.

4.2 SELEX Apparatus

SELEX detector was a spectrometer (60 m. long) which was composed of five parts:

- Beam spectrometer
- Vertex spectrometer
- M1 spectrometer
- M2 spectrometer
- M3 spectrometer

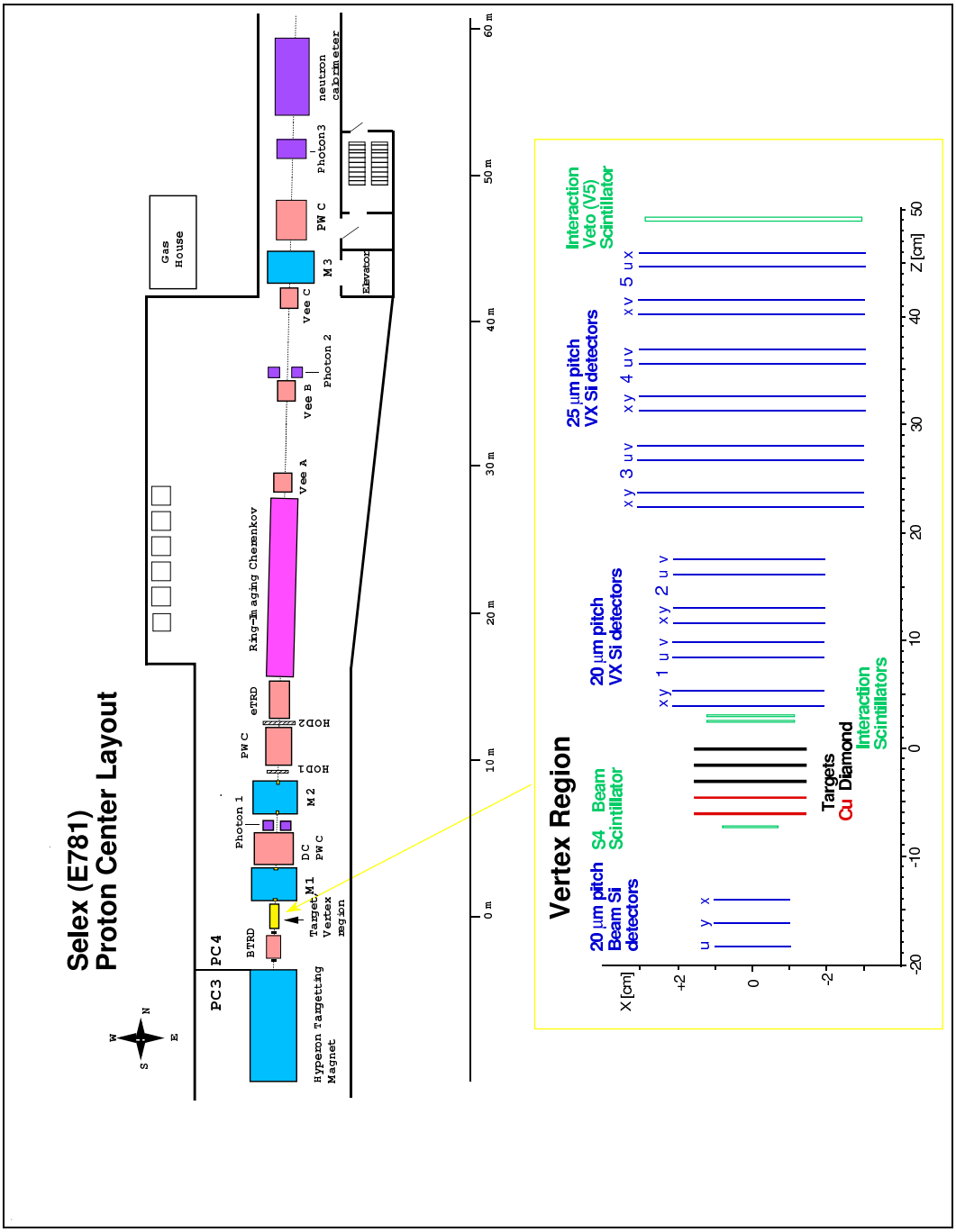

Figure 4.1: Schematic view of SELEX spectrometer.

Figure 4.2 shows a diagram of the five spectrometers, for each one of them, but the vertex, there were particle detectors and a magnet, so it was possible to measure the momentum of the charged particles. The vertex spectrometer did not contain a magnet because it was designed for high resolution tracking of particles near the interaction target.

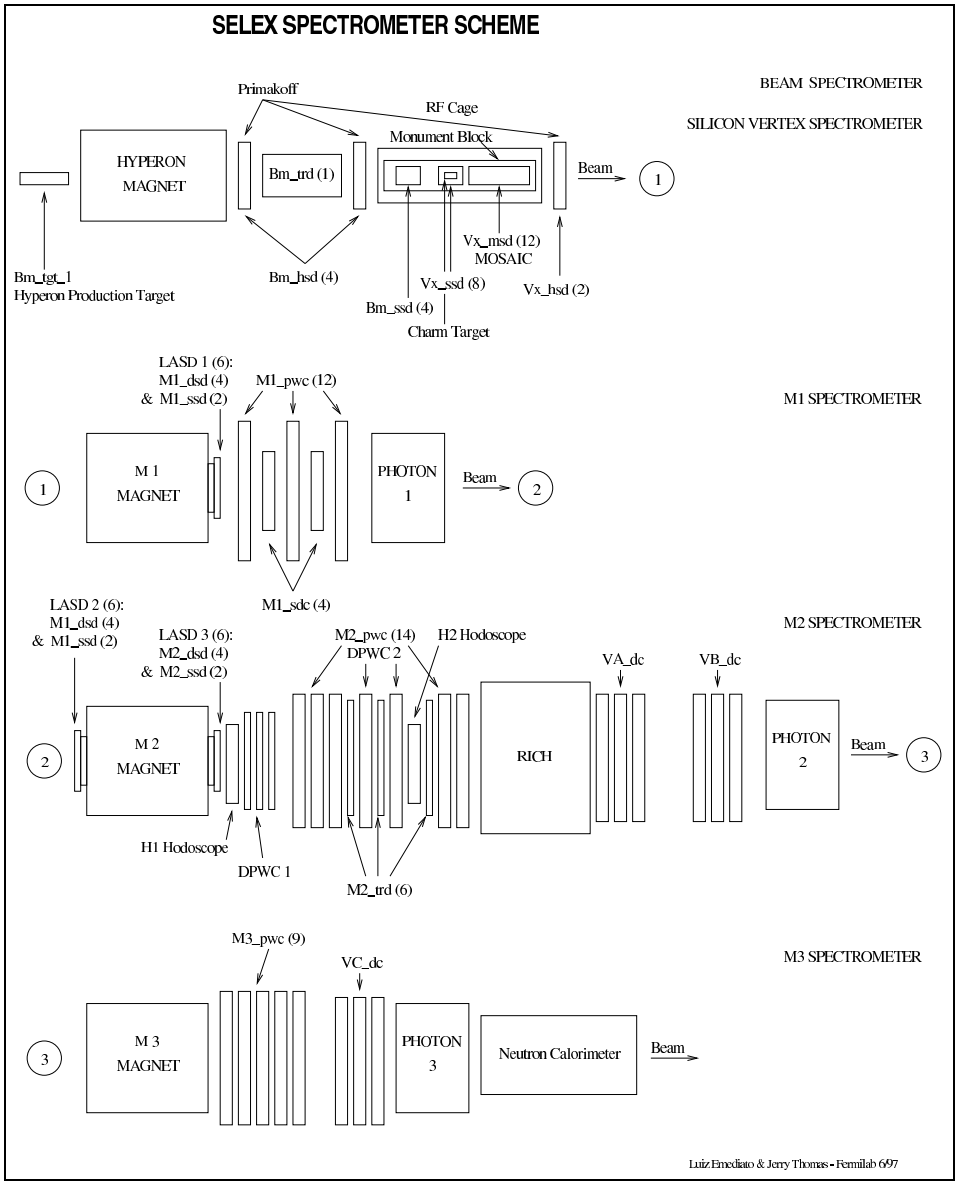

Figure 4.2: SELEX spectrometer scheme

4.2.0.1 Coordinate systems

The origin of the coordinate system was chosen to be in the middle of the downstream surface of the most downstream target as it is shown in

Figure 4.3. The z-axis was along the beam direction, the y-axis was vertically up and the x-axis completed a right-handed coordinate system (the units used to measure distance were centimeters).

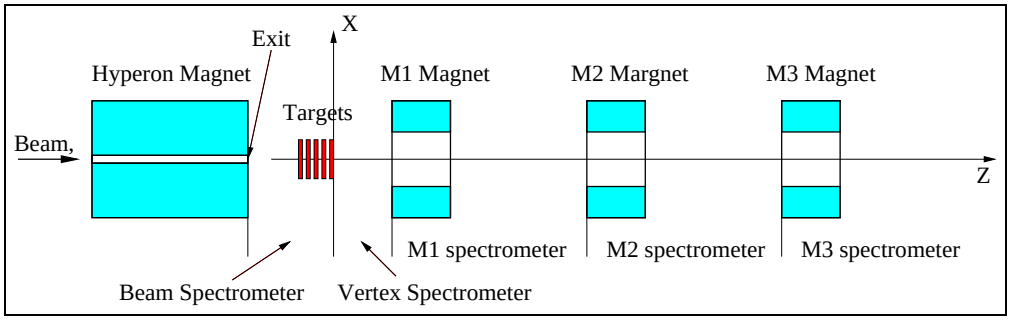

Figure 4.3: SELEX coordinate system and spectrometers.

In addition, each spectrometer had a local coordinate system typically aligned in position and angles with the overall coordinate system but its z origin shifted to the magnetic center of the magnet of that spectrometer.

4.2.1 Beam Spectrometer

The beam spectrometer consisted of everything upstream the last charm target (also included the targets).

Figure 4.4 shows an schematic view of this spectrometer.

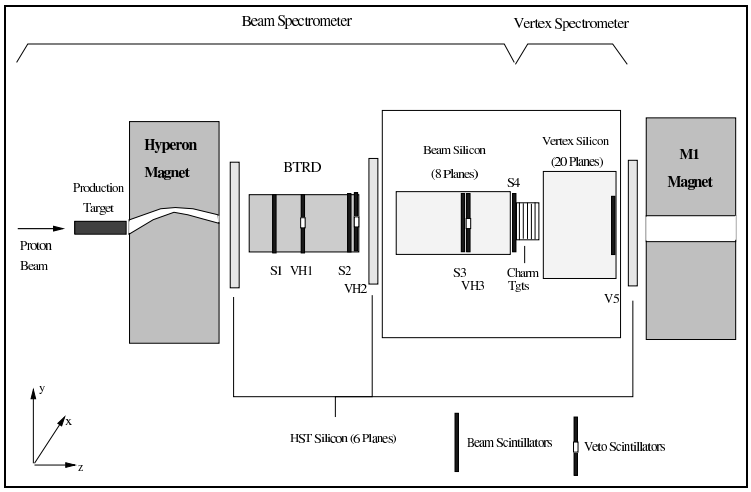

Figure 4.4: Schematic view of the beam spectrometer.

4.2.1.1 Hyperon Beam

The Tevatron accelerator produced a 800 GeV beam of protons, which was directed to the SELEX fixed target experiment. Under normal condi-

tions, the Tevatron delivered 5×10^{10} protons/second during a 20-second burst in periods of 60 sec. The proton beam spot size was on the order of $1\,mm$ full width at half-maximum. This protons beam hit a beryllium target (one interaction length, about $30\,cm$) producing secondary particles that entered a narrow (about $0.5 \times 0.5\,cm^2$) long curved channel of $7.3\,m$ inside the hyperon magnet (Figure 4.5) with a magnetic field of $3.5\,T$. The walls of the channel (made of tungsten) served to collimate the beam, so only high momentum particles, $600 \pm 50\,\mathrm{GeV/c}$, could go through the magnet. The main purpose to use this momentum is that the relative fraction of hyperons in the secondary beam grows with the momentum. At the target region, the $600\,\mathrm{GeV/c}$ negative secondary beam consisted of approximately 50.9% of pions (π^-), 46.3% of sigmas (Σ^-), 1.6% of kaons (K^-) and 1.2% of cascades (Ξ^-). By changing the magnet polarity, it was possible to produce a positive beam which mainly consisted of 89.2% of protons (p), 5.7% of pions (π^+), 2.7% of sigmas (Σ^+) and 2.4% of kaons (K^+) [38, 39, 40].

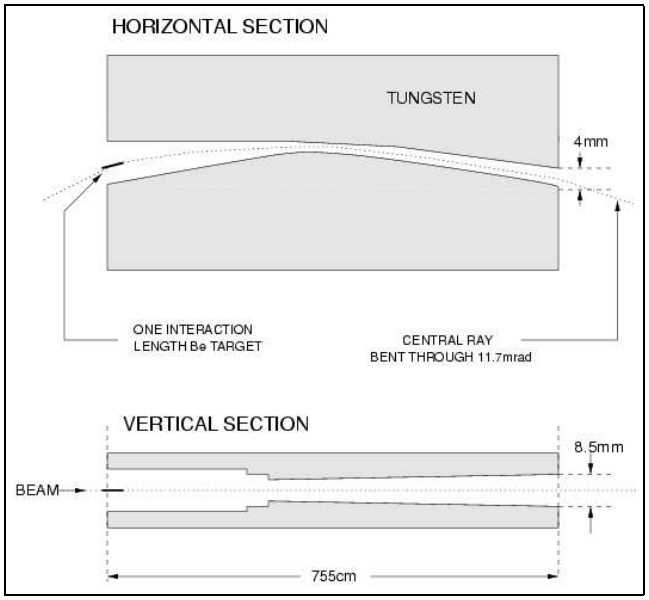

Figure 4.5: Hyperon Magnet.

4.2.1.2 Beam Transition Radiation Detectors (BTRD)

A TRD detects electromagnetic radiation emitted by charged particles as they traversed the boundary between media with different dielectric properties. A charged particle moving towards a boundary forms together with its mirror charge an electric dipole, whose field strength varies with time, i.e., with the movement of the particle. The field strength vanishes when the particle enters the medium and the time dependent dipole electric field causes the emission of electromagnetic radiation.

Particles in the hyperon beam were tagged in the identical 10 modules of the Beam TRD. Each module had a radiator made of 200 polypropylene foils 17 μm thick, followed by 3 proportional wire chambers filled with the mixture of Xe+30%CH_4 gas to detect transition radiation (the gas mixture maximizes the absorption of photons) [41]. The proportional wire chambers (PWC) gave an output signal(hit) when they detected energy above a fixed threshold. The number of activated planes was equal to the sum of all the output signals in the PWC. As mention in the last paragraph; when a relativistic particle crosses the boundary of media with different dielectric constants it emits transition radiation photons. Typically, the energy of such photons is a few KeV and they are detectable by multiwire proportional chambers. The probability of radiation is proportional to the Lorentz γ-factor of the particle; hence a π^- (meson) produces more hits in the BTRD detectors than a Σ^- (baryon) of the same energy since the π^- mass is much less than that of the Σ^-. The total number of hits in the BTRD was used to separate the baryon component from the meson component of the beam (Figure 4.6).

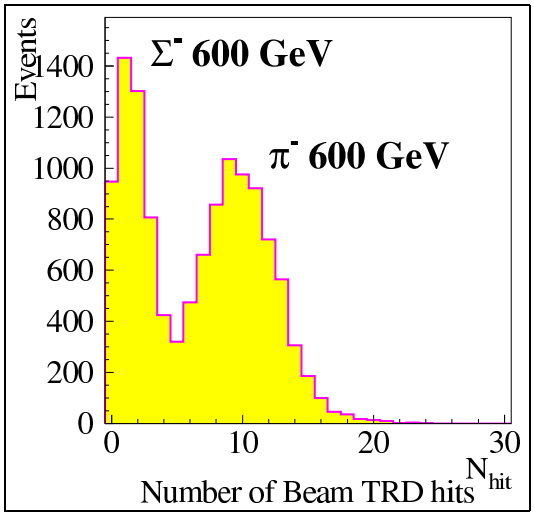

Figure 4.6: Hits in BTRD.

4.2.1.3 Beam Silicon Strip Detectors (BSSD)

The beam track position and direction of motion were measured with 8 planes of Silicon Strip Detectors (SSD). Each detector had 1024 strips of 20 μm pitch, with a $2 \times 2\, cm^2$ sensitive area. The position of the beam track in the charm targets had a 4 μm resolution approximately and the strips were readout by SVX chips. Because the integration gate of the readout electronics was a few microseconds long, information about several beam tracks from the 700 kHz beam was stored in the beam SSD hit output along with the triggering beam.

4.2.1.4 Hardware scattering trigger Silicon Detectors (HSD)

The beam track which triggered the event was identified using the Hardware scattering Silicon Detectors (HSD) (it also used hit information from the vertex SSD, to be discussed later). The system consisted of 4 Silicon Strip Detectors (each one $50\,\mu m$ pitch), and they employed $80\,ns$ gates, so only hits from the beam particle that triggered the event were readout. Beam track candidates were extrapolated from the Beam SSD to the HSD planes, such feature benefits all SELEX physics projects, by identifying the in-time beam track using first two stations of the HSD, and a third station, which was mounted on the downstream end of the RF cage, could be used as a single outgoing in-time track identifier. The track that had 2 or more matching hits in the HSD was identified as the trigger beam track.

4.2.1.5 Charm Targets

Beam particles interacted in 5 targets with combined interaction length of 4.3%. They were spaced $1.5\,cm$. Two of them were from copper (Cu) and the other three of diamond (C). Its properties are summarized in Table 4.1.

target	material	thickness $[mm]$	z $[cm]$	atomic number A	density $[g/cm^3]$	interaction length [%]
1	copper	1.6	-6.13	63.5	8.96	1.06
2	copper	1.1	-4.62	63.5	8.96	0.76
3	diamond	2.2	-3.10	12	3.20	0.82
4	diamond	2.2	-1.61	12	3.20	0.82
5	diamond	2.2	-0.11	12	3.20	0.82

Table 4.1: Information of the targets.

4.2.2 Vertex Spectrometer

The vertex spectrometer started at the downstream edge of the last target, and ended at the middle of the M1 magnet.

Figure 4.7 shows an schematic view of this spectrometer (the segmented charm target can also be seen).

4.2.2.1 Vertex Silicon Detectors (SSD)

20 silicon detectors planes downstream of the charm targets detected secondary tracks with high spatial resolution. The first 8 detectors ($5\,cm$ detectors) had $20\,\mu m$ pitch with an effective area of $5.1 \times 5.0\,cm^2$. The last

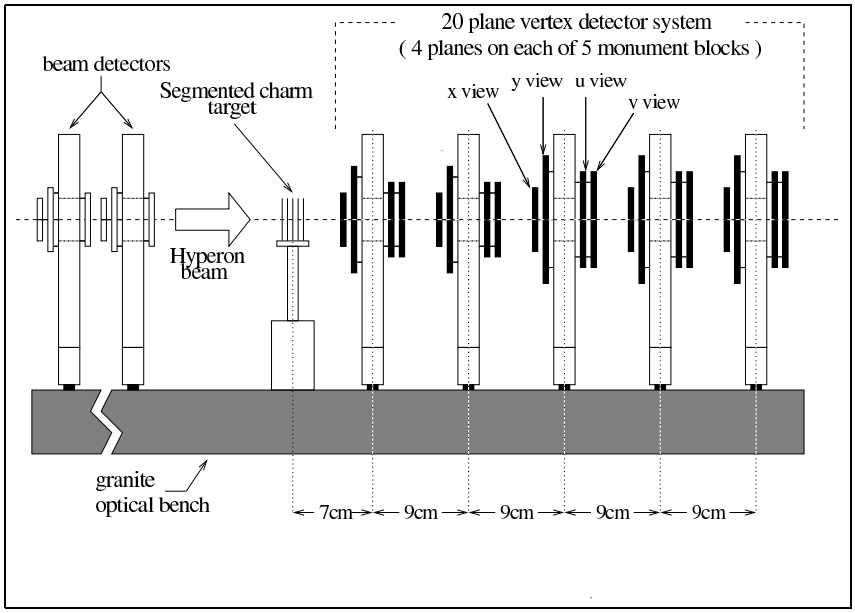

Figure 4.7: Schematic view of the vertex spectrometer and the target region.

12 detectors (mosaic detectors) had $25\,\mu m$ pitch with an effective area of $8.3 \times 9.6\,cm^2$. They were mounted on special granite optical bench, and measured tracks in x, y, u and v projections.

Each of the detectors had more than 98% hit detection efficiency and a spatial resolution of about $6.5\,\mu m$.

The Beam silicon, Vertex silicon, charm targets and trigger scintillators were enclosed in a light-tight aluminum box for RF shielding, which was also cooled with air chilled to 19^o C.

4.2.3 M1 Spectrometer

The M1 spectrometer consisted of the M1 magnet and the detectors between the M1 and M2 magnets.

Figure 4.8 shows a schematic view of this spectrometer.

4.2.3.1 Multiwire Proportional Chambers (MWPC)

A MWPC consists of equally spaced anode wires centered between two cathode planes. The chamber is filled with a gas combination that ionizes when a charged particle passes through it; the ionized gas consists of electrons and positively charged ions, where the positive ions would drift in the electric field to the cathode and the electrons would drift to the anode. When the electrons are close to an anode wire, a process of avalanche formation occurs greatly increasing the signal collected by the wire. This signal is read out

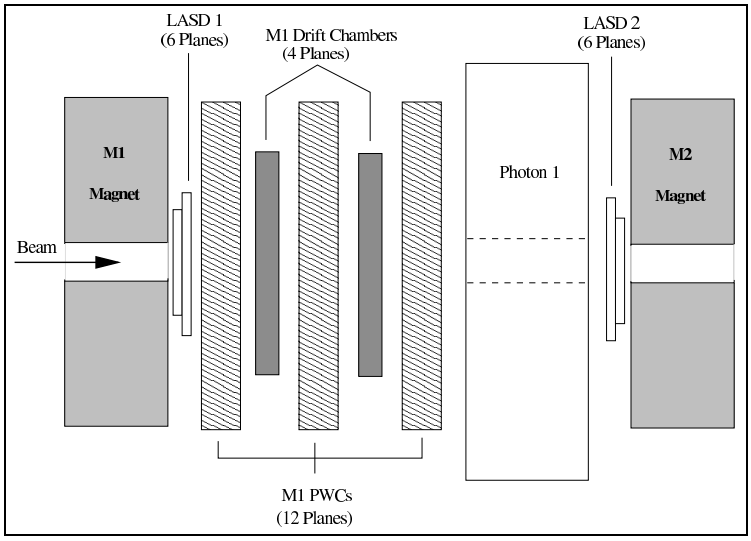

Figure 4.8: Schematic view of the M1 spectrometer.

and the wire position of the passing charged particle is determined.

The M1 spectrometer had 3 chambers with $3\,mm$ wire spacing and about $2 \times 2\,m^2$ of active area. Each chamber had 4 sensitive planes in 4 projections (x, y, u and v) as it can be seen in Figure 4.9.

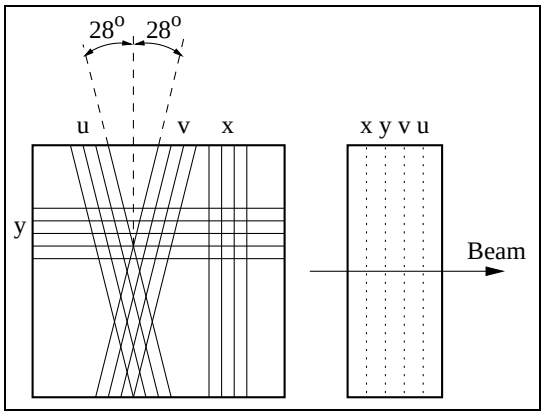

Figure 4.9: M1 chamber.

These chambers had more than 90% hit detection efficiency and a spatial resolution of about $0.9\,mm$.

4.2.3.2 Drift Chambers

A drift chamber uses the fact that if the drift velocity of the ionized particles is held constant and known, and the time of passing of the particle is also known, then a finer position resolution of the particle can be determined.

In M1, there were also 2 drift chambers, each one with 2 sensitive planes

measuring hits in x projection. They were about 80% efficient and had about $0.7\,mm$ resolution.

4.2.3.3 Large Area Silicon Detectors (LASD)

There were 3 stations of LASD located at the end plates of M1 and M2 magnets as it is shown in Figure 4.10.

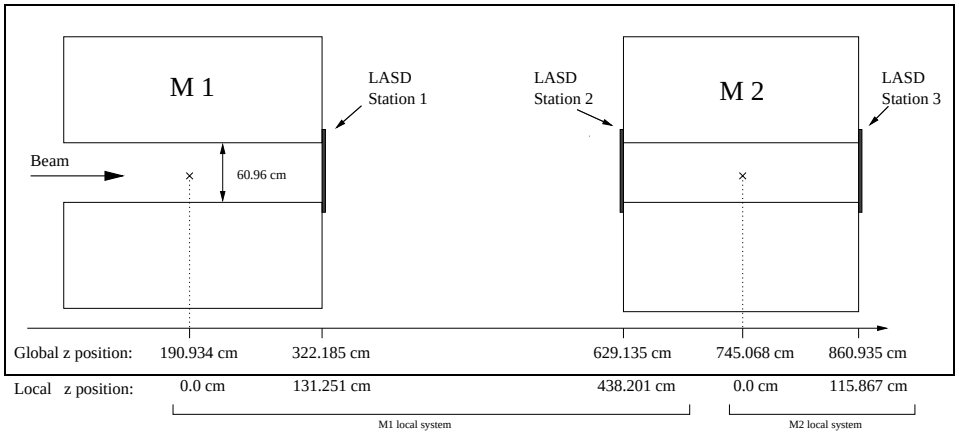

Figure 4.10: 3 LASD stations.

Each station had 2 planes of double-sided silicon strip detectors with $50\,\mu m$ strip pitch and $3.2 \times 2.6\,cm^2$ of sensitive area. It also contained 2 other planes, these were single-sided silicon strip detectors with $50\,\mu m$ strip pitch and $3.2 \times 3.2\,cm^2$ of sensitive area. The double-sided SSD measured hits in x and y projections while the single-sided did it in u and v projections. Detectors had $95 - 99\%$ hit detection efficiency and a spatial resolution of about $15\,\mu m$.

4.2.3.4 Lead Glass Electromagnetic Calorimeters

High energy electrons lose their energy almost exclusively by bremsstrahlung and photons lose it by electron-positron pair production. The electromagnetic shower is produced in the lead glass of the calorimeter and the integrated energy can be used to estimate the energy of the incident particle.

In the experiment, 3 electromagnetic calorimeters were positioned at the end of M1, M2 and M3 spectrometers. Each calorimeter had a hole in the middle to let beam and high energy particles go through them. The first 2 calorimeters were composed of blocks of 2 different sizes with the smaller ones ($4.25 \times 4.25 \times 34\,cm^3$) covering the inside of the detector and the bigger ones ($8.5 \times 8.5 \times 34\,cm^3$) covering the outside of the detector. The third calorimeter was built out of the same size blocks ($3.8 \times 3.8 \times 45\,cm^3$) [42]. Lead glass has density of $4.1\,g/cm^3$ and radiation length equal to $2.5\,cm$.

4.2.4 M2 Spectrometer

The M2 spectrometer consisted of the M2 magnet and the detectors between the M2 and M3 magnets.

Figure 4.11 shows an schematic view of this spectrometer.

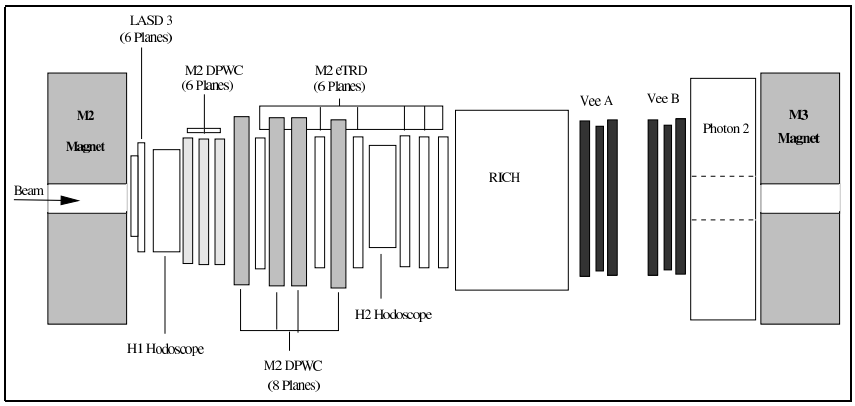

Figure 4.11: Schematic view of the M2 spectrometer.

4.2.4.1 Multiwire Proportional Chambers (MWPC)

The M2 spectrometer had 7 chambers with $2\,mm$ wire spacing. The 3 upstream chambers had a $60 \times 60\,cm^2$ aperture. The 4 downstream chambers had a $60 \times 100\,cm^2$ aperture as it is shown in Figure 4.12.

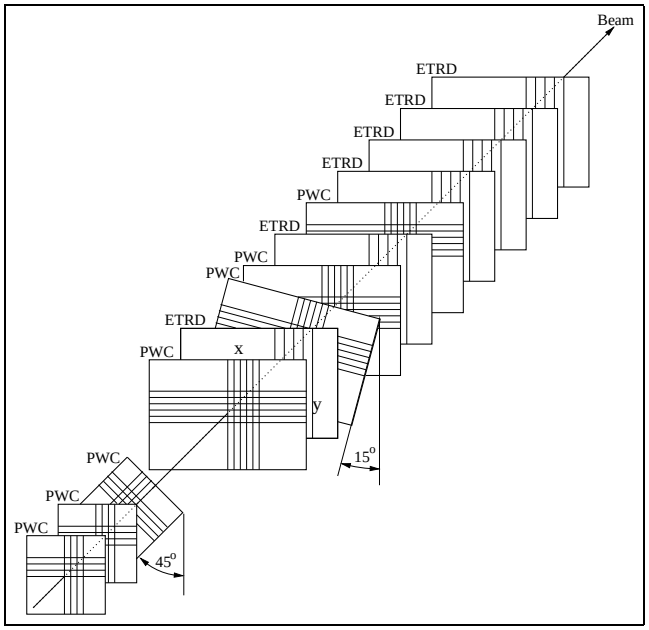

Figure 4.12: M2 chamber.

Each chamber had 2 sensitive planes in 2 orthogonal projections. These chambers had more than 95% hit detection efficiency with a spatial resolution of $0.6\,mm$.

4.2.4.2 Electron Transition Radiation Detector (ETRD)

To mainly identify electrons there were 6 Electron TRD modules. The transition radiation was generated in 200 polypropylene foils, $17\,\mu m$ thick, positioned in front of each chamber. The radiation was detected by $103 \times 63\,cm^2$ MWPC with $4\,mm$ wire spacing and filled with a mixture of Xe and methane [43, 44].

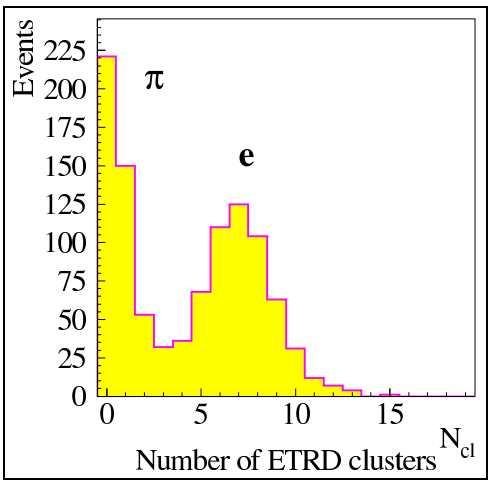

Figure 4.13: e/π separation in ETRD.

4.2.4.3 Ring Imaging Cherenkov Counter (RICH)

Cherenkov radiation is emitted when a charged particle traverses a medium with refractive index n with a velocity v exceeding the velocity of light c/n in that medium. Cherenkov radiation is emitted because the charged particle polarizes the atoms along its track so that they become electric dipoles. The time variation of the dipole leads to the emission of electromagnetic radiation. The opening angle of the resulting cone is related to the particle's velocity by the equation:

$$\cos\beta = \frac{1}{n\sqrt{1-\frac{1}{\gamma^2}}}$$

The major particle identification device in the SELEX apparatus was the RICH detector, where particles passed through $10\,m$ long vessel filled with Ne gas emitting Cherenkov light along the way.

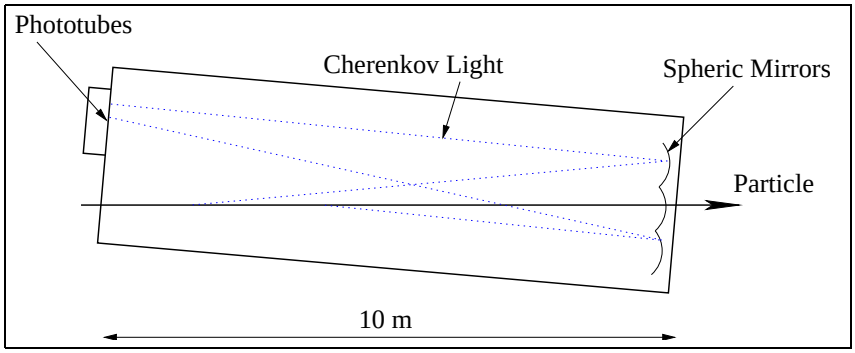

Figure 4.14: RICH detector.

This light was reflected on spherical mirrors with $20\,m$ curvature and focused on a 2848 phototube array. The ring radius grows with the velocity of the particle. A particle with $\beta = 1$ produces a ring radius of $11.5\,cm$ with 13.6 hits on the ring, each one was measured with a spatial resolution of $5.5\,mm$ and the ring radius was measured with $\sigma = 1.8\,mm$ resolution in multi-track events, which allowed π/K separation up to 165 GeV/c [45, 46, 47].

The fact that it is not possible to distinguish between a kaon and a pion for particles with momentum above 165 GeV/c, leads to a mis-identification of the particles that produces background in the reconstructions performed. This problem is expected and it needs to be taken into account in the post-recon analysis (see section 5.3.1.1).

4.2.4.4 Vector Drift Chambers (VDC)

There were 9 VDC joined in 3 stations VeeA, VeeB (located in M2 spectrometer) and VeeC (located in M3 spectrometer). The stations had $116 \times 116\,cm^2$ aperture, with about 90% efficiency and $100\,\mu m$ resolution. The stations measured tracks in x, y, u or x, y, v projections. Each chamber had 8 sensitive planes in the fine cells of the center region of the chamber and 6 sensitive planes in the coarse cells, which allowed to measure the track vector and not just its position [48].

4.2.5 M3 Spectrometer

A third spectrometer was expected to measure decay products for long-ranged hyperons, unfortunately it did not work. M3 magnet had a field strength of $1.3\,T$. It consisted of three MWPCs, two of them with a size of $64 \times 64\,cm^2$ and the other one $115 \times 89\,cm^2$. Finally the third VDC, the third photon detector and the neutron calorimeter.

4.2.6 Magnets

The magnetic fields for each magnet were measured with a flip-coil apparatus that determined B_x, B_y and B_z components on a 1-inch grid with a precision of 0.1%. The main parameters of the magnets are summarized in Table 4.2.

magnet	z (center pos.) [cm]	B [T]	p_T-kick	Longitude [cm]	Width [cm]
M1	190	1.35	0.7371	262.50	50.00
M2	745	1.54	0.8285	231.73	85.09
M3	4240	1.30	0.4170	231.73	85.09

Table 4.2: Magnets information.

4.3 Trigger

SELEX used an open trigger requiring an interaction in the targets, besides the common trigger used in most charm experiments that just selects events with interactions.

The trigger system used a set of scintillation counters (S1-S4), veto counters (V1-V4), interaction counters (IC) and 2 hodoscopes (H1, H2). An schematic view of these elements can be seen in Figure 4.15.

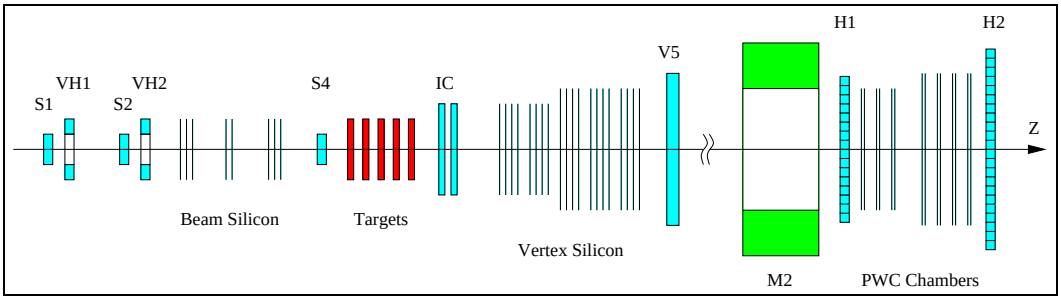

Figure 4.15: SELEX trigger.

The IC produced an output signal with the amplitude proportional to the numbers of particles that crossed them, it consisted of two thin counters (separated), and the amplitude of the signal in each counter was measured.

The T0 trigger defined a beam particle as the coincidence of S1, S2 and S4 counters with no hits in veto counters VH1 and VH2. Trigger T1 required an interaction in the targets, a signal from the BTRD and 2 hits in the positive region of the hodoscope H1. An interaction in the targets was defined as the

signal from the IC larger than the signal from 3 minimum ionizing particles. In early runs the signal from the BTRD was not used, so that interactions from both π^- and Σ^- were accepted. In later runs the BTRD was used to trigger only on baryons (Σ^- and protons). In addition to the charm trigger, there were other triggers like special calibration ones to check apparatus performance [49, 50].

4.4 Data Acquisition

If an event passed the trigger, it was digitized, packed and read out into dual-ported memories. There were about 100,000 events read out during a 20-second beam spill, followed by 40 seconds of no beam. They were processed by a 22-processor SGI Challenge computer by the SELEX Online Filter code (it passed about 1 event in 8). These events were written out to disk that later were sampled by the monitoring program to check the apparatus performance during data-taking. The size of one event was about 6.5KB; the events from disk were combined in 200 MB files which were written out to tapes and stored for further processing.

4.5 Filter

One of the innovations of the SELEX experiment was the online filter. This was a program which processed data to reject events that did not have evidence for a secondary vertex.

First the filter program reconstructed tracks in the downstream (M2) PWC system. Only tracks with momentum greater than 15 GeV/c could make it through the magnets to reach these chambers. After that, a beam track was reconstructed. The tracks from the downstream PWC were extrapolated back to the vertex silicon, using beam track information as a guidance to the approximate primary vertex location, then a special fast reconstruction program searched for track segments in the vertex silicon, using downstream track extrapolations as an initial starting parameters and looking for hits in searching windows around them. The size of the searching windows were calculated based on the resolutions of the detectors and the effects of multiple scattering. Because only relatively large momentum tracks (> 15 GeV/c) were extrapolated back to the vertex silicon, multiple scattering errors were kept under control. Finally, the beam track and tracks reconstructed in the vertex silicon and the downstream chambers were fit to a primary vertex. If the fit had an acceptable χ^2 and used all tracks, the event was rejected as non-charm. On the other hand, if one or more tracks did not point to the common vertex, the event was kept.

The online filter decreased the background by a factor of 8 and was about

50 % efficient for a typical charm signal; so the experiment was benefited by decreasing the time to process the tapes by a factor of 8 at the cost of modest sacrifice in charm signal.

4.6 Data Taking

SELEX started to take data in July 1996. First runs were taken to verify the trigger, to check apparatus, to establish chamber efficiencies, to calibrate photon detectors, to optimize online filter and to perform similar tasks dedicated to establish a high quality of the data written to tape. Data written to tape since February 1997 was used in the final charm analysis.

Group	Run numbers	Files
b1	5587-6312	p2b01
b2	6313-7012	p2b02
c1	7018-7381	p2c01
d1	7382-8079	p2d01
e1	8087-8673	p2e01
f1	8683-9046	p2f01
g1	9057-9411	p2g01
h1	9502-9789	p2h01
x1	9806-10243	p2x01
z1	10244-10858	p2z02
p1	10876-11313	p2p01

Table 4.3: Groups and run numbers for data taking.

The first part of these data did not use the signal from the Beam TRD in the trigger, so interactions from both π^- and Σ^- were written to tape (pb and pc groups). The second part used the Beam TRD response in the T1 trigger and mostly Σ^- interactions were written to tape (pd, pe, pf, pg, ph, px and pz groups). In the third part the polarity of the hyperon beam was reversed, which provided beam composed of mostly protons (pp group) as it can be seen in Figure 4.16 and in Table 4.3 that summarize the SELEX data sets. The 15.2 billion interactions were reduced to a factor of ~ 2 by the trigger and a factor of ~ 8 by the filter, so around 1 billion interactions were stored. The experiment took data for almost year and a half, and the interactions stored were divided in three types of files: charm (using trigger at different levels and filter), calib (calibration of detectors turning off the magnetic fields) and prim (used mainly for Primakoff studies).

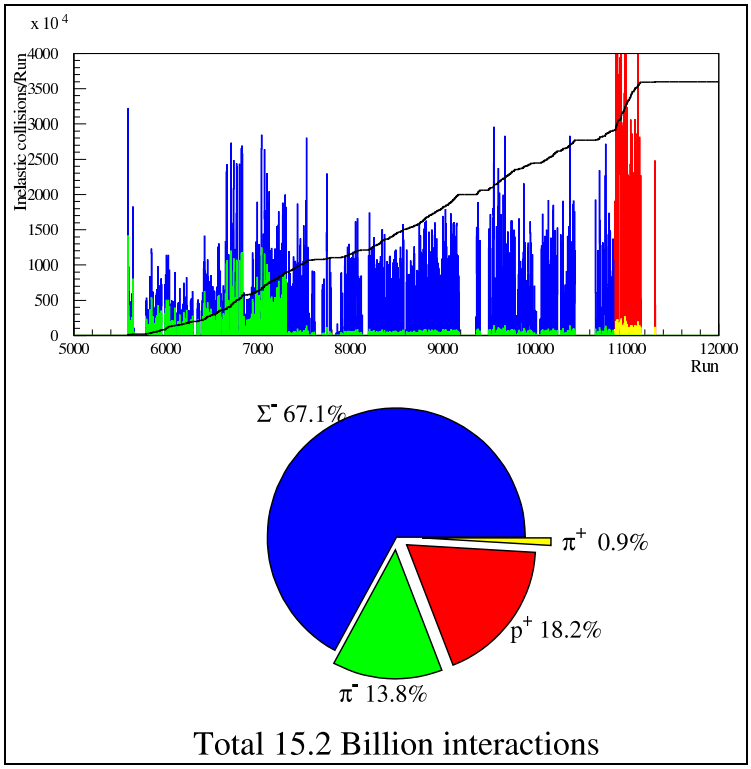

Figure 4.16: SELEX Data Sets.

4.6.1 Detector Performance

During the running time of the experiment special alignments runs were taken every day to verify the geometrical position of silicon detectors and downstream PWC chambers. The detector performance and the Online Filter were constantly monitored; there were also many improvements in the apparatus and optimization in the codes. Noise levels were reduced, trigger and data acquisition were modified to read out events faster. By the last half of data-taking the yield of reconstructed charm events per billion interactions was three times higher than at the beginning of data taking.

4.7 SOAP: Selex Off-line Analysis Physics

In order to analyze the huge amount of information SELEX designed a complete code called SOAP (Selex Off-line Analysis Physics) mainly written in Fortran. SOAP is basically divided in 5 parts. A description of the main 5 parts is detailed:

- UNPACK: Loading of raw data into common blocks.
  For each detector, the hardware created a list of which wire, silicon

strip or phototube had a signal. The software converted the list of hits to positions in the local coordinate system of the detector.

- TRACKING: The goal of the charge particle tracking analysis is to correctly find and measure the parameters of all the charged tracks within the acceptance of the SELEX apparatus. A charged track is completely described by a set of 8 parameters: the 3 coordinates in space of the point where it first was observed, the z coordinate where it was last observed, its vector 3 momentum and its particle ID.
  Charged particle tracking is a four step process:

  1. Straight line track segments are found in each spectrometer: a spectrometer track segment is, by definition, a list of the coordinates in each of the detectors of that spectrometer which are believed to belong to one charged track (some of these coordinates may be missing, indicating that the particular track has no coordinate assigned in a given detector; this can be due to an inefficiency of the detector, a software inefficiency of the algorithm in assigning the hit in that detector correctly to the track or the simple fact that the particle actually missed that detector, either because it was outside the aperture or because it was born after that detector). The pattern which defines a track segment is that all coordinates fit a straight line in space. The algorithm consist of a basic straight line search based upon two assumptions: tracks will be found in 3 dimensional space and each coordinate measurement (hit) will be assigned to at most one track segment. A straight line in space is described by five space variables (two slopes, two intercepts and a fixed point in z)

  2. Segments are linked across spectrometers to form candidate tracks: the basic idea for the algorithm is analogous to the track segment algorithm. All track segments in pairs of spectrometers are fit to the hypothesis that they form a continuous track with a kink (called p_T-*kick*) in the equivalent magnet bend plane (see Table 4.2). Track segment pairs which make an acceptable chi-squared to this hypothesis are assigned as part of a track. This is also programmed at a high level.

  3. Individual hits in each plane which make up a track are momentum fit: the track momentum fitting algorithm matches the individual coordinates which make up the segments assigned to a track to the function describing the trajectory of a particle through the magnets and chambers of the spectrometers. The fit parameters are the slopes and intercepts of the track at the origin of the chosen coordinate system and the curvature of the track ($q/\vec{p}$).

Each chamber coordinate is treated as an independent measurement and the error assigned is the measurement error of the plane ($w/\sqrt{12}$, where w is the wire spacing). Multiple Coulomb scattering is neglected; besides magnets are treated in the bend plane and small angle approximations are made.
Track fits are 8 parameter objects, in addition to the 5 track parameters described above, the global z coordinate of the first and last measurement on a track is saved along with the spectrometer whose origin is used for the track. The origin of a track is chosen as the origin of the spectrometer of the most upstream segment of that track.

4. Fit tracks are extrapolated to the particle ID (IDentification) detectors (BTRD, RICH) where the particle ID is determined based upon the tracks parameters and the PID (Particle IDentification) detector responses [51].

- PARTID: Particle identification uses information from BTRD, RICH and ETRD. The major device of identification for charged particles coming from a decay is the RICH. The RICH software produces likelihoods that the track is a certain particle, normalized to the hypothesis with the greatest likelihood; its information from detectors outside the RICH determines the momentum and the position of the ring center. Particles with different masses have different radii, and the measured radius is compared to the predictions.
A likelihood function was formed to describe how close the predicted radius matched the measured radius [46]. The likelihood was then normalized to that of the most likely hypothesis, which was assigned 1. The hypothesis of interest are for the proton, kaon, pion and background. This procedure gives the relative likelihood that a given track is of a particular kind. As an example, a track is identified as a pion when the likelihood is greater than 0.1 (any track with $\mathcal{L} > 0.1$ can be a pion) and a proton or a kaon are required when the likelihood is equal or greater than the likelihood assigned to a pion. In Figure 4.17 two pions are identified in the RICH as an example of the likelihood hypothesis.

  A file called *recpid.ocs* carries the information about the particle identification with the likelihood required for the definition of that particle. This file is shown below for some particles, where several cuts are made according to the type of particle required (this file is used by the RECON package). The information that appears in this file is: abbreviated name of the particle (see RECON for description), the system used for its identification (RICH, ETRD, none), and cuts in the likelihood, the minimum and maximum momentum, the minimum

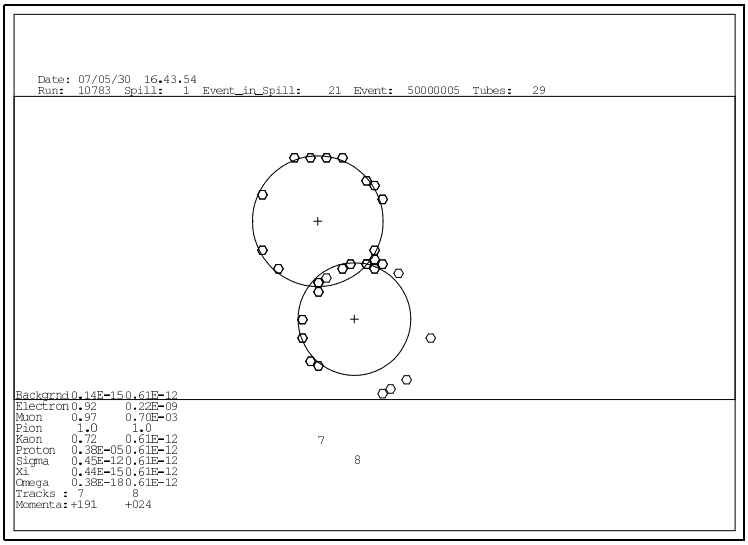

Figure 4.17: Identification of two pions in the RICH.

and maximum miss distance, the minimum and maximum transverse momentum of the particle, as well as the spectrometer and logic combinations for the particles to be identified. These are soft cuts applied by SOAP necessary to reduce the output signal and the running time which will allow to apply harder cuts in the post-recon analysis (see Chapter 5).

```
#recpid 0 0 fill anal v04.12 21-Nov-1997 23:00 psc !Particle id
!
name system cut  pmin pmax mdmin mdmax ptmin ptmax spectro logic
 e   etrd  e>0.5    0.   0.  0.   0.   0.    0.    m2     none
 i   rich  i<0.1    0.   0.  0.   0.   0.    0.    any    not
 k   rich  k/i>=1   0.   0.  0.   0.   0.    0.    m2     none
 p   rich  p/i>=1   0.   0.  0.   0.   0.    0.    m2     none
 s   none  none    40. 600.  0.   0.   0.    0.   vxm1nm2 none
 x   none  none    40. 600.  0.   0.   0.    0.   vxm1nm2 none
 o   none  none   100. 600.  0.   0.   0.    0.   vxm1nm2 none
*end
```

- VERTEX: A space point where two or more tracks intersect is called a vertex. The vertex package finds the primary interaction vertex and any secondary vertices. The primary vertex includes the beam track, the target foil where the beam particle interacted and the charged tracks that were produced from its initial interaction. The secondary vertices represent places where short-lived particles decay into charged tracks. The code used to find vertices in this analysis was vtx2.
  vtx2 starts by generating a list of tracks that are believed to start

near the target foils. In general, this consists of tracks with a vertex segment and another downstream segment to provide a momentum estimate, here the beam track is included to improve primary vertex position resolution. All these tracks are fit to a single (primary) vertex. For events that fail this single vertex selection, all combinations of 2, 3, 4 and 5 tracks in the track list are checked to see if they intersect at a common (secondary) vertex. A nonlinear fit to find the best three dimensional space point for this vertex is made. The quality of the vertex is measured by χ^2, based on how far the tracks in the fit missed the space point, weighted by the track parameters uncertainties. If this secondary vertex is of reasonable quality, a search is made for a primary vertex. The remaining tracks not involved in the secondary vertex fit are checked to see if a subset is found that would intersect with the beam track at one of the targets. A fit is made to find the primary vertex space point. Tracks that miss the primary vertex are removed and the vertex is re-fit, also based on χ^2. If the primary vertex is of reasonable quality, then the secondary-primary vertices pair is added to the list of possible vertices, and the next permutation is tried [52, 53].

- RECON: A reconstruction is a recipe for combining tracks in the experiment to form a particle candidate. Masses are assigned to the tracks, so the relativistic mass and momentum can be computed for the combination of tracks (random combinations of tracks produce background in the mass plots). For real particles, the mass of the reconstruction should, within a narrow range, depend on the detector resolution and the mass width of the particle (in the invariant mass distribution for the reconstruction this shows up as an excess of events, a peak, above the background).
  A high level language is used to reconstruct particle hypothesis using vertex, pid (Particle IDentification) and track information. The parameters of a reconstructed particle hypothesis are vertex location and separation from the primary vertex (L) and error (σ), four momentum (p_μ), mass (m) and error, track pid (Particle IDentification of the track, see explanation below) and charge (q).
  The recon package executes the high level program stored in an OCS (Open Constant System) table (a filed called *recdf.ocs*). Each line of this table causes the recon package to search in the current event for a reconstructed particle hypothesis that matches the described criteria. Several different types of searches are possible. An example of a *recdf.ocs* file is shown below (actually the one used for this analysis), in this file some soft cuts may be done in order to reduce the running time and the size of the output files (see the section Vtuples):

```
#recdf 0 0 fill anal v04.12 Jan 19 1998 14:31 psc
id name from pr q pid ls_min ls_max mass_min mass_max out
!
400 lc+_pkpi    v2 3 +1 p+k-i+   6.  800. 2.100 2.600 $2
520 xc+_xi2pi   v2 3 +1 x-i+i+   6.  800. 2.100 2.600 $2
522 xc+_s+k-pi  v2 3 +1 s+k-i+   6.  800. 2.100 2.600 $2
440 lc+_s+2pi   v2 3 +1 s+i+i-   6.  800. 2.100 2.600 $2
442 lc+_s-2pi   v2 3 +1 s-i+i+   6.  800. 2.100 2.600 $2
!
*end
```

The criteria for each line is:

id	unique number for the reconstruction
name	reconstruction name
from	search type
pr	reconstruction prong count
q	reconstruction charge
pid	particle id requirements
ls_min/max	L/σ range required
mass_min/max	mass window required
bit	output status bits

Table 4.4: Criteria for *recdf.ocs* table.

For the particle id requirements it is necessary to specify a 2 or 3 character code:

- Particle: e(electron), m(muon), i(pion), k(kaon), p(proton), s(sigma), x(cascade), o(omega) or g(photon).
- Numbers from 1 through 9 to specify different pid requirement (coming from *recpid.ocs*).
- Particle charge: +(positive), –(negative) or 0(neutral).

The reconstruction package (search type) used in the analysis is called "v2". This package is based on vertex package vtx2 that finds vertices. It builds reconstructions from the list of secondary vertices applying the specified cuts on prong count, charge, L/σ and mass required in the *recdf.ocs* file.
The reconstruction package called "kink by disappearance" was used to find hyperons ($\Sigma^{\pm}$ and Ξ^{-}). The most favored decay channels in hyperons are in two particles; one of them is neutral and the other one is charged. This kind of topology is known as a "kink" because the

neutral particle does not leave a trace in the detectors. This package selects a hyperon candidate when there is a track with segments in the vertex and M1 spectrometers but not in the M2 spectrometer. The missing segment of the track in the M2 spectrometer means that the hyperon has decayed.
It is worthy to mention that there is a package that reconstructs the hyperons (kink_ds), but at this time some fixes are needed for that package. It is mentioned in this work because it led to the discovery of the new Ξ_c^+ decay modes but it is not used in the branching ratios calculations. The main problem appears when the efficiency is calculated, this is done with a Monte Carlo simulation as it will be explained below. The problem is that when one kink (hyperon) is simulated, the package reconstructs 2, 3, 4 or sometimes even 5 hyperon candidates. The primary vertex for each reconstruction is the same, but they have different decay points. This multiplicity in the number of hyperon candidates reconstructed clearly affects the determination of the efficiency. A brief description is given on Appendix A for those interested in the package usage.

In order to reduce the running time and the size of the output files (see the section Vtuples) as well as to use some specific parts of the packages described above, there exists a file called *soap.cmd*. A typical file used during the analysis in this work is shown below.

The packages described above (unpack, tracking, partid, vertex and recon) can independently be turned on/off with the command *"execute"* in the *soap.cmd* file. For each package there is a set of cuts and switches (for example, in the vertex package it is possible to cut in the χ^2 from the fit of the primary vertex with the command: *"set cut vertex vtx3 5.0"*, this means that when running soap, only primary vertices with a χ^2 below 5 are written to the output files). It is also indicated the data files to run and the number of events to be analyzed.

```
!  Command file pass2.cmd
!  CVS/RCS keywords
!  $Id: pass2.cmd,v 1.4 2000/12/04 21:34:27 syjun Exp $
!  $Author: syjun $  command file used for passII production
!
 noexec   filter

 execute  unpack
  set  on  unpack    adc cros rmh svx ! hist

 execute  tracking
 set  on  tracking  segment link fit0 silmatch silm3d guided fit hist
 set  on  tracking  vx_radial m1_guide vx_lasd tr_seg2 ! tr_subset tr_user
```

```
!set  on  tracking  tr_addlasd tr_crack ! tr_kink ! sil_vee Dauwe m1kink
 set  on  tracking  m1_share            ! m1pwc s-y hit share
 set  cut tracking  lasd_wid     2.   ! inflate LASD res by factor 2
 set  cut tracking  max_bmsi   250.
 set  cut tracking  max_vxsi  1000.
 set  cut tracking  max_pwc    260.
 set  cut tracking  max_svx   1000.
 set  cut tracking  segment       0 ! all spectrometers on in track_segment
 set  cut tracking  ptm1     0.7371 ! use fixed spectrometer pt_kicks
 set  cut tracking  ptm2     0.8285 ! use fixed spectrometer pt_kicks
 set  cut tracking  trajectory kink ! parabolic trajectory as a default
 prog     tracking  pass2.tseg
 ocs  class main anal

 exec     photon
 set  on  photon    full m1_pht m2_pht m3_pht
 set  cut photon    min_count  4.        ! pass11 5.
 set  cut photon    min_energy 1.5       ! pass11 2.

 exec     partid
 set  on  partid rich btr etr etr_track  ! etr_hist

 execute  user
 set  on  user   hist
 set  cut user   report        1000

 exec     vertex
 set on vertex bmvtx2
 set  on  vertex vtx2  err2  secint  prim  sec
 set  cut vertex prong           4
 set  cut vertex vtxd          4.0
 set  cut vertex vtx2          9.0
 set  cut vertex vtx3          5.0
 set  off vertex secint

 exec     recon
 set  on  recon  hist  vtuple vtup1 vtup2 ! vtup3 ! ntuple
 set  cut recon  tgt_rec       0.05
 set  cut recon  pscale        1.0000  ! pass11_11_v1
 set  cut recon  cand_csec     5.0
 set  cut recon  cand_cpri     5.0

 disk in  reset
 disk in infile
 ana 0
 exit
```

4.8 Data Processing

Raw data were processed using SOAP and it was used a basic algorithm of reconstruction with soft cuts in order to reduce the size of the data. This raw data running has been done two times:

- pass1: A list with reconstructions was elaborated. The reconstructions were divided in 5 groups:

  1. Charmed mesons
  2. Charmed baryons and partial states
  3. Semileptonic decays
  4. Strange states
  5. Exotic states

  If there were found 2, 3, 4 or even 5 reconstructions from different groups, the event was written to each group, so, it was be stored up to 5 times.
  Some output information was written to ftuples files (tuples with a fixed size where 82 variables can be stored) for every reconstruction. Ftuples were designed to store important information of the reconstructions (invariant mass, coordinates of the vertices, momentum, etc.) in order to be used later, in a post-recon analysis.

- pass2: Some bugs were fixed, the alignment was optimized, the FORTRAN code (software) was increased (photon, V0, vee, kink, etc.) and new reconstructions were added to the list. The reconstructions were also divided in 5 groups:

  1. Charmed mesons
  2. Charmed baryons and partial states
  3. V0 states
  4. Strange states
  5. Downstream charm

  If at least one reconstruction from the list was found, the event was written to a file called out1 (just once, no matter what group it belonged). If none reconstruction from the list was found then the event was written to a file called out2. This was a significant difference between pass2 and pass1 where the events could be stored more than once.
  Some output information of the reconstructions was written to vtuples files (see below) for the post-recon analysis (see Chapter 5).

4.8.1 Vtuples

Vtuples are variable size tuples created in pass2 (using an object oriented approach) to handle more information. Vtuples consist of a header and a number of blocks where there is usually one beam track block, one primary vertex block and a different number of other blocks. Presence and number of other blocks depend on the type of reconstruction the vtuple is built for. There could be some secondary vertices, some secondary tracks, some vee-kink downstream blocks, some V0 kink blocks, photon calorimeter blocks and/or user blocks. Every mentioned block represents a physical object and can be treated as it is in the corresponding software.

Vtuples, also known as vtups, are produced when "vtuple" is switched on in recon package (*"set on recon vtuple vtup1"*, see *soap.cmd* file). The maximum number allowed is 5, due to the number of groups designed in pass1 and kept for pass2, but with different characteristics.

Table 4.5 shows the number of variables in each vtuple block.

Block name	Length (1 word = 4 bytes)
Header; recon info	14
Prim. vertex	9
Beam track	8
Sec. vertex	16
Vertex track	10
Kinks; recon_sv	14
Vees-kinks	15
Gamma	8
User	8

Table 4.5: Vtuples structure.

The general structure of the vtuples, as well as the files used to read them are described in Appendix B. This appendix is included because the FORTRAN code to read vtuples was done as one of the first tasks of this investigation and up to now several students have used it in their analysis (for example, M. A. Olivo [54], A. Flores [55], J. L. Sánchez [56], G. Hinojosa [57]).

4.9 Simulation

To check the SELEX apparatus efficiency and to understand the variables behavior involved in the analysis, a simulation of events in the experiment is needed, which is carried out with a Monte Carlo method.

The simulation is divided in two main features: firstly the events are generated, secondly they are embedded into the SELEX routines. This is an important issue in the analysis, so, this method is explained in detail.

4.9.1 Embedded Data Generator (EDG)

EDG is the event generator for SELEX that allows to obtain a sample of particles [58]. Its name is QQ and it was designed by the CLEO collaboration [59].

The production of the particle is simulated with a phenomenological function as follows:

$$\frac{d\sigma}{dx_F dp_T^2} = A \cdot (1 - x_F)^n \cdot e^{-bp_T^2} \tag{4.1}$$

This equation was obtained by certain quark counting rules and phase space arguments [60].

The file needed to generate events (*name.dec*) has two parts:

- Production of the particle
- Decay of the particle

Decays are specified in a file called "decay.dec" (standard decay file that is similar to a decay dictionary). The various properties of particles production are defined using the commands shown in Table 4.6 along with an example (production of Ξ_c^+):

Property	Name	ID	Stable ID	mass	charge	spin	$c \cdot \tau$
Example	CSU0	125	-1	2.467900	1.0	0.5	0.000106

Table 4.6: Particle properties in *name.dec*.

To define the decay properties of the particle, the branching ratio and the daughter particles of the decay are needed.

An example of the *name.dec* file used to generate Ξ_c^+ in the channel $\Xi^-\pi^+\pi^+$ is shown:

```
PARTICLE  CSU0    125   -1  2.467900  1.0  0.5   0.000106
PDG       CSU0   4232
;
DECAY  CSU0
CHANNEL  0 1.0000  XI-   PI+   PI+
ENDDECAY
```

```
;
DECAY XI-
CHANNEL  0 1.0000  LAM   PI-
ENDDECAY
;
DECAY LAM
CHANNEL  0 1.000   P+   PI-
ENDDECAY
```

In this example, the decay properties include the Ξ^- (in the $\Lambda\pi^-$ channel) and the Λ (in the $p\pi^-$ channel). One important property is the branching ratio, which should be included in the *name.dec* file (CHANNEL 0 **1.0000** XI- PI+ PI+). The reason to use 1.0 in the example file is because in the efficiency determination only one channel at a time is measured, so the whole sample of events need to be embedded (see Event Embedding) and not just a fraction. The efficiency needs to be corrected by the branching ratio in case the real value is used.

Another important point to mention is that before running the EDG generator, some other parameters need to be specified, such as: the type of beam used to generate the particles (ID of the particle and momentum), the x_F, actually the "n" in Equation 4.1, the p_T distribution desired to be followed by the mother particle and of course the number of particles required for the simulation.

The file generated (*name.emb*) contains information of the mother particle and all of the charged daughter particles. The parameters in the file for each particle are:

- Point of generation: 3 coordinates (x, y and z)
- Directional cosines (α, β and γ)
- Momentum of the particle
- Mass of the particle

The primary vertex is in (0, 0, 0,).

4.9.2 Event Embedding

Event embedding is a tool incorporated into SOAP. It simulates generated events in the SELEX apparatus. The generated events can be embedded with or without underlying events from data.

Embedding is enabled by running SOAP with appropriate switches turned on in the *soap.cmd* file. The package starts by reading in an event from the

embed file, *name.emb*; then, the parent track is translated and rotated so that the beam and the interaction point which produces this track are coincident with the beam and primary vertex from data. A track which is a daughter of another track is transformed respective to its parent in the same way. When embedding is performed without underlying events from data the primary vertex is determined by embedding two extra tracks, so the vertex package works.

When the embedding package is turned on, the event from data is first reconstructed to get the primary vertex and the beam direction (unless unpacking is turned off). Afterwards, the same event from data, together with the embedded tracks is reconstructed again.

The embedding package turned on in the *soap.cmd* file used for the simulation is shown below:

```
execute mcmatch
set on mcmatch embed smear match
disk embed name.emb
```

First of all the Monte Carlo package is turned on, then some switches are turned on: embed (turns on embedding), smear (Multiple Coulomb scattering may be included) and finally, the *name.emb* file is read [61].

It is important to know that the coordinate of the embedded hit for each plane in the apparatus is calculated using a standard SOAP trajectory function (geometrical acceptance is taken into account based on the OCS (Open Constant System) constants for each plane and magnets). The embedded hit is assigned to the closest strip/wire/cell based on the geometrical parameters of the plane and added to a common block for that plane.

The reconstruction of generated events once they are embedded in the SELEX apparatus is performed in the same way as it is in the reconstruction of events from data.

Summary

Summing up, the SELEX experiment took data during 1996 and 1997 and stored around 1 billion interactions. The complex code used for data analysis which is a high language code, built by the SELEX collaboration allowed to find two new Ξ_c^+ decay modes.

Furthermore, some problems such as memory overwritten were found and solved; besides new features such as extra information handled by the vtuples files were added while performing this analysis.

The next chapter describes the methodology of the post-recon data analysis carried out over the events gotten from running SOAP.

Chapter 5

Methodology of Data Analysis

SELEX was the first experiment to observe a Cabibbo-suppressed decay mode of the Ξ_c^+ particle [7], so one of the first tasks was to measure the branching ratio of this Cabibbo-suppressed mode to corroborate that the methodology applied in this analysis was working (a control mode), moreover, two Λ_c^+ decay modes reported by other collaborations are also used as control modes. The reason to use Λ_c^+ decay modes is because they have the same decay channels than Ξ_c^+ (actually every Cabibbo-favored decay in Λ_c^+ is also a Cabibbo-suppressed decay in Ξ_c^+).

An absolute branching fraction has been measured just for a very few particles, most of the times a branching fraction relative to a very well known mode is measured. For the case of the Ξ_c^+ particle the reference mode used is the $\Xi^-\pi^+\pi^+$ channel as it was mentioned before.

The methodology applied to the data analysis described in this chapter starts with a description of how the Ξ_c^+ candidates are obtained and how the branching ratio is measured, including the determination of the number of events and the efficiency calculation.

5.1 Data Description

After the data processing in pass2 is performed (it is worth remembering that some soft cuts were applied in SOAP while doing pass2) there is information in the pass2-vtuples for each of the reconstructions from the list elaborated, which was described in Section 4.8. Fortunately, the interesting reconstructions for this work are in that list. For the post-recon analysis two possible options can be selected : the first one is to use these vtuples and perform the post-recon analysis; the second one is to extract the run and event numbers for the reconstructions from these vtuples (actually, those with an invariant mass[3] close to the interesting particle), then, re-run SOAP

[3]The invariant mass is a Lorentz invariant quantity, in this work is calculated at the rest frame of the particle. See the variables involved in the post-recon analysis.

over the data (actually just over the out1 files) and select all the events that match the run and event numbers extracted before (this is called a "strip file"), finally a re-running over SOAP can be done every time is needed to produce new vtuples in order to perform the post-recon analysis with them.

The second option could be interpreted as a waste of time and disk space but it has the advantage that the whole information for each event is available (in case checks are needed, fixes are done to the code, etc.); moreover the size of these strip files is considerably small because specific reconstructions (interesting for the work) are stored and a re-running over SOAP would be a fast task; besides the first option has the disadvantage that reduced information for the reconstruction is stored in the pass2-vtuples, and in case that extra information is needed nothing can be done to recover it.

It can be inferred that the second option is better, so, strip files with the specific reconstructions, useful for this work, were produced.

The Ξ_c^+ reconstructions under study are:

- $\Sigma^+\pi^-\pi^+$ and $\Sigma^-\pi^+\pi^+$: These decay channels are the new decay modes of the Ξ_c^+ (found in this work) and their branching ratios will be reported.

- $\Xi^-\pi^+\pi^+$: This Ξ_c^+ decay is the reference mode. The branching ratio will be taken relative to this mode as it was explained in Chapter 3.

- $pK^-\pi^+$: This Ξ_c^+ decay was reported by SELEX in 2000 [7] (the first Cabibbo-suppressed observed of the Ξ_c^+) and it will be used as a control mode.

The Λ_c^+ reconstructions are:

- $\Sigma^+\pi^-\pi^+$ and $\Sigma^-\pi^+\pi^+$: These Λ_c^+ decay channels will be used as control modes because they are the same as in Ξ_c^+ and they have been reported before, as well as their branching ratios [4, 6].

- $pK^-\pi^+$: This Λ_c^+ decay is used as a reference mode for the other Λ_c^+ decays reported before, so it needs to be considered as well.

The strip files used are named:

- strip400-p2 (for $pK^-\pi^+$)

- strip-pass2.520 (for $\Xi^-\pi^+\pi^+$)

- striplckbd-p2 (for $\Sigma^+\pi^-\pi^+$ and $\Sigma^-\pi^+\pi^+$)

5.2 Variables in the post-recon analysis

Once the vtuple files are obtained from re-running SOAP, they have to be carefully analyzed, because of this, some variables need to be discussed.

Studies are performed to each of the variables described below and a set of cuts are fixed for the determination of all the branching ratios. This set of cuts is different from the ones used for the evidence of the decay modes.

5.2.1 Invariant Mass

If certain particle (such as Ξ_c^+) decays into some group of particles, the square of the four-momentum for this "mother" particle is computed as:

$$P^2 = P^\mu P_\mu = \frac{E^2}{c^2} - |\vec{p}|^2 \tag{5.1}$$

In the rest frame of the mother particle (momentum $\vec{p} = \vec{0}$), Equation 5.1 gives:

$$P^2 = \frac{E^2}{c^2} \tag{5.2}$$

and using $E = mc^2$ in Equation 5.2:

$$P^2 = m^2 c^2 \tag{5.3}$$

Finally, solving for m:

$$m = \sqrt{P^2}/c \tag{5.4}$$

The quantity m is called the *invariant mass*, since it is a Lorentz invariant. P^2 is calculated as the sum of the four-momenta for all the particles coming from the decay ("daughter" particles) as it is shown in Equation 5.5:

$$P^2 = \sum_{i=1}^{N} (m_{d_i}^2 c^2 - |\vec{p}_{d_i}|^2) \tag{5.5}$$

where $\vec{p}_d$ and m_d are the momentum and mass of a daughter particle and N is the number of daughter particles in the decay. The invariant mass is calculated using the momenta and the masses of the daughter particles because these are quantities which can be measured in the experiment.

If the invariant mass of a specific decay needs to be calculated (this variable comes in the vtuples files since it was evaluated in SOAP, but it can also be re-calculated in the post-recon analysis) then the daughter particles momenta[4] are used in the calculations, while the masses used are assigned

[4]The momenta were measured with the particles detectors and the magnetic fields, see Chapter 4

according to the likelihood given by the particle identification devices (see PARTID in Section 4.7) and on the type of reconstruction required as in the case of the "kink by disappearance" package.

It is worth to note that the type of particle (p, K, π, Ξ, ...) for the daughter particles used in the invariant mass calculation is, at certain level, "guessed", using information from its likelihood given by a detector. For example, in the $pK^-\pi^+$ reconstruction the RICH (particle identification device) gives a likelihood in order to label certain track as a proton and the corresponding proton mass is used for the invariant mass calculation; this is also done for the K^- and π^+. As another example, in the $\Xi^-\pi^+\pi^+$ reconstruction the Ξ^- is identified with the "kink by disappearance" package, so any track with segments in the vertex and M1 spectrometers but not in the M2 spectrometer (see Section 4.7) is labeled as a Ξ^- and the mass of such particle is used for the invariant mass calculation.

In this work, histograms are filled with the invariant mass of certain reconstructions:

- $\Sigma^+\pi^-\pi^+$
- $\Sigma^-\pi^+\pi^+$
- $\Xi^-\pi^+\pi^+$
- $pK^-\pi^+$

Since the particles under study (Ξ_c^+ and Λ_c^+) decay into this reconstructions the histograms filled are opened with a window around the corresponding masses ($2468\,\mathrm{MeV}/c^2$ and $2287\,\mathrm{MeV}/c^2$, respectively). After a set of specific cuts is applied to the invariant mass distributions it is expected to have an excess of events around the Ξ_c^+ and Λ_c^+ masses, meaning that sometimes the hypothesis for the mass of the daughter particles was right. Some invariant mass distributions are shown and explained in detail in this chapter and in the next one about the results obtained.

5.2.2 $\boldsymbol{\sigma = \sqrt{\sigma_p^2 + \sigma_s^2}}$

The uncertainty coming from primary and secondary vertices in z direction. It is important to have well defined vertices and this is indicated by their associated errors.

5.2.3 L / $\boldsymbol{\sigma}$

L is the separation along the z-axis between the primary vertex and the secondary vertex ($L = z_{sec} - z_{prim}$) and σ is the error associated to the measurement of both vertices ($\sqrt{\sigma_p^2 + \sigma_s^2}$). It is one of the most important

variables because the particle Ξ_c^+ has a long lifetime ($\sim 442 \times 10^{-15}\, sec$) and most of the background is short living. This is enhanced because SELEX has an excellent vertex resolution, which gives a small vertex uncertainty; besides the boost is very large, which gives a large separation between primary and secondary vertices.

5.2.4 *pvtx*

Point-back is another important variable. It is calculated when the vector resulted from the sum of the trajectories of the daughters particles is extrapolated back to the z-plane of the primary vertex. The distance from this extrapolation to the primary vertex in this plane is measured and the point-back is the square of that distance divided by its error. Trajectories from a real decay have a small pvtx value.

5.2.5 χ^2

χ^2 associated to the fit of the secondary vertex. A small value indicates a good fit performed.

5.2.6 *scut*

In this case, the trajectories of the daughters particles are extrapolated back to the z-plane of the primary vertex and the distance to this vertex is measured to each one of them. Scut is the second closest trajectory divided by its error; this quantity is required to be greater than some value because this rejects trajectories coming from the primary vertex that pass close to the secondary vertex and they are included by accident in the fit of the secondary vertex.

5.2.7 p_π

The momentum of the pions is relevant to take into account because slow pions produce a lot of background due to multiple scattering.

5.2.8 p_T

The total transverse momentum of the reconstructed daughter particles with respect to the charm particle.

5.2.9 p_{hyp}

The momentum of the hyperons is also relevant to take into account because they have to reach the M1 spectrometer but not the M2 spectrometer

according to the package used to identify them.

5.2.10 *btk_pid*

It gives information about the planes switched on the BTRD. It is possible to distinguish between a π^- and a Σ^- particle coming from the beam (see Chapter 4). It is known that the Ξ_c^+ production is larger with a Σ^- beam than with a π^- beam [63].

5.2.11 RICH likelihood, $\mathcal{L}$

The identification of the daughter particles in the RICH, the likelihood $\mathcal{L}$, is an important cut to check, so an observation will be done in each decay mode.

5.3 Branching Ratio (BR)

Experimentally the Branching Ratio (BR) is measured with a division between the number of total events of the two decay modes (the decay of interest and the reference mode):

$$BR = \frac{N_c\ (Decay\ of\ Interest)}{N_c\ (Reference\ Mode)} \tag{5.6}$$

where N_c stands for the number of particles produced in the SELEX experiment (number of events corrected by the efficiency of the experiment). For the case of the Ξ_c^+:

$$BR = \frac{N_c\ (Decay\ of\ Interest)}{N_c\ (\Xi^-\pi^+\pi^+)} \tag{5.7}$$

Due to unavoidable inefficiencies in the particle reconstruction in the SELEX spectrometer, the number of particles reconstructed is not equal to the number of particles produced in the experiment, moreover it is a complicated function of many variables. Fortunately, the Monte Carlo simulation performed, allows to compute the efficiency in order to correct the number of reconstructed events. In this way, it will be possible to get the number of produced events. This can be observed in equation 5.8:

$$N = \epsilon \cdot N_c \tag{5.8}$$

where N_c is the number of events produced in the SELEX experiment, N is the number of reconstructed events in the SELEX spectrometer and ϵ is the efficiency obtained from the Monte Carlo simulation.

It is seen from equation 5.8 that the number of produced events in the SELEX spectrometer is:

$$N_c = \frac{N}{\epsilon} \tag{5.9}$$

Using Equation 5.7, the branching ratio (BR) for a Ξ_c^+ decay is:

$$\frac{\frac{N\ (Decay\ of\ Interest)}{\epsilon\ (Decay\ of\ Interest)}}{\frac{N\ (\Xi^-\pi^+\pi^+)}{\epsilon\ (\Xi^-\pi^+\pi^+)}}$$

which can be written as:

$$BR = \frac{N\ (Decay\ of\ Interest)}{N\ (\Xi^-\pi^+\pi^+)} \cdot \frac{\epsilon\ (\Xi^-\pi^+\pi^+)}{\epsilon\ (Decay\ of\ Interest)} \tag{5.10}$$

Finally, if

$$\epsilon_{rel} = \frac{\epsilon\ (\Xi^-\pi^+\pi^+)}{\epsilon\ (Decay\ of\ Interest)}$$

the branching ratio can be written as:

$$BR = \frac{N\ (Decay\ of\ Interest)}{N\ (\Xi^-\pi^+\pi^+)} \cdot \epsilon_{rel} \tag{5.11}$$

where ϵ_{rel} is the relative efficiency between the two decay modes, i.e., the ratio between the two absolute efficiencies.

A very important point is that the cuts applied to the invariant mass distributions of both decays need to be very similar when computing the branching ratio, in order to get the number of events and to determine the efficiencies (actually, they are the same in this study). This avoids to take one region on a variable for one mode and a different region for that variable on the other mode where the dependency of the efficiencies can vary. It is also expected that any other dependence on the variables is canceled when taken the division between the two efficiencies in order to reduce the systematical error of the relative efficiency ϵ_{rel}. This will be demonstrated later by some systematical studies.

The branching ratios of the new decay modes ($\Xi_c^+ \to \Sigma^+\pi^-\pi^+$ and $\Xi_c^+ \to \Sigma^-\pi^+\pi^+$) that will be measured are:

$$BR_1 = \frac{\Gamma(\Xi_c^+ \to \Sigma^+\pi^-\pi^+)}{\Gamma(\Xi_c^+ \to \Xi^-\pi^+\pi^+)}$$

and

$$BR_2 = \frac{\Gamma(\Xi_c^+ \to \Sigma^- \pi^+ \pi^+)}{\Gamma(\Xi_c^+ \to \Xi^- \pi^+ \pi^+)}$$

Their relative branching fraction is also measured:

$$BR_3 = \frac{\Gamma(\Xi_c^+ \to \Sigma^- \pi^+ \pi^+)}{\Gamma(\Xi_c^+ \to \Sigma^+ \pi^- \pi^+)}$$

The next branching ratios will also be measured:

$$BR_4 = \frac{\Gamma(\Xi_c^+ \to p K^- \pi^+)}{\Gamma(\Xi_c^+ \to \Xi^- \pi^+ \pi^+)}$$

as a control mode (reported by SELEX in 2000 [7]),

$$BR_5 = \frac{\Gamma(\Lambda_c^+ \to \Sigma^+ \pi^- \pi^+)}{\Gamma(\Lambda_c^+ \to p K^- \pi^+)}$$

as another control mode (reported by CLEO [4]),

$$BR_6 = \frac{\Gamma(\Lambda_c^+ \to \Sigma^- \pi^+ \pi^+)}{\Gamma(\Lambda_c^+ \to \Sigma^+ \pi^- \pi^+)}$$

as a third control mode (reported by E687 [6]), and

$$BR_7 = \frac{\Gamma(\Lambda_c^+ \to \Sigma^- \pi^+ \pi^+)}{\Gamma(\Lambda_c^+ \to p K^- \pi^+)}$$

It is worth to mention that in the measurement of Λ_c^+ branching ratios the reference mode is in one case $pK^-\pi^+$ and in the other case $\Sigma^+\pi^-\pi^+$. The reason to choose these reference modes is that other measurements, previously reported, were performed in this way and a comparison is expected at the end.

5.3.1 Number of events in data

One important part in Equation 5.11 is the number of particles reconstructed in the SELEX apparatus, specially because some problems appear in its determination as it is explained below.

To determine the number of events in the invariant mass data distributions (an histogram is filled with this variable) a set of standard cuts for the variables of the post-recon analysis (described in Section 5.2) is applied. Two methods are considered for the determination of the number of events:

- A Gaussian plus a linear fit is performed using a fixed width given by the Monte Carlo simulation. The Gaussian function used is (x is the invariant mass and x_0 is the Ξ_c^+ mass equal to 2467 MeV/c^2):

$$gauss(x) = p_1 \frac{1}{\sqrt{2\pi}\,\sigma_g} e^{-\frac{(x-x_0)^2}{2\sigma_g^2}} + p_3 + p_4 \cdot (x - x_0) \tag{5.12}$$

  The first parameter in the fit (p_1) gives N, the number of reconstructed events in the SELEX spectrometer, the second parameter is the width (in this case fixed and written as σ_g to distinguish it from the uncertainty σ calculated above), the last ones, p_3 and p_4, are part of the linear fit to the background.
  As an example, the invariant mass of the reference mode ($\Xi^-\pi^+\pi^+$) is shown with the Gaussian fit performed (Figure 5.1).

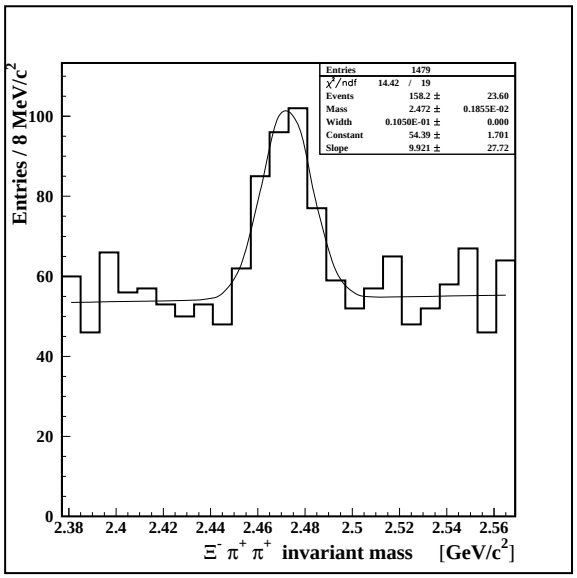

Figure 5.1: Invariant mass distribution for $\Xi^-\pi^+\pi^+$ with a Gaussian plus a linear fit.

  One of the main difficulties found in the study of the new decay modes ($\Sigma^+\pi^-\pi^+$ and $\Sigma^-\pi^+\pi^+$) is the fact that the pass2 run over raw data to select this reconstruction was done with a cut in the invariant mass close to the mass of the Ξ_c^+ particle. This causes problems estimating the number of events in the signal and the behavior of the background. The cut in the invariant mass distribution is at 2485 MeV/c^2 for such reason the fit is performed with a Gaussian plus a linear function for values below the cut and just a linear fit above the cut.

- A counting method is also performed using the background distribution function obtained from the Gaussian fit. This background function is

extrapolated to the bins with an excess of events (the gray region seen in Figure 5.2) in order to define a signal region.

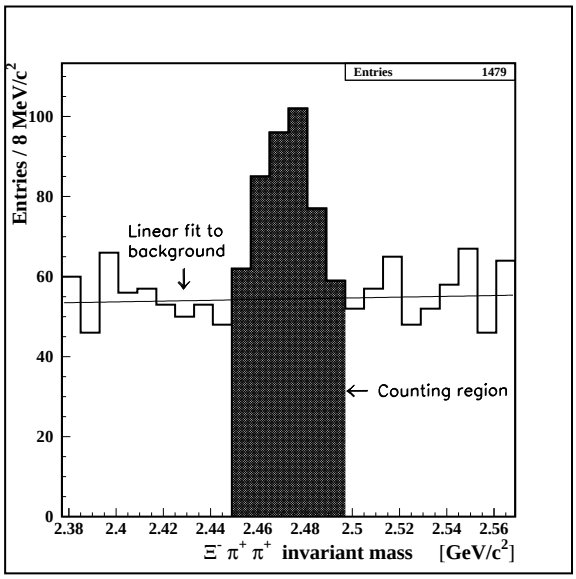

Figure 5.2: Invariant mass distribution for $\Xi^-\pi^+\pi^+$ with the counting region in gray color.

The Signal+Background number, (S+B), with an error $\Delta(S+B) = \sqrt{S+B}$ is the total content of entries within the counting region and the background number B is the area (number of entries) under the linear fit inside the counting region, with an error ΔB obtained from the fit described above. The number of events is calculated with a simple subtraction:

$$S = (S+B) - B \tag{5.13}$$

with error $\Delta S = \Delta(S+B) + \Delta B$ (see section 5.3.4 about statistical errors).

The counting method is used to compare the number of events obtained from the Gaussian fit because the distribution sometimes does not behave as a Gaussian-like function and there are problems with the results obtained from the fit, hence, along with the Gaussian fit, this will be used in the determination of the number of events for the evidence of the new decay modes, so this will not let any doubt about the first observation of the Cabibbo-suppressed decay modes $\Sigma^+\pi^-\pi^+$ and $\Sigma^-\pi^+\pi^+$.

The use of both methods will decrease the probability of doing a wrong determination in the number of events and it will allow a systematical check. For the example shown above the Gaussian fit gives 158 ± 24

events while the counting method gives 151 ± 32 events. There is no difference between both results which indicates that the determination of the number of events is consistent within the methods.

5.3.1.1 Reflections

The determination of the number of events, N, is not so easy. Sometimes particles are not well identified due to the procedure used to calculate the invariant mass. This problem is expected when computing the invariant mass and it produces the background in the distributions.

It is expected to have background because the particle identification works with likelihoods for its determination, moreover each detector has a finite range where it can work (as an example, the RICH was capable of K/π separation up to 165 GeV, see Chapter 4) so outside the region, the particle can be mis-identified. Another problem is that sometimes the detector can fail the identification even in the range where it can work. Important to note is that the detectors in SELEX have an excellent resolution (most of them above 90%) but the particles under study are very rare, so the probability for the detector to make a mistake increases.

Background also appears due to certain requirements of the codes used to reconstruct particles; for example in the case of the hyperon reconstruction (kink by disappearance, see Recon in section 4.7) a lot of background is produced since the code only requires a missing track to label it as a hyperon; such track could disappear not for a decay but just for the geometry of the detector or because of some detector failure; moreover the decay could correspond to another particle.

A description of the main problem and its solution is explained next using an example.

The point to discuss is the ambiguous identification of the daughter particles. These mis-identifications, called "reflections", are detected when it is supposed that at least one of the daughter particles is a different one. As an example the $\Xi^-\pi^+\pi^+$ reference mode is used; its invariant mass is shown in Figure 5.3.

An excess of events, a peak, associated to a Ξ_c^+ particle is observed around $2468\,\mathrm{MeV}/c^2$, but to the left of the Ξ_c^+ peak there is another excess of events around $2400\,\mathrm{MeV}/c^2$. A reflection is the first idea which comes to mind and because of the methodology of the hyperon reconstruction (see Recon in Section 4.7) it could be that the assumed Ξ^- is in reality a Σ^-.

In order to verify this assumption, the invariant mass corresponding to $\Sigma^-\pi^+\pi^+$ is calculated for the events used in the $\Xi^-\pi^+\pi^+$ reconstruction (the invariant mass for all the entries in Figure 5.3 is calculated changing the mass of the Ξ^- to the mass of the Σ^-) and an excess of events around $2287\,\mathrm{MeV}/c^2$ is found, corresponding to the Λ_c^+ decay $\Sigma^-\pi^+\pi^+$ (see Figure 5.4).

The events that are around the Λ_c^+ mass in Figure 5.4 (a $\pm 20\,\mathrm{MeV}/c^2$ in-

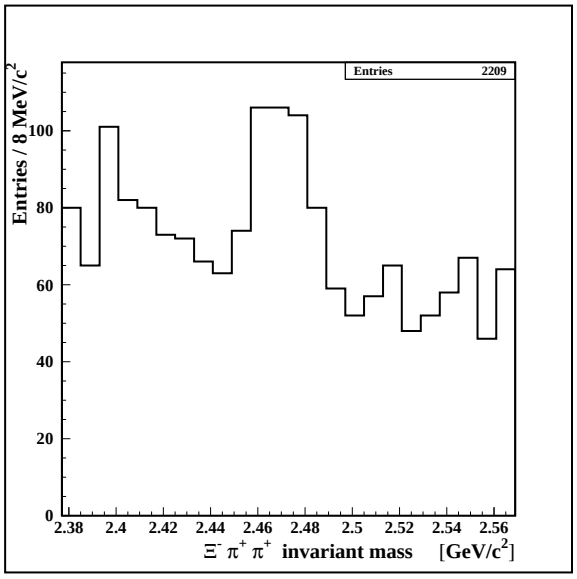

Figure 5.3: Invariant mass distribution for $\Xi^-\pi^+\pi^+$ (reflections have not been removed).

terval in this case) are eliminated from the original distribution (Figure 5.3).

The reason to eliminate the reflections is that the background behaves better (better means softly, sometimes linear), as it can be seen in Figure 5.5, where the excess of events around $2400\,\mathrm{MeV}/c^2$ has disappeared (this histogram was used in Section 5.3.1 as the example for the determination of the number of events).

The nature of the reflections can be inferred most of the time due to the different lifetimes between the particle under study (Ξ_c^+ in this case) and the particles that produced them; this is observed when the reflection appears/disappears from the Ξ_c^+ invariant mass distribution at short or long values for L/σ or they can also be detected due to specific details of the reconstruction package. A blind search was made to correctly identify all the reflections that could appear in the distributions, i.e., the whole combinations between possible and not possible decays of all the known particles was taken into account and the invariant mass was re-calculated; at the end histograms were filled. Peaks were searched at the invariant mass of known particles over the resulting histograms.

Different reflections are removed for all the decay modes under study, so a specific comment will be given to each one of them.

5.3.1.2 Corrections of events

The treatment of reflections leads to a loss of a fraction of events that needs to be taken into account for the determination of the number of events in the branching ratio measurements.

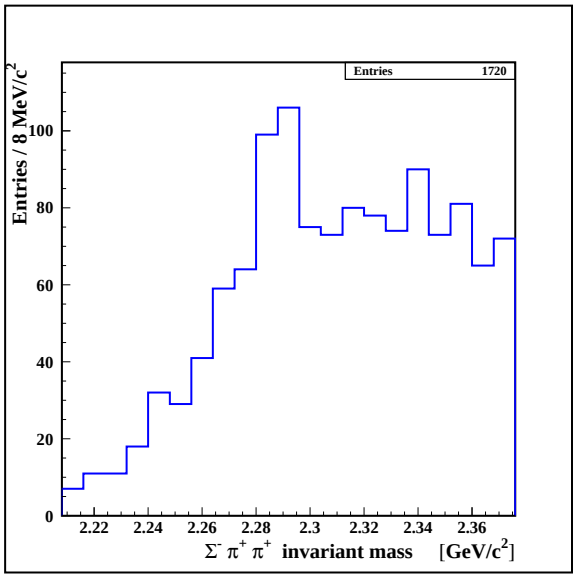

Figure 5.4: Invariant mass distribution for $\Sigma^-\pi^+\pi^+$ "reflected" from the inv. mass dist. for $\Xi^-\pi^+\pi^+$ due to a wrong identification of the Ξ^-.

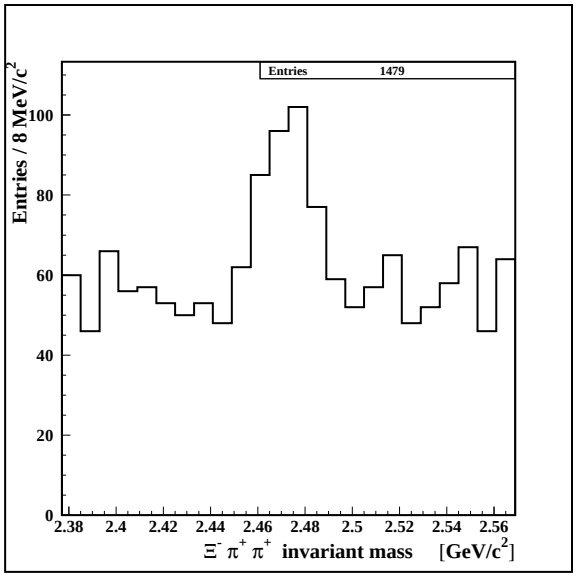

Figure 5.5: Invariant mass distribution for $\Xi^-\pi^+\pi^+$ after $\Lambda_c^+ \rightarrow \Sigma^-\pi^+\pi^+$ reflection is removed.

Once a reflection was removed some of the left out events were distributed along the invariant mass window, being some of them outside the peak region and some others inside the region of the peak. The removed events inside the peak should be included in the determination of the number of events and to estimate the lost events a Monte Carlo simulation is used.

First, the fraction of removed events that were inside the region of the peak needs to be determined, this is performed using Monte Carlo. As an example, if $\Xi_c^+ \to \Xi^-\pi^+\pi^+$ has a reflection of $\Lambda_c^+ \to \Sigma^-\pi^+\pi^+$ and it is removed, then the fraction of events under the peak is determined simulating events for $\Lambda_c^+ \to \Sigma^-\pi^+\pi^+$ and reconstructing them as $\Xi_c^+ \to \Xi^-\pi^+\pi^+$. The number of particles close to the mass of the Ξ_c^+ divided by the total number of reconstructed Λ_c^+ is the fraction that needs to be taken into account. In the example, 1774 Λ_c^+'s were reconstructed from 100,000 generated, see Figure 5.6, and once they are reconstructed as $\Xi^-\pi^+\pi^+$, 268 events are placed in a band corresponding to the width of the Ξ_c^+ and centered in the Ξ_c^+ mass, see Figure 5.7. This means that for every 1774 Λ_c^+'s, 268 of them are reconstructed as a Ξ_c^+; so the fraction is $268/1774 = 0.15$

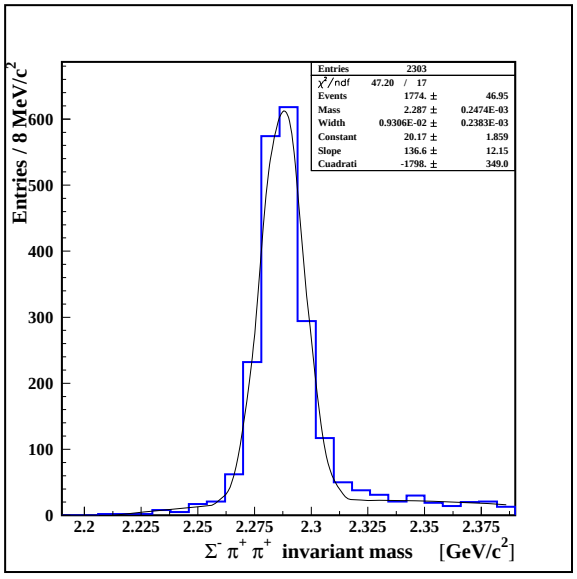

Figure 5.6: Reconstructed events corresponding to $\Sigma^-\pi^+\pi^+$ from a simulation of 100,000 events with a Gaussian plus a second degree polynomial fit.

Second, the number of events taken from the invariant mass distribution for data needs to be calculated. In the example, it is necessary to know how many Λ_c^+'s were misidentified as Ξ_c^+'s. This is performed by reconstructing the events for data in the $\Xi^-\pi^+\pi^+$ invariant mass as $\Sigma^-\pi^+\pi^+$ and then by

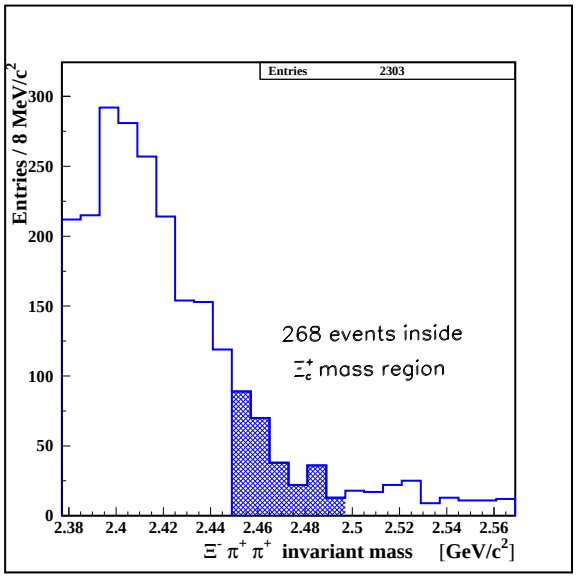

Figure 5.7: Events reconstructed as $\Xi^-\pi^+\pi^+$ from $\Sigma^-\pi^+\pi^+$ Monte Carlo simulation (Fig. 5.6).

estimating the number of events corresponding to a Λ_c^+ particle (sometimes a fit can be done but with a reduced number of events in the reflection, the counting method still works). In this example, 84 events were reconstructed as $\Lambda_c^+ \rightarrow \Sigma^-\pi^+\pi^+$ as it can be seen in Figure 5.8, and using a fraction of 0.15, it is seen that only $0.15 \times 84 = 12.6$ Ξ_c^+'s were removed from the original distribution and they should be included in the total number of events, giving 171 ± 24 $((158.2 + 12.6) \pm 23.6)$ events.

Since the number of corrected events is small compared to the total number of events relative errors are kept.

5.3.2 Signal significance

The determination of the signal significance for the evidence of the new decay modes is described in this section. This is a very important task because the signal significance is obtained with a statistical method to know if the peaks observed are due to fluctuations of the background.

The signal significance is calculated as $S/\sqrt{B}$ or in a more conservative way $S/\sqrt{S+B}$, in which S is the number of signal events and B is the number of background events in the signal region.

These calculations are only approximations, so as to correctly obtained the signal significance, the Poisson probability for the signal to be a statistical fluctuation is calculated.

If the signal plus background is $N = S + B$ then the Poisson probability for the signal to be a statistical fluctuation of the background is:

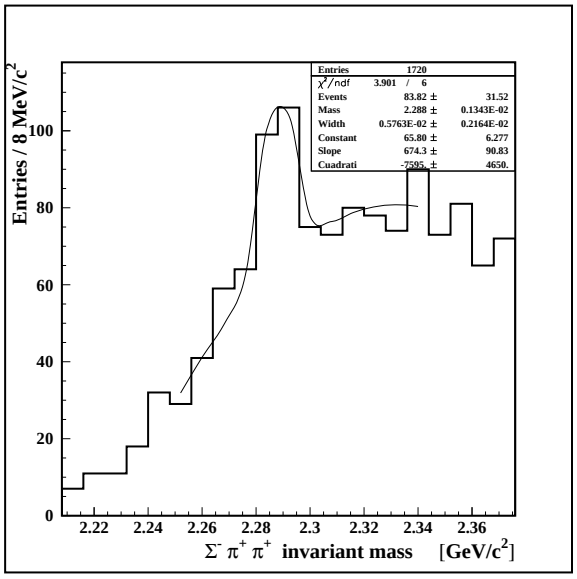

Figure 5.8: Data invariant mass distribution for $\Sigma^-\pi^+\pi^+$ "reflected" from the inv. mass dist. for $\Xi^-\pi^+\pi^+$ due to a wrong identification of the Ξ^-. Data are fitted to a Gaussian plus a second degree polynomial.

$$P(x >= N) = 1 - \sum_{x=0}^{N-1} \frac{B^x e^{-B}}{x!} \tag{5.14}$$

The methods described in this section are used for the significance determination of the new decay modes $\Xi_c^+ \to \Sigma^+\pi^-\pi^+$ and $\Xi_c^+ \to \Sigma^-\pi^+\pi^+$ (see Tables 6.1 and 6.2).

5.3.3 Efficiency

Another important task to do is to determine the reconstruction efficiency for all the Ξ_c^+ and Λ_c^+ modes observed, in order to compute the relative efficiency that appears in the branching ratio measurement (ϵ_{rel}).

The absolute efficiency, ϵ, is determined with a simple division:

$$\epsilon = \frac{REC}{GEN} \tag{5.15}$$

where GEN is the number of generated events via Monte Carlo simulation and REC is the number of those generated events that are reconstructed by the routines of the SELEX experiment once they are embedded.

For all the decay modes (for Ξ_c^+ and Λ_c^+) 200,000 events are generated. The number of reconstructed events is determined by fitting a Gaussian to the signal plus a linear fit to the background of the invariant mass distribution, as it was on data, but in this case σ_g is a free parameter (the value given by

this fit is the fixed one used for the determination of events in data).

As an example, using the Ξ_c^+ decay mode in $\Xi^-\pi^+\pi^+$ again, the invariant mass distribution for the reconstructed events is shown in Figure 5.9 and a Gaussian fit is performed for the determination of the number of events.

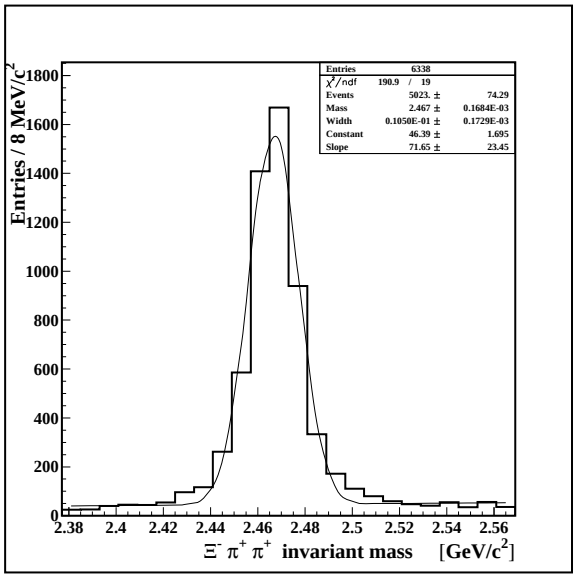

Figure 5.9: Invariant mass distribution for $\Xi^-\pi^+\pi^+$ from Monte Carlo.

Around 5023 ± 74 events are reconstructed and since 200,000 events were generated the resulting efficiency is around 2.5% (a detailed determination of the efficiencies is summarized in Chapter 6).

Of course, the efficiency may depend on the transverse momentum (p_T) or on the longitudinal momentum (actually on x_F), or even on another variable. As it was explained before it is not necessary to correct the absolute efficiencies as function of p_T or x_F, or not even as function of both of them because the important variable is the relative efficiency and any dependency should cancel, moreover, a systematical study will be performed (see Section 5.3.5 about systematical errors).

5.3.4 Statistical Error

The known theory about error propagation is used to compute the statistical error.

In the case of two uncorrelated quantities a and b with errors Δa and Δb, if an operation c is computed between variables a and b ($c = f(a, b)$) then the associated error to c, called Δc, is determined by a first order Taylor expansion:

$$(\Delta c)^2 = \left(\frac{\partial f}{\partial a}\right)^2 (\Delta a)^2 + \left(\frac{\partial f}{\partial b}\right)^2 (\Delta b)^2 \tag{5.16}$$

If $c = a \pm b$, then:

$$(\Delta c)^2 = (\Delta a)^2 + (\Delta b)^2 \tag{5.17}$$

If $c = ab$ or $c = a/b$, then:

$$(\Delta c)^2 = c^2 \left[\left(\frac{\Delta a}{a} \right)^2 + \left(\frac{\Delta b}{b} \right)^2 \right] \tag{5.18}$$

In this analysis, the variables involved are sometimes correlated; in the case presented here of two correlated variables, i.e., when one of the samples is totally included in the other one, a classical binomial error should be computed (as an example, to determine the efficiency, there is a correlation between the number of generated and reconstructed events):

If $p = \langle n \rangle / N$ (mean successes) and $q = 1 - p$ (mean failures) with $\sigma^2 = Npq$ (variance) then for n "accepted" events out of N tries, the observed success probability (acceptance) is:

$$r = n/N \tag{5.19}$$

and the error on acceptance is:

$$\sigma_r = \sqrt{r(1-r)/N} \tag{5.20}$$

5.3.5 Systematical Error

In order to see how the systematics affect the results, the dependence of the branching ratio on some of the variables involved in the analysis is checked (actually, those that are critical to get the signal). The systematical study is performed to the final branching ratio result. The variables taken into account are L/σ, pvtx, χ^2, scut and p_T^2; moreover the study was done for three different values of n for the production distribution function (proportional to $(1 - x_F)^n$ as it was seen in section 2.7, Equation 4.1). SELEX measured the n value for the production of the particle Λ_c^+ with a Σ^- beam and the value reported is $n = 2.45 \pm 0.18$ [62]. A similar value is expected for the Ξ_c^+ due to the similar valence quark composition ($\Lambda_c^+ = \{cdu\}$, $\Xi_c^+ = \{csu\}$) and to the quark composition of the beam particle ($\Sigma^- = \{sdd\}$) that has quarks in common with the baryons; besides a preliminary result of A. Blanco Covarrubias' analysis on charm production gives a value of $n = 2.06 \pm 0.77$ for Ξ_c^+ production with a Σ^- beam [63].

The values considered for the systematic study are $n = 1.5$, $n = 2.5$ and $n = 3.5$.

5.3.6 Resonances

Some of the decay modes under study may decay via a resonant state; so, the presence of some resonances is checked for those Ξ_c^+ modes with a hyperon in the final state. The decay modes are $\Sigma^+\pi^-\pi^+$, $\Sigma^-\pi^+\pi^+$ and the reference mode $\Xi^-\pi^+\pi^+$; and it is possible to have resonances decaying to $\pi^-\pi^+$, $\Sigma\pi$ and $\Xi^-\pi^+$ according to the different combinations between two of the three particles.

Summary

Once some difficulties are solved; the methodology of data analysis is clear: after applying some cuts, the number of events on both modes is counted and the relative efficiency between them is determined with a Monte Carlo simulation. The branching ratio is the division between the numbers of events times the relative efficiency, undoubtedly errors need to be taken into account. The results are shown in the next chapter.

Chapter 6

Results

Several decay modes have been observed for the Ξ_c^+, but around 500 candidates were found for all the decay channels in 1 billion interactions stored by the SELEX collaboration. This surely can be called "more difficult than looking for a needle in a haystack".

The results for the analysis performed are presented next. First, the invariant mass distributions for all the decay modes under study, both in data and Monte Carlo, are shown along with the cuts used to obtain them. Then, the results for all the branching ratios measured are presented along with the number of events found and the absolute and relative efficiencies. Finally, the results for all the systematical studies are detailed.

6.1 Evidence of the decay modes

The invariant mass distribution for the reference mode ($\Xi_c^+ \to \Xi^-\pi^+\pi^+$) is presented, and the distributions that evidence the discovery of the new (found in this work) Ξ_c^+ decay modes are shown, besides the corresponding distributions to the modes used for control are also presented. The results include data and Monte Carlo.

The results presented here are based on the Gaussian fit performed. The counting method will only be used in the evidence of the new Ξ_c^+ decay modes. For the reference and control modes the counting method is consistent with the Gaussian fit performed.

6.1.1 Reference mode: $\Xi_c^+ \to \Xi^-\pi^+\pi^+$

6.1.1.1 Data

The invariant mass distribution corresponding to the reference mode is shown in Figure 6.1.

The cuts applied are:

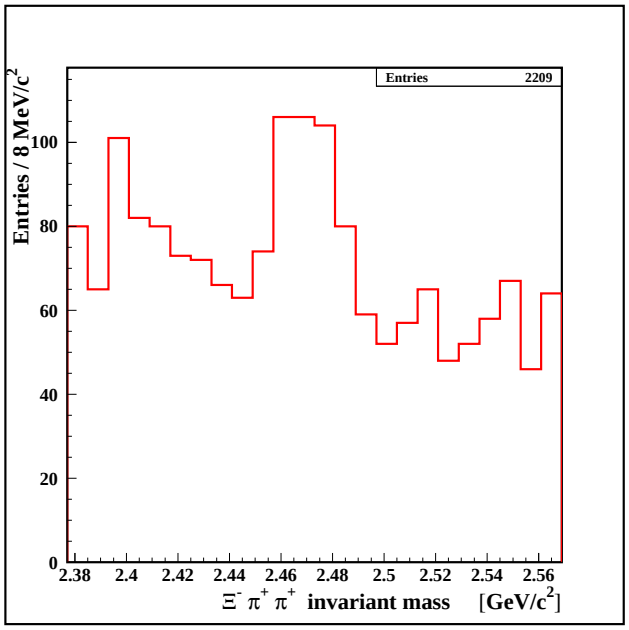

Figure 6.1: Invariant mass distribution for $\Xi^-\pi^+\pi^+$ (no reflections have been removed).

- $L/\sigma > 8$
- $pvtx < 10$
- $\chi^2_{\rm sec} < 5$
- $p_\pi > 10$ GeV/c
- $p_T^2 > 0.3$ $(\mathrm{GeV}/c)^2$
- $scut > 4$
- $\sigma < 0.17cm$
- Σ^- and proton beam

A reflection is observed in the distribution due to a wrong identification of the Ξ^-. In this decay mode, the Ξ^- is changed to a Σ^-, which gives $\Sigma^-\pi^+\pi^+$ instead of $\Xi^-\pi^-\pi^+$. A peak around $2287\,\mathrm{MeV}/c^2$ corresponding to a Λ_c^+ is seen (events $\pm 10\,\mathrm{MeV}/c^2$ around this mass are removed) and Figure 6.2 shows this reflection.

Figure 6.3 shows the invariant mass distribution after the Λ_c^+ reflection is removed. The number of events under the peak is determined with a Gaussian plus a linear fit and a fixed width of $\sigma_g = 10.5\,\mathrm{MeV}/c^2$ given by Monte Carlo (Figure 6.4), leading to 158 ± 24 events.

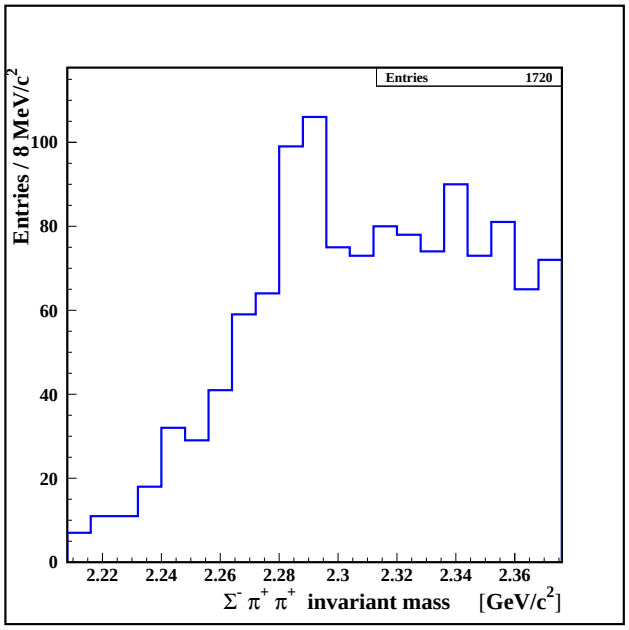

Figure 6.2: Invariant mass distribution for $\Sigma^-\pi^+\pi^+$ "reflected" from the inv. mass dist. for $\Xi^-\pi^+\pi^+$ due to a wrong identification of the Ξ^-.

6.1.1.2 Simulation

Figure 6.4 shows the invariant mass distribution corresponding to the reconstructed events with the same cuts applied to data. The width of this Gaussian distribution is used to fit the data. The generation of events was performed with $p_T = 1.0$ and $n = 2.5$

The file *cascade-cas_pi_pi.dec* used to generate the events is:

```
PARTICLE  CSU0    125   -1  2.467900  1.0  0.5   0.000106
PDG       CSU0   4232
;
DECAY  CSU0
CHANNEL  0 1.0000  XI-   PI+   PI+
ENDDECAY
;
DECAY XI-
CHANNEL  0 1.0000  LAM   PI-
ENDDECAY
;
DECAY LAM
CHANNEL  0 1.000   P+   PI-
ENDDECAY
```

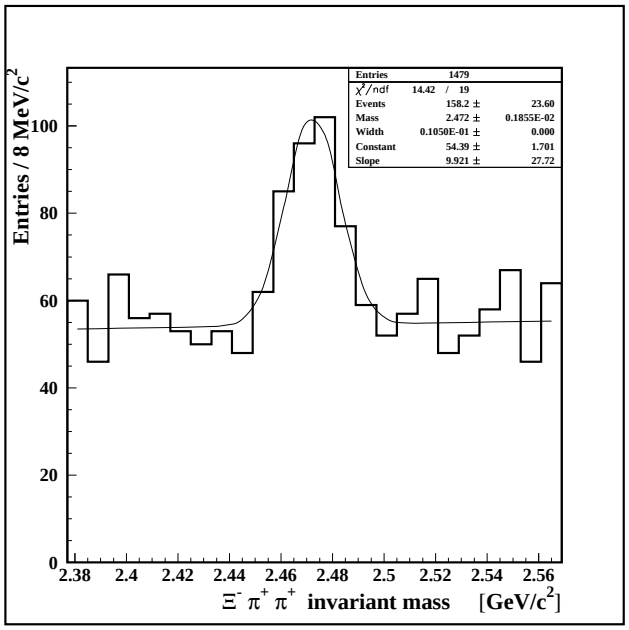

Figure 6.3: Invariant mass distribution for $\Xi^-\pi^+\pi^+$ with $\Lambda_c^+ \rightarrow \Sigma^-\pi^+\pi^+$ reflection removed.

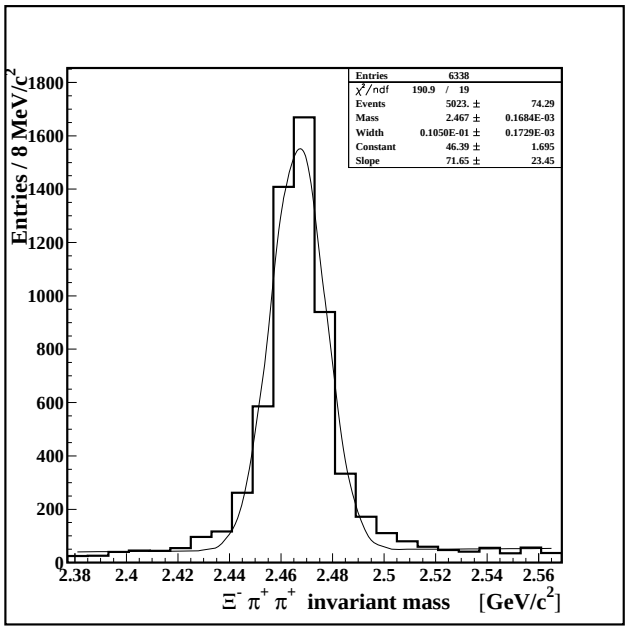

Figure 6.4: Invariant mass distribution for $\Xi^-\pi^+\pi^+$ from Monte Carlo with $p_T = 1.0$ and $n = 2.5$.

6.1.2 $\Xi_c^+ \to pK^-\pi^+$

6.1.2.1 Data

The invariant mass distribution corresponding to $pK^-\pi^+$ is shown in Figure 6.5.

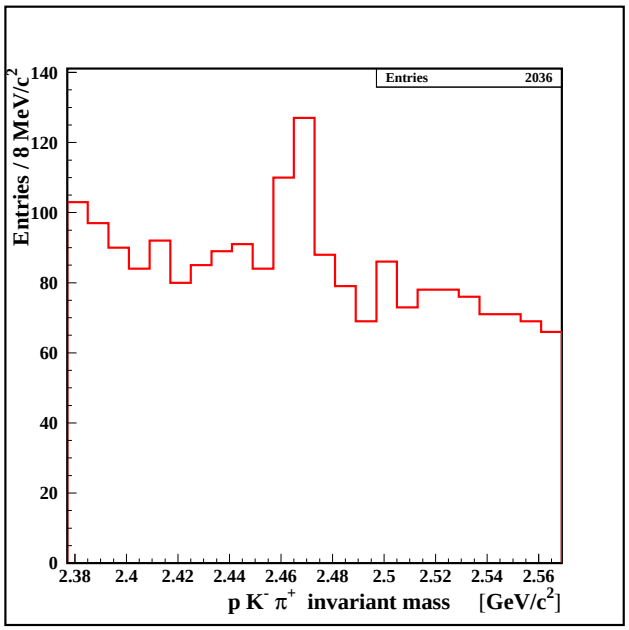

Figure 6.5: Invariant mass distribution for $pK^-\pi^+$ in the Ξ_c^+ mass region (no reflections have been removed).

The cuts applied to this reconstruction are:

- $L/\sigma > 10$
- $pvtx < 9$
- $\chi^2_{\text{sec}} < 8$
- $p_\pi > 5$ GeV/c
- $p_T^2 > 0.3$ $(\text{GeV}/c)^2$
- $scut > 5$
- $\sigma < 0.17cm$
- Σ^- and proton beam
- $\mathcal{L}(K)/\mathcal{L}(\pi) \geq 1$
- $\mathcal{L}(p)/\mathcal{L}(\pi) \geq 1$

The last two cuts mean the condition of the likelihood required for the identification of the particle in the RICH.

The reflections that are observed in this channel are:

1. A possible wrong identification of the proton: the invariant mass of $\pi^+K^-\pi^+$ is reconstructed and a peak around $1869\,\mathrm{MeV}/c^2$ is seen; the particle at this mass is the D^+ meson (Figure 6.6).

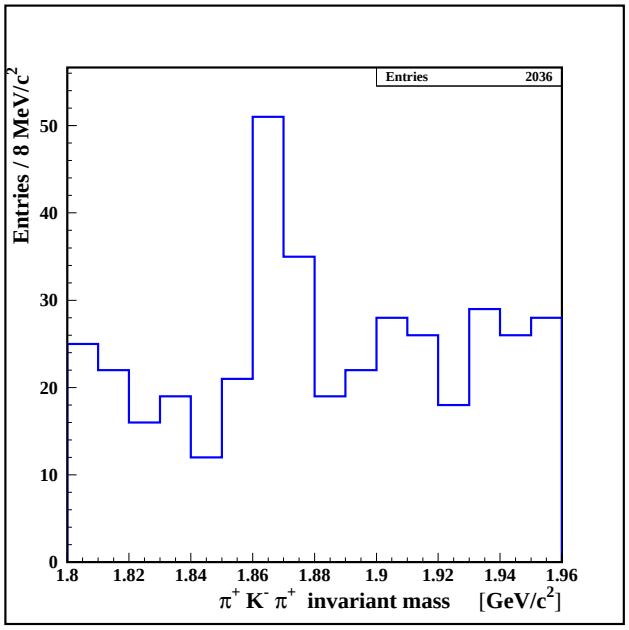

Figure 6.6: Invariant mass distribution for $\pi^+K^-\pi^+$ "reflected" from the inv. mass dist. for $pK^-\pi^+$ due to a wrong identification of the proton.

2. Ambiguous identification of the proton: the invariant mass of $K^+K^-\pi^+$ is reconstructed instead of $pK^-\pi^+$. There are two excesses of events, one around $1869\,\mathrm{MeV}/c^2$ corresponding to a D^+ meson and another one around $1968\,\mathrm{MeV}/c^2$ associated to a D_s^+ meson (Figure 6.7).

The events that are $\pm 20\,\mathrm{MeV}/c^2$ around these three peaks are eliminated from the original distribution in $pK^-\pi^+$.

Figure 6.8 shows the invariant mass distribution for $pK^-\pi^+$ after the reflections described are removed. The number of events under the peak is determined with a Gaussian plus a linear fit with a fixed width of $\sigma_g = 8.9\,\mathrm{MeV}/c^2$ given by Monte Carlo (Figure 6.9), resulting in 95 ± 19 events.

6.1.2.2 Simulation

Figure 6.9 shows the invariant mass distribution for the simulation which corresponds to this mode with the tighter cuts mentioned above.

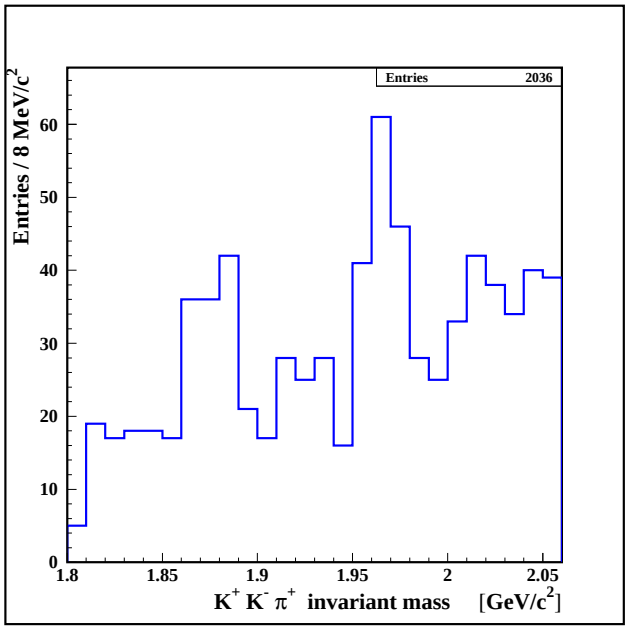

Figure 6.7: Invariant mass distribution for $K^+K^-\pi^+$ "reflected" from the inv. mass dist. for $pK^-\pi^+$ due to a wrong identification of the proton.

The file *cascade-p_k-_pi+.dec* used to generate the events is:

```
PARTICLE  CSU0    125   -1  2.467900  1.0  0.5   0.000106
PDG       CSU0   4232
;
DECAY  CSU0
CHANNEL  0 1.0000  P+   K-   PI+
ENDDECAY
```

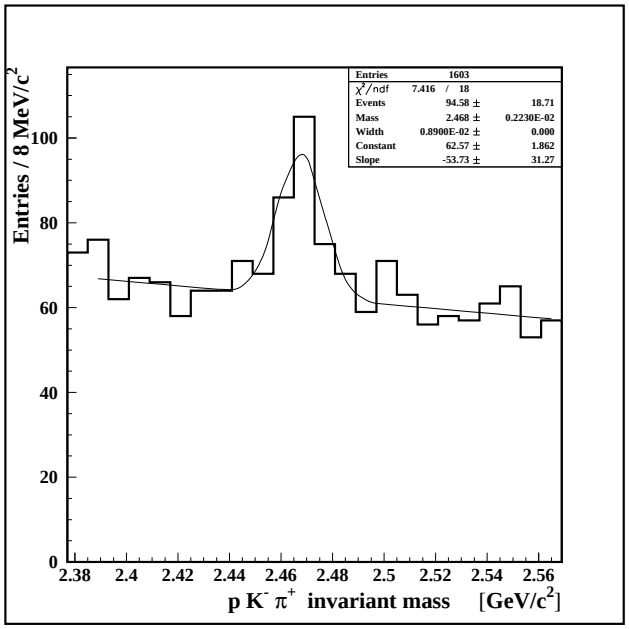

Figure 6.8: Invariant mass distribution for $pK^-\pi^+$ in the Ξ_c^+ mass region (reflections have been removed).

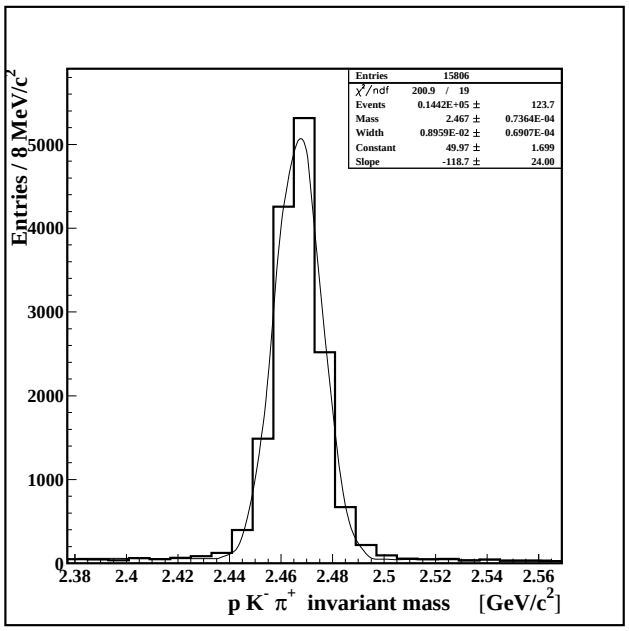

Figure 6.9: Invariant mass distribution for $pK^-\pi^+$ from Monte Carlo in the Ξ_c^+ mass region with $p_T = 1.0$ and $n = 2.5$.

6.1.3 $\Lambda_c^+ \to pK^-\pi^+$

6.1.3.1 Data

This Λ_c^+ mode is very clean due to the efficiency in the reconstruction of the daughter particles and to the branching fraction ($(5.0 \pm 1.3)\%$, the biggest in the hadronic modes of the Λ_c^+).

Figure 6.10 shows the invariant mass distribution for $pK^-\pi^+$ where a huge excess of events corresponding to a Λ_c^+ signal can be observed.

The number of events is determined with a Gaussian plus a linear fit with a fixed width of $\sigma_g = 7.9\,\mathrm{MeV}/c^2$ given by Monte Carlo (Figure 6.11), and 2067 ± 63 events are found.

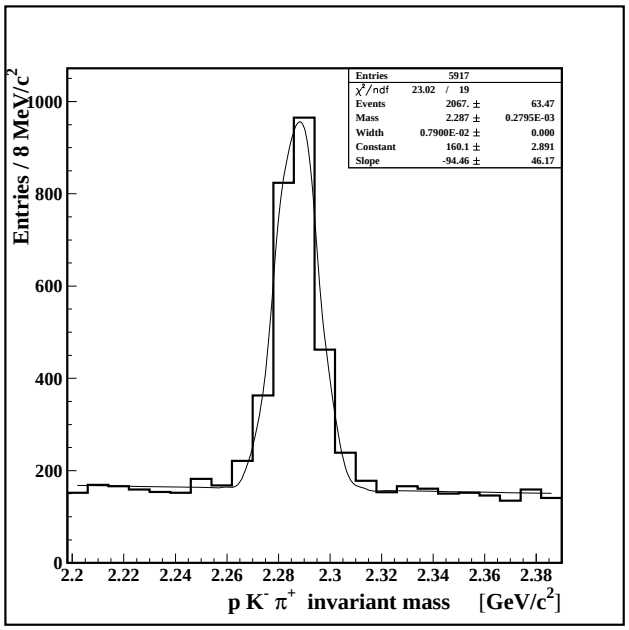

Figure 6.10: Invariant mass distribution for $pK^-\pi^+$ in the Λ_c^+ mass region.

The cuts applied to this distribution are:

- $L/\sigma > 8$
- $pvtx < 12$
- $\chi^2_{\mathrm{sec}} < 5$
- $p_\pi > 5$ GeV/c
- $p_T^2 > 0.3$ $(\mathrm{GeV}/c)^2$
- $scut > 4$
- $\sigma < 0.17cm$

- $\mathcal{L}(K)/\mathcal{L}(\pi) \geq 1$
- $\mathcal{L}(p)/\mathcal{L}(\pi) \geq 1$
- Σ^- and proton beam

No reflection was removed from this invariant mass distribution.

6.1.3.2 Simulation

Figure 6.11 shows the invariant mass distribution for the simulation corresponding to this mode with the tighter cuts mentioned above.

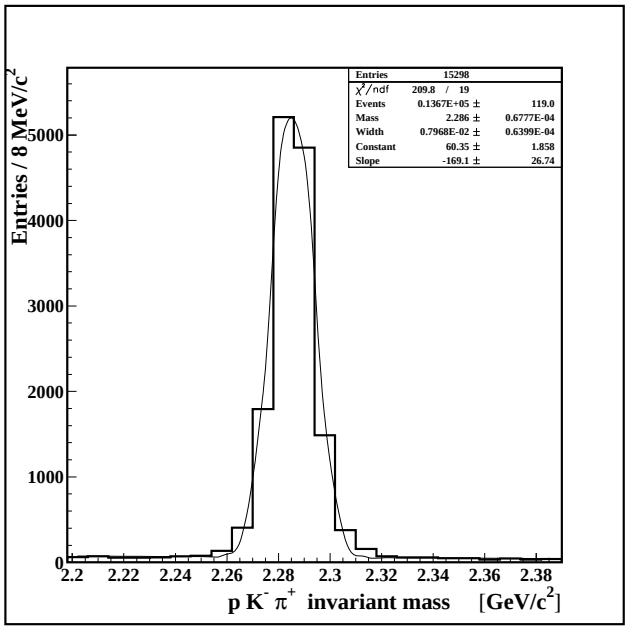

Figure 6.11: Invariant mass distribution for $pK^-\pi^+$ from Monte Carlo in the Λ_c^+ mass region with $p_T = 1.0$ and $n = 2.5$.

The file *lambda-p_k-_pi+.dec* used to generate the events is:

```
PARTICLE  LAMC   123   -1  2.285000  1.0  0.5   0.000060
PDG       LAMC       4122
;
DECAY  LAMC
CHANNEL  0 1.0000  P+   K-   PI+
ENDDECAY
```

6.1.4 $\Sigma^+\pi^-\pi^+$

This reconstruction has two important excesses of events in its invariant mass distribution. The first one corresponds to the Λ_c^+, its mass is around $2288\,\mathrm{MeV}/c^2$ (this decay mode has been reported before [4, 5]) and the second one corresponds to the Ξ_c^+, its mass is around $2472\,\mathrm{MeV}/c^2$ and it has not been reported before.

During the production phase of the data analysis candidate events were selected when the selection criteria were fulfilled and the invariant mass of the charm candidate was within a pre-defined window, resulting in an artificial cutoff slightly above the Ξ_c^+ mass, at $2485\,\mathrm{MeV}/c^2$. For this study the mass window was extended with a re-running over the data, but the results do not significantly change with the cutoff in the mass window.

Figure 6.12 shows the invariant mass distribution where both peaks can be observed; the sum of two Gaussians with fixed widths (given by Monte Carlo) and a second degree polynomial are adjusted. The cuts are fixed in order to easily appreciate both particles in the same window. Details for each of the particles are explained below.

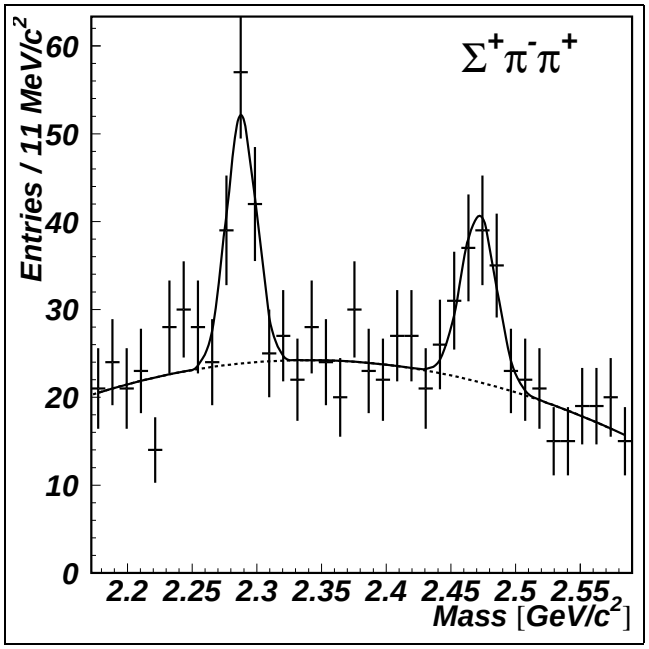

Figure 6.12: Invariant mass distribution for $\Sigma^+\pi^-\pi^+$; Λ_c^+ is around $2288\,\mathrm{MeV}/c^2$ and Ξ_c^+ is around $2472\,\mathrm{MeV}/c^2$.

6.1.5 $\Xi_c^+ \to \Sigma^+\pi^-\pi^+$

6.1.5.1 Data

The invariant mass distribution corresponding to $\Xi_c^+ \to \Sigma^+\pi^-\pi^+$ is shown in Figure 6.13 (same as Figure 6.12 but close up to the Ξ_c^+ invariant mass). The width is fixed at $\sigma_g = 12.3\,\mathrm{MeV}/c^2$ and it is given by Monte Carlo (Figure 6.14).

The number of events is calculated with a Gaussian plus a second degree polynomial fit and the counting method described before is also used in order to corroborate that the statistical significance of the signal is well determined. The number of events is 59 ± 14 using the Gaussian fit and 55 ± 15 using the counting method. The background under the signal region is 87 ± 7 events. Counting and fitting the number of entries above a extrapolated linear background, and using a second-order polynomial for the background, give within errors the same number of events.

The significance is calculated as $S/\sqrt{B}$ or in a more conservative way $S/\sqrt{S+B}$, in which S is the number of signal events and B is the number of background events in the signal region. These calculations are only approximations, so the Poisson probability that the signal could be a statistical fluctuation is also computed. Table 6.1 summarizes the results obtained.

Method for Significance	Significance for Gaussian	Significance for Counting
$S/\sqrt{B}$	6.3 ± 1.5	5.9 ± 1.6
$S/\sqrt{S+B}$	4.9 ± 1.1	4.6 ± 1.3
Poisson probability (%)	6.2×10^{-7}	4.0×10^{-6}
Signal events S	59 ± 14	55 ± 15
Background events B	87 ± 7	87 ± 9

Table 6.1: Significance determination and number of evidence events for the signal of the decay $\Xi_c^+ \to \Sigma^+\pi^-\pi^+$.

The cuts applied to get the distribution are:

- $L/\sigma > 12$
- $pvtx < 13$

- $\chi^2_{\rm sec} < 7$
- $p_T^2 > 0.4$ $(\mathrm{GeV}/c)^2$
- $p_{hyp} > 70$ GeV/c
- $scut > 0$
- $\sigma < 0.10cm$
- $\mathcal{L}(\pi) > 0.1$ for one of the pions
- Σ^- and proton beam

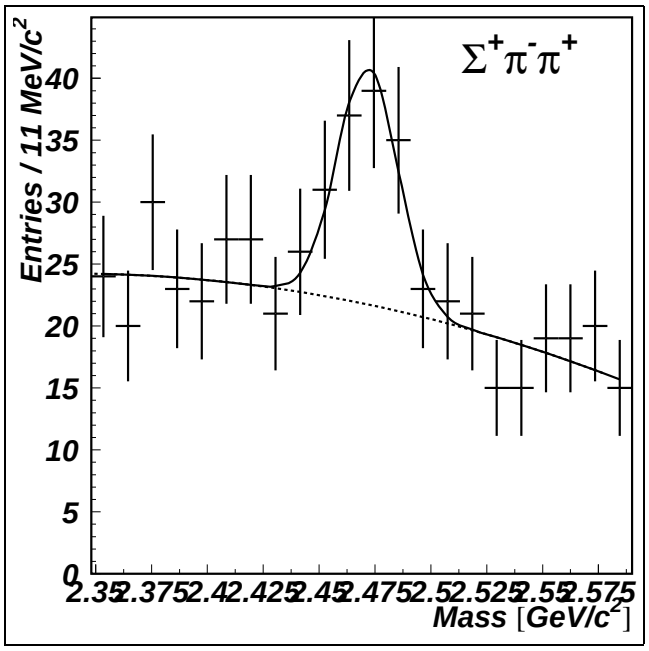

Figure 6.13: Invariant mass distribution for $\Sigma^+\pi^-\pi^+$ in the Ξ_c^+ mass region (same as Figure 6.12 but close up to the Ξ_c^+ invariant mass).

The reflection removed in this channel is:

1. Ambiguous identification of the π^-: the invariant mass for $\Sigma^+K^-\pi^+$ is reconstructed instead of $\Sigma^+\pi^-\pi^+$. A peak around $2468\,\mathrm{MeV}/c^2$ corresponding to a Ξ_c^+ is seen. The events that are $\pm 15\,\mathrm{MeV}/c^2$ around this peak are eliminated from the original distribution in $\Sigma^+\pi^-\pi^+$.

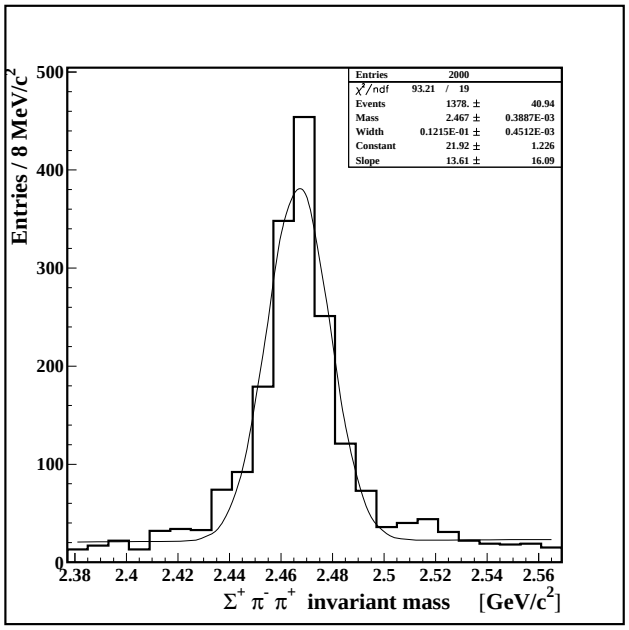

Figure 6.14: Invariant mass distribution for $\Sigma^+\pi^-\pi^+$ from Monte Carlo in the Ξ_c^+ mass region with $p_T = 1.0$ and $n = 2.5$.

6.1.5.2 Simulation

Figure 6.14 shows the corresponding invariant mass distribution to this mode with the same cuts applied to data. The generation of events was performed with $p_T = 1.0$ and $n = 2.5$

The files *cascade-sig_pi_pi-n_pi+.dec* and *cascade-sig_pi_pi-p_pi0.dec* used to generate the events are shown below. It is important to note that the two files correspond to the two main decay modes of the Σ^+ hyperon ($n\pi^+$ and $p\pi^0$). Both modes nearly have a branching fraction of 50% ($(48.31 \pm 0.30)\%$ for $n\pi^+$ and $(51.57 \pm 0.30)\%$ for $p\pi^0$), so 100,000 events for each mode are generated.

For $\Sigma^+\pi^-\pi^+$ with the Σ^+ hyperon in the $n\pi^+$ channel, the file is:

```
PARTICLE  CSU0    125   -1  2.467900  1.0  0.5   0.000106
PDG       CSU0   4232
;
DECAY  CSU0
CHANNEL  0 1.0000  SIG+   PI-   PI+
ENDDECAY
;
DECAY SIG+
CHANNEL  0 1.0000  N0    PI+
ENDDECAY
```

and also with the Σ^+ hyperon in the $p\pi^0$ channel, the file is:

```
PARTICLE  CSU0    125   -1  2.467900  1.0  0.5   0.000106
PDG       CSU0   4232
;
DECAY  CSU0
CHANNEL  0 1.0000  SIG+   PI-   PI+
ENDDECAY
;
DECAY SIG+
CHANNEL  0 1.0000  P+    PI0
ENDDECAY
```

6.1.6 $\Lambda_c^+ \rightarrow \Sigma^+\pi^-\pi^+$

6.1.6.1 Data

Figure 6.15 shows the invariant mass distribution $\Sigma^+\pi^-\pi^+$ where an excess of events corresponding to a Λ_c^+ can be observed.

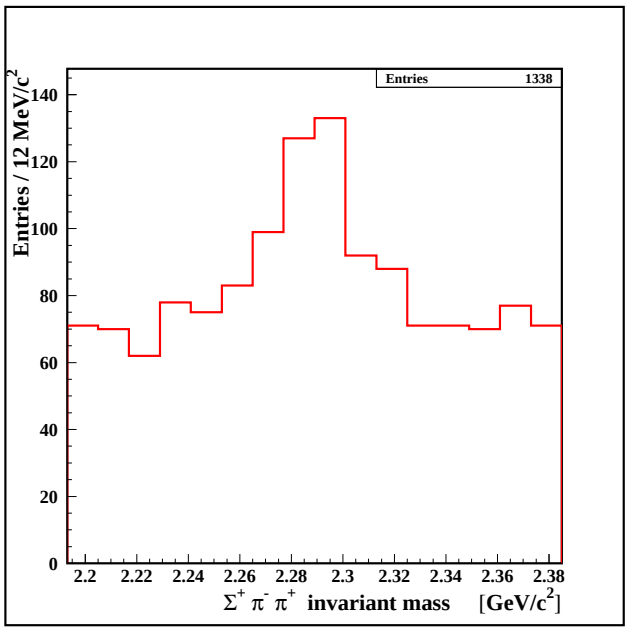

Figure 6.15: Invariant mass distribution for $\Sigma^+\pi^-\pi^+$ in the Λ_c^+ mass region (no reflections have been removed and a different set of cuts was applied in comparison to those in Figure 6.12).

The cuts applied to this distribution are:

- $L/\sigma > 9$
- $pvtx < 4$

- $\chi^2_{\text{sec}} < 5$
- $p_\pi > 10$ GeV/c
- $p_T^2 > 0.3$ $(\text{GeV}/c)^2$
- $scut > 4$
- $\sigma < 0.17cm$
- Σ^- and proton beam

One reflection to be removed from this histogram is an ambiguous identification of two particles: the Σ^+ is changed to a K^+ and the π^- is changed to a K^-, which gives $K^+K^-\pi^+$ instead of $\Sigma^+\pi^-\pi^+$. A peak around 1968 MeV/c^2 associated to a D_s^+ meson is seen and the events ± 20 MeV/c^2 around this mass are removed. Figure 6.16 shows the $K^+K^-\pi^+$ invariant mass distribution.

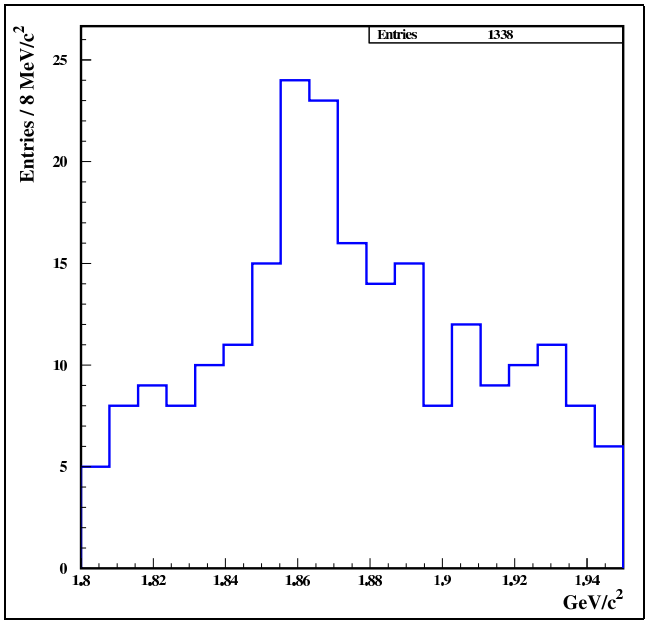

Figure 6.16: Invariant mass distribution for $K^+K^-\pi^+$ "reflected" from the inv. mass dist. for $\Sigma^+\pi^-\pi^+$ due to a wrong identification of the Σ^+ and the π^-.

Another reflection taken into account is a wrong identification of the same two particles: in this case, the Σ^+ is changed to a π^+ and the π^- is changed to a K^- again, which gives $\pi^+K^-\pi^+$ instead of $\Sigma^+\pi^-\pi^+$. A peak around 1869 MeV/c^2 associated to a D^+ meson is seen (Figure 6.17) and the events ± 20 MeV/c^2 around this mass are removed.

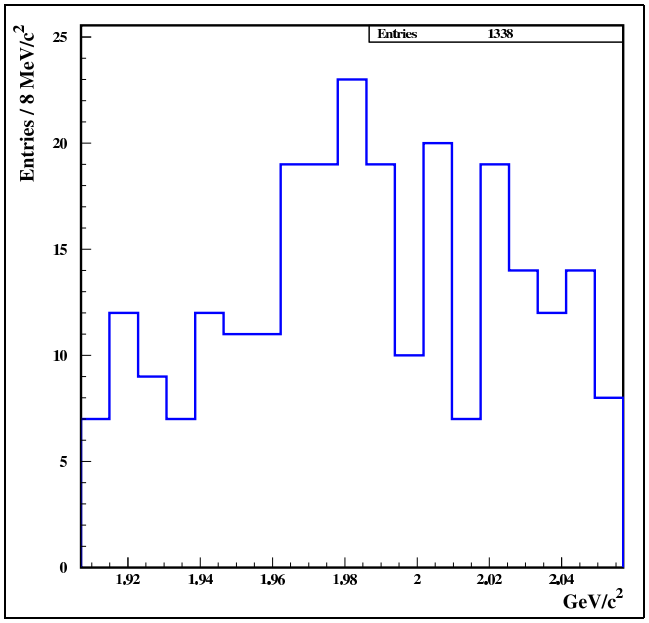

Figure 6.17: Invariant mass distribution for $\pi^+K^-\pi^+$ "reflected" from the inv. mass dist. for $\Sigma^+\pi^-\pi^+$ due to a wrong identification of the Σ^+ and the π^-.

Figure 6.18 shows the invariant mass distribution for $\Sigma^+\pi^-\pi^+$ after the reflections described above are removed. The number of events under the peak is determined with a Gaussian plus a linear fit with a fixed width of $\sigma_g = 12.7\,\mathrm{MeV}/c^2$ given by Monte Carlo (Figure 6.19), leading to 169 ± 23 events.

6.1.6.2 Simulation

A Monte Carlo simulation is performed as usual. Figure 6.19 shows the corresponding invariant mass distribution with the same cuts that are applied to the data. The generation of events is performed with $p_T = 1.0$ and $n = 2.5$

As in the case of the $\Xi_c^+ \to \Sigma^+\pi^-\pi^+$ decay, two files are used to generate events (100,000 for each Σ^+ decay mode). The files are shown next, *lambda-sig_pi_pi-n_pi+.dec* for $\Sigma^+\pi^-\pi^+$ with the Σ^+ hyperon in the $n\pi^+$ channel and *lambda-sig_pi_pi-p_pi0.dec* for $\Sigma^+\pi^-\pi^+$ with the Σ^+ hyperon in the $p\pi^0$ channel, respectively.

```
PARTICLE  LAMC   123   -1  2.285000  1.0  0.5   0.000060
PDG       LAMC       4122
;
DECAY  LAMC
CHANNEL  0 1.0000  SIG+   PI-   PI+
ENDDECAY
```

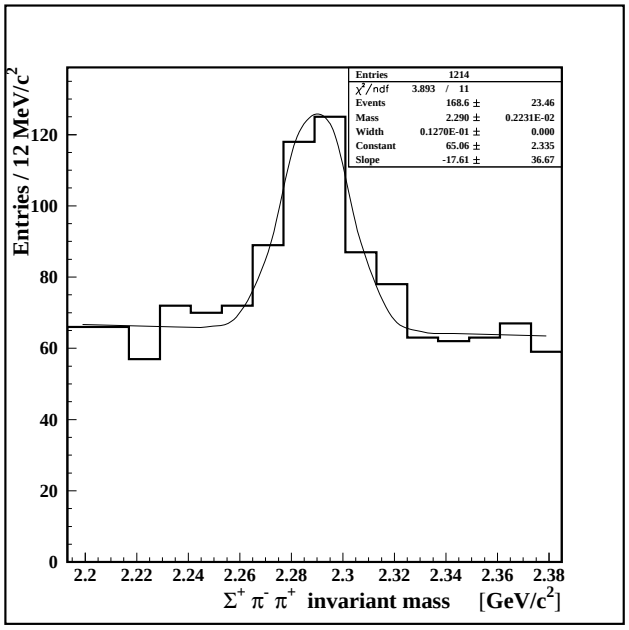

Figure 6.18: Invariant mass distribution for $\Sigma^+\pi^-\pi^+$ in the Λ_c^+ mass region (reflections have been removed).

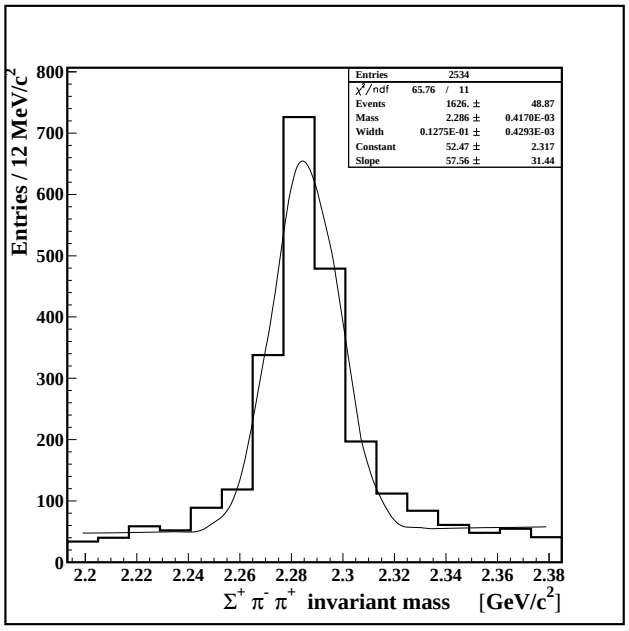

Figure 6.19: Invariant mass distribution for $\Sigma^+\pi^-\pi^+$ from Monte Carlo in the Λ_c^+ mass region with $p_T = 1.0$ and $n = 2.5$.

```
;
DECAY SIG+
CHANNEL  0 1.0000  N0    PI+
ENDDECAY

PARTICLE  LAMC   123   -1  2.285000  1.0  0.5   0.000060
PDG       LAMC       4122
;
DECAY  LAMC
CHANNEL  0 1.0000  SIG+   PI-   PI+
ENDDECAY
;
DECAY SIG+
CHANNEL  0 1.0000  P+    PI0
ENDDECAY
```

6.1.7 $\Sigma^-\pi^+\pi^+$

This reconstruction has two important excesses of events in its invariant mass distribution. The first one corresponds to the Λ_c^+, its mass is around $2286\,\mathrm{MeV}/c^2$ (this decay mode has been reported before [6]) and the second one corresponds to the Ξ_c^+, its mass is around $2463\,\mathrm{MeV}/c^2$ and it has not been reported before.

Figure 6.20 shows the invariant mass distribution where both peaks can be observed; the sum of two Gaussians with fixed widths (given by Monte Carlo) and a second degree polynomial are adjusted. Details for each of the particles are explained below.

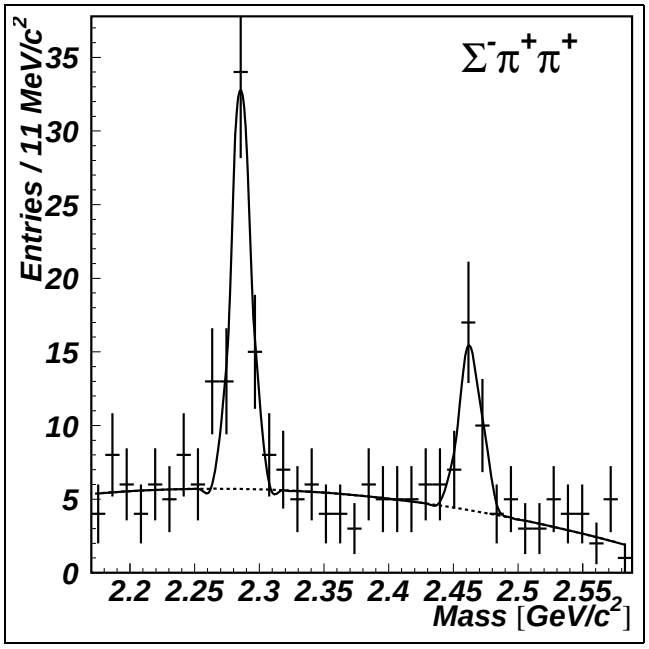

Figure 6.20: Invariant mass distribution for $\Sigma^-\pi^+\pi^+$; Λ_c^+ is around $2286\,\mathrm{MeV}/c^2$ and Ξ_c^+ is around $2463\,\mathrm{MeV}/c^2$.

6.1.8 $\Xi_c^+ \to \Sigma^-\pi^+\pi^+$

6.1.8.1 Data

During the production phase of the data analysis candidate events were selected when the selection criteria were fulfilled and the invariant mass of the charm candidate was within a pre-defined window, resulting in an artificial cutoff slightly above the Ξ_c^+ mass, at $2485\,\mathrm{MeV}/c^2$. For this study the mass window was extended with a re-running over the data, but the results do not significantly change with the cutoff in the mass window.

The invariant mass distribution is shown in Figure 6.21 (same as Figure 6.20 but close up to the Ξ_c^+ invariant mass), the width is fixed at

9.6 MeV/c^2 and it is given by Monte Carlo (Figure 6.23).

As in the case of the $\Sigma^+\pi^-\pi^+$ channel, the number of events is calculated with a Gaussian plus a linear fit and the counting method is also used in order to corroborate that the statistical significance of the signal is well determined. The number of events is 22 ± 8 using the Gaussian fit and 14 ± 4 using the counting method. The background under the signal region is 13 ± 3 events. Counting and fitting the number of entries above a extrapolated linear background, and using a second-order polynomial for the background, give within errors the same number of events.

The significance is calculated as $S/\sqrt{B}$ or in a more conservative way $S/\sqrt{S+B}$, in which S is the number of signal events and B is the number of background events in the signal region. These calculations are only approximations so the Poisson probability that the signal can be a statistical fluctuation is also computed. Table 6.2 summarizes the results obtained.

Method for Significance	Significance for Gaussian	Significance for Counting
$S/\sqrt{B}$	6.2 ± 2.2	5.9 ± 2.1
$S/\sqrt{S+B}$	3.8 ± 1.3	3.6 ± 1.2
Poisson probability	2.3×10^{-5}	7.7×10^{-5}
Signal events S	22 ± 8	22 ± 7
Background events B	13 ± 3	14 ± 4

Table 6.2: Significance determination and number of evidence events for the signal of the decay $\Xi_c^+ \to \Sigma^-\pi^+\pi^+$.

The cuts applied to get the distribution are:

- $L/\sigma > 8$
- $pvtx < 10$
- $\chi^2_{\rm sec} < 6$
- $p_T^2 > 0.5$ (GeV/c)^2
- $p_{hyp} > 80$ GeV/c

- $scut > 4$
- $\sigma < 0.08cm$
- $\mathcal{L}(\pi) > 0.1$ for one of the pions
- Σ^- and proton beam

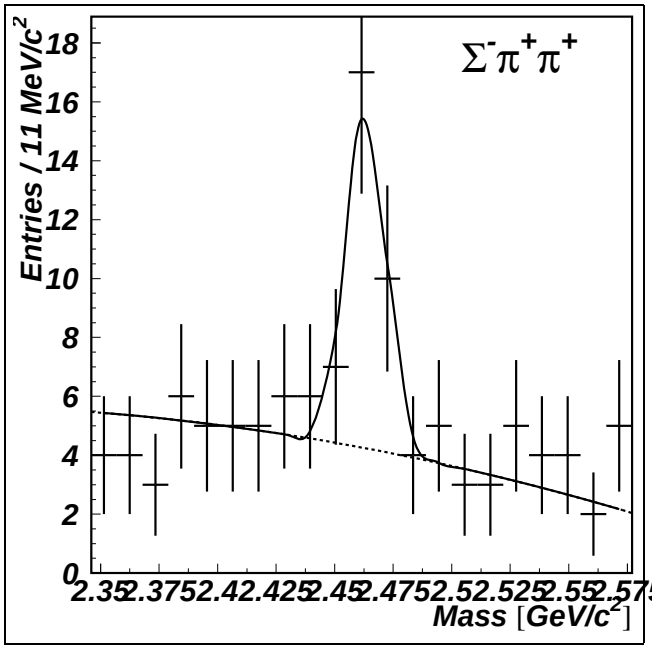

Figure 6.21: Invariant mass distribution for $\Sigma^-\pi^+\pi^+$ in the Ξ_c^+ mass region with $\Xi_c^+ \to \Xi^-\pi^+\pi^+$ reflection removed (same as Figure 6.20 but close up to the Ξ_c^+ invariant mass).

The reflection removed in this channel is:

1. Ambiguous identification of the Σ^-: the invariant mass for $\Xi^-\pi^+\pi^+$ is reconstructed instead of $\Sigma^-\pi^+\pi^+$. A peak around $2468\,\mathrm{MeV}/c^2$ corresponding to a Ξ_c^+ is seen. This reflection barely affects the invariant mass distribution; however it will be important in the reconstruction of the Λ_c^+ in this channel. Figure 6.22 shows the invariant mass distribution for $\Xi^-\pi^+\pi^+$ using the events in the reconstruction for $\Sigma^-\pi^+\pi^+$. The events that are $\pm 12\,\mathrm{MeV}/c^2$ around this peak are eliminated from the original distribution in $\Sigma^-\pi^+\pi^+$.

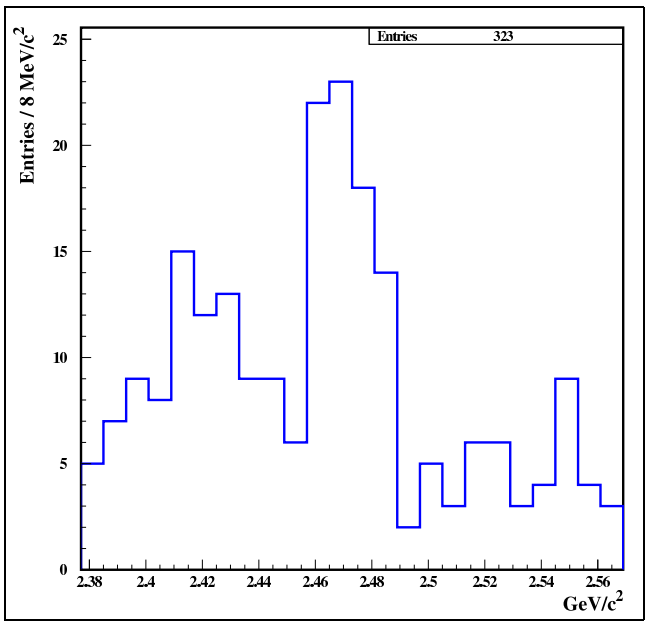

Figure 6.22: Invariant mass distribution for $\Xi^-\pi^+\pi^+$ "reflected" from the inv. mass dist. for $\Sigma^-\pi^+\pi^+$ due to a wrong identification of the Σ^-.

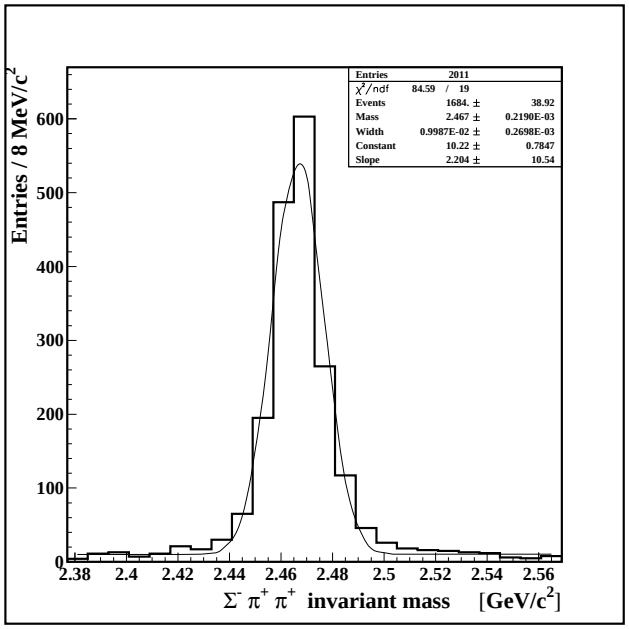

Figure 6.23: Invariant mass distribution for $\Sigma^-\pi^+\pi^+$ from Monte Carlo in the Ξ_c^+ mass region with $p_T = 1.0$ and $n = 2.5$.

6.1.8.2 Simulation

Figure 6.23 shows the corresponding invariant mass distribution for the simulation of this mode with the same cuts applied to data. The generation of events was performed with $p_T = 1.0$ and $n = 2.5$

The file *cascade-sig_pi_pi-n_pi-.dec* used to generate the events is:

```
PARTICLE  CSU0    125   -1  2.467900  1.0  0.5   0.000106
PDG       CSU0   4232
;
DECAY  CSU0
CHANNEL  0 1.0000  SIG-   PI+   PI+
ENDDECAY
;
DECAY SIG-
CHANNEL  0 1.0000   N0    PI-
ENDDECAY
```

6.1.9 $\Lambda_c^+ \rightarrow \Sigma^-\pi^+\pi^+$

6.1.9.1 Data

The invariant mass distribution corresponding to this mode is shown in Figure 6.24.

The cuts applied to get this distribution are:

- $L/\sigma > 9$
- $pvtx < 4$
- $\chi^2_{\text{sec}} < 5$
- $p_T^2 > 0.3$ $(\text{GeV}/c)^2$
- $scut > 4$
- $\sigma < 0.17cm$
- Σ^- and proton beam

As it was mentioned before, the reflection observed is an ambiguous identification of the Σ^-: the invariant mass of $\Xi^-\pi^+\pi^+$ is reconstructed instead of $\Sigma^-\pi^+\pi^+$. A peak around $2468\,\text{MeV}/c^2$ corresponding to a Ξ_c^+ is seen (Figure 6.25).

The events $\pm 10\,\text{MeV}/c^2$ around the Ξ_c^+ mass are removed from the original distribution for Λ_c^+. The resulting invariant mass distribution is shown in Figure 6.26. The number of events is determined with a Gaussian plus a linear fit with a fixed width of $11.1\,\text{MeV}/c^2$ given by Monte Carlo (Figure 6.27), resulting in 151 ± 19 events.

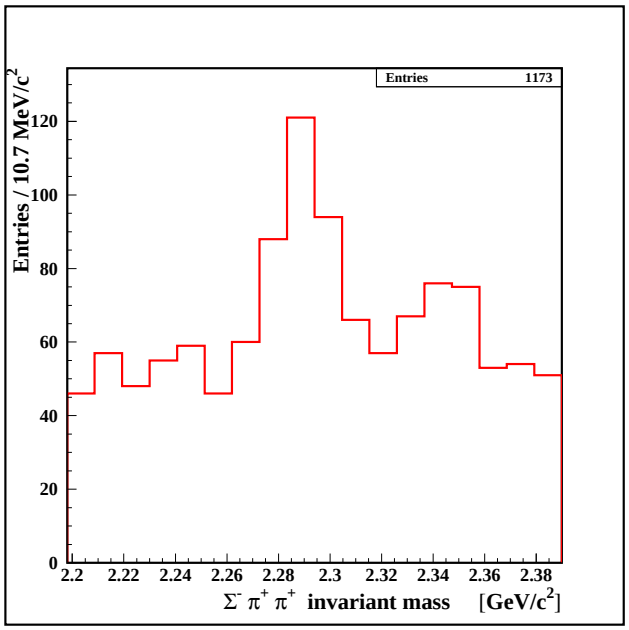

Figure 6.24: Invariant mass distribution for $\Sigma^-\pi^+\pi^+$ in the Λ_c^+ mass region (no reflections have been removed and a different set of cuts was applied in comparison to those in Figure 6.12).

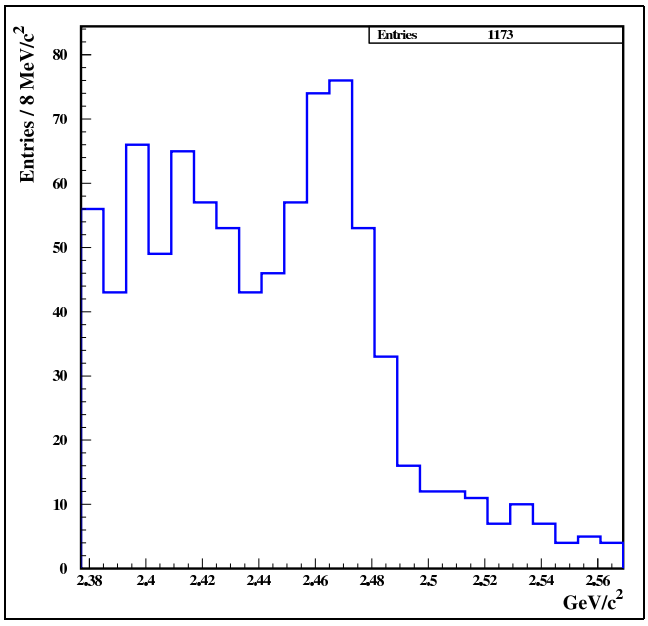

Figure 6.25: Invariant mass distribution for $\Xi^-\pi^+\pi^+$ "reflected" from the inv. mass dist. for $\Sigma^-\pi^+\pi^+$ due to a wrong identification of the Σ^-.

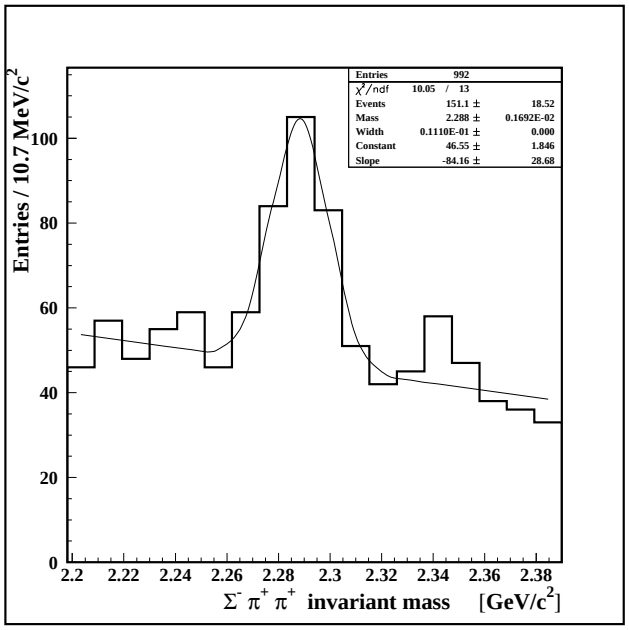

Figure 6.26: Invariant mass distribution for $\Sigma^-\pi^+\pi^+$ in the Λ_c^+ mass region with $\Xi_c^+ \to \Xi^-\pi^+\pi^+$ reflection removed.

6.1.9.2 Simulation

Figure 6.27 shows the corresponding invariant mass distribution for the simulation of this mode with the same cuts applied to data. The generation of events was performed with $p_T = 1.0$ and $n = 2.5$

The file *lambda-sig_pi_pi-n_pi-.dec* used to generate the events is:

```
PARTICLE  LAMC   123   -1  2.285000  1.0  0.5   0.000060
PDG       LAMC       4122
;
DECAY  LAMC
CHANNEL  0 1.0000  SIG-   PI+   PI+
ENDDECAY
;
DECAY SIG-
CHANNEL  0 1.0000   N0    PI-
ENDDECAY
```

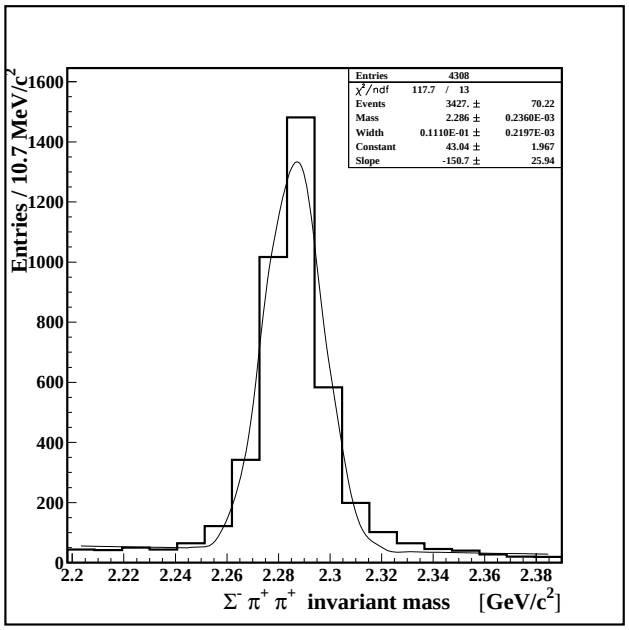

Figure 6.27: Invariant mass distribution for $\Sigma^-\pi^+\pi^+$ from Monte Carlo in the Λ_c^+ mass region with $p_T = 1.0$ and $n = 2.5$.

6.2 $\Xi_c^+ \to \Xi^- K^+ \pi^+$ and $\Xi_c^+ \to \Sigma^+ K^+ \pi^-$

Two more modes are considered as an example of future activities related to branching ratios of the charm-strange baryon Ξ_c^+.

The decay modes presented in this section are reported because they have a similar topology to the decays introduced earlier: a hyperon plus two mesons (pions and kaons); besides, they were consired in the blind analysis of the reflections.

The first mode, $\Xi_c^+ \to \Xi^- K^+ \pi^+$, is a Cabibbo-suppressed decay. Its invariant mass is shown in Figure 6.28. Using the counting method, 7.0 ± 2.6 events are found over a background of 4.0 ± 2.0 events.

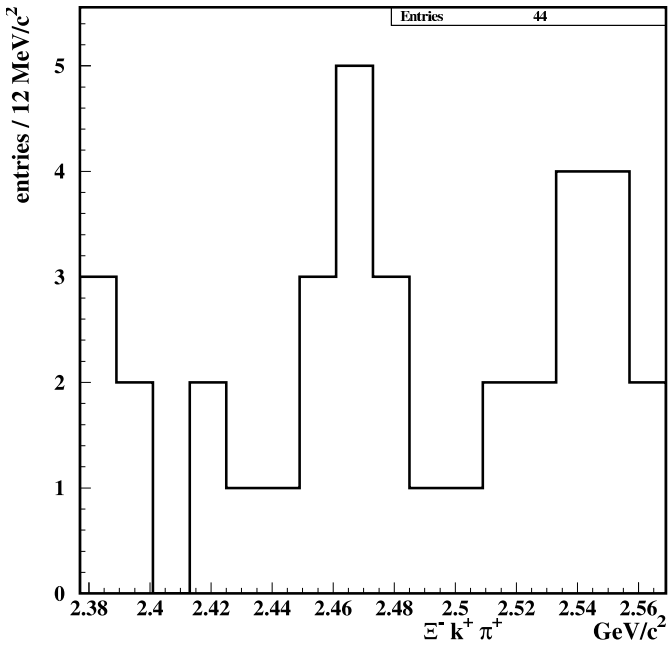

Figure 6.28: Invariant mass distribution for $\Xi^- K^+ \pi^+$ in the Ξ_c^+ mass region.

The second mode, $\Xi_c^+ \to \Sigma^+ K^+ \pi^-$, is a doubly Cabibbo-suppressed decay. Its invariant mass is shown in Figure 6.29. Using the counting method, 9.0 ± 3.0 events are found over a background of 7.0 ± 2.6 events. The decay $\Xi_c^+ \to \Sigma^+ K^+ \pi^-$ would be the first doubly Cabibbo-suppressed reported decay of the Ξ_c^+.

The signal significances are about 3.5 and 3.4, respectively, considering the most enthusiastic calculation $S/\sqrt{B}$.

More studies are needed to clear the signals with a different set of cuts, so a larger samples and statistical significances can be obtained, moreover, some reflections can be observed in the invariant mass distributions. The branching ratios are not either measured since it is necessary to perform the systematical studies for all the variables involved in the analysis and

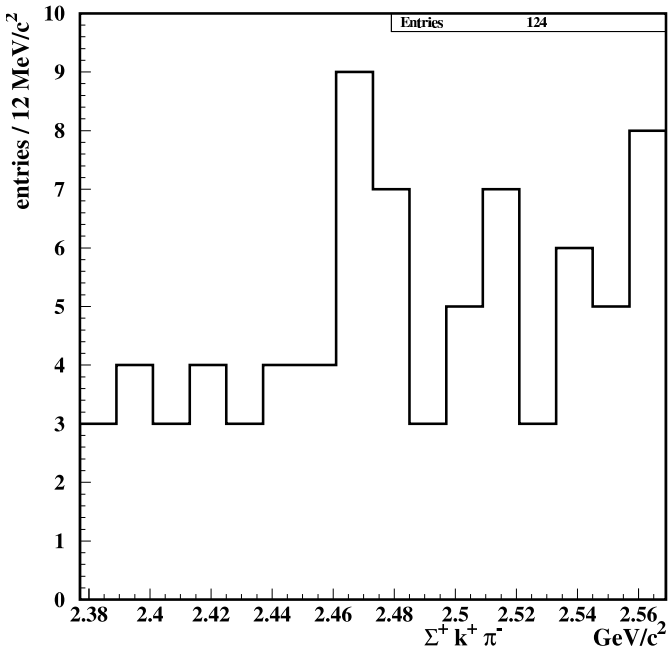

Figure 6.29: Invariant mass distribution for $\Sigma^+ K^+ \pi^-$ in the Ξ_c^+ mass region.

undoubtedly a Monte Carlo simulation is crucial to evaluate the efficiencies, which are expected to be similar to the modes previously presented.

There have been observed some other decay modes, besides the two modes described here: $\Lambda_c^+ \to pK^+\pi^-$ and $D_s^+ \to K^+K^+\pi^-$, both doubly Cabibbo-suppressed decays, and more rare decays can be observed using the SELEX spectrometer in future analysis. These signals are not enough to be reported in a publication; they are presented as part of a set of activities that can be performed in the future, in order to continue with the study of the charm-strange baryon Ξ_c^+ and some other charm particles.

6.3 Resonances

Dalitz plots have been made in order to verify the possible resonances that may appear in the Ξ_c^+ decay modes. Figure 6.30 shows the plots for the decay modes $\Xi_c^+ \to \Sigma^+\pi^-\pi^+$ and $\Xi_c^+ \to \Sigma^-\pi^+\pi^+$.

It is observed that due to the low number of events is very difficult to identify a possible resonance, so the projections to the corresponding axes where particles may form a resonance are analyzed. Projections are made for the signal region and a sideband containing the same number of background events, where the background is only distributed to the left due to the cutoff in the invariant mass, since this study was done before the re-running over the data, which gave a wider mass window.

The first decay mode analyzed is $\Xi_c^+ \to \Sigma^+\pi^-\pi^+$, where the first pro-

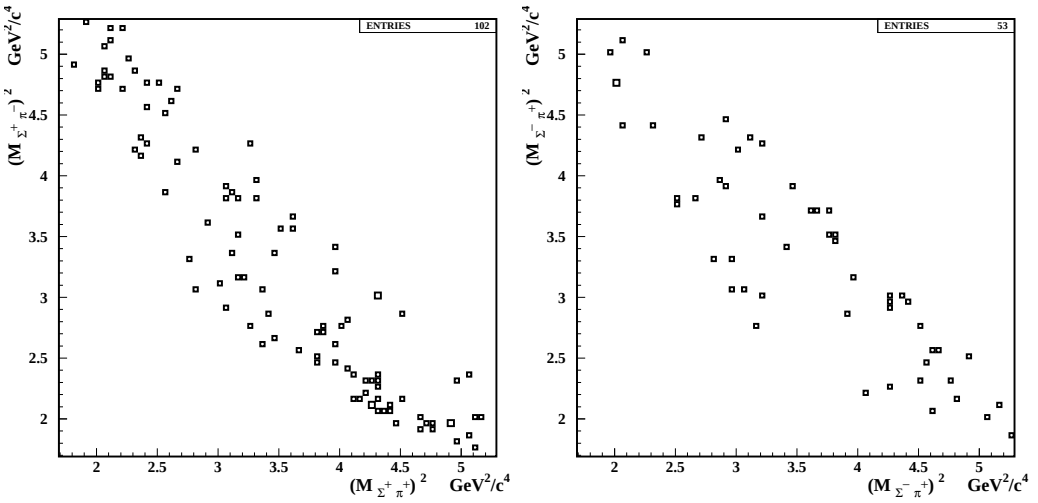

Figure 6.30: Dalitz plot for $\Xi_c^+ \to \Sigma^+\pi^-\pi^+$ and $\Xi_c^+ \to \Sigma^-\pi^+\pi^+$ decay modes.

jection observed in Figure 6.31, corresponds to the $\pi^-\pi^+$ combination and the second projection observed in Figure 6.32, to the $\Sigma^+\pi^-$ combination. Distributions in blue correspond to the signal region, while distributions in red correspond to the left sideband region; moreover the sideband subtraction is also shown. Projection for the $\Sigma^+\pi^+$ combination is not shown since there are not doubly charged resonances (Δ^{++}, for example) decaying to the daughter particles of this Ξ_c^+ decay.

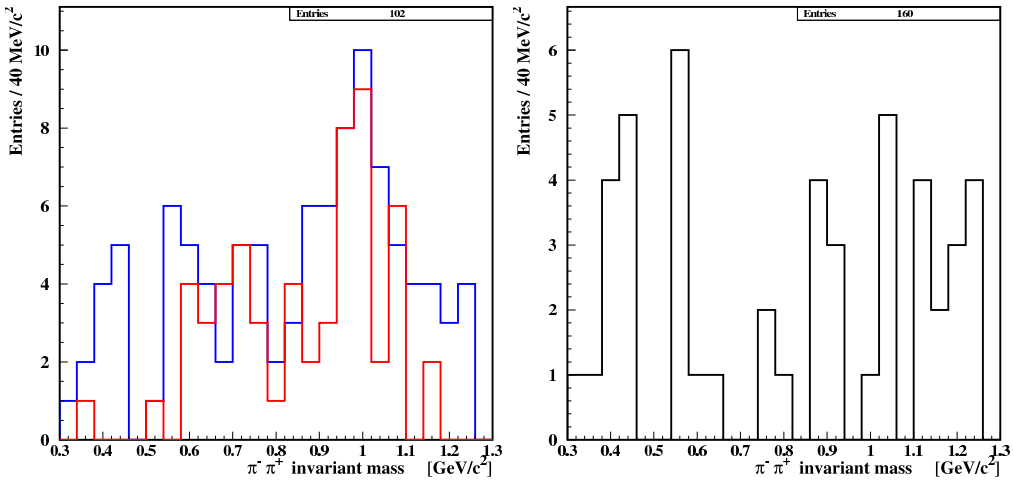

Figure 6.31: $\pi^-\pi^+$ invariant mass for the decay $\Xi_c^+ \to \Sigma^+\pi^-\pi^+$ (left), where the blue histogram corresponds to the signal region and the red histogram corresponds to the sideband region. Subtracted sideband is also shown (right).

There is no clear evidence for a resonance in the decay since it is observed that the background and the signal regions have a similar behavior. If some Ξ_c^+ particles decay via a resonance, then, they are a small fraction of the

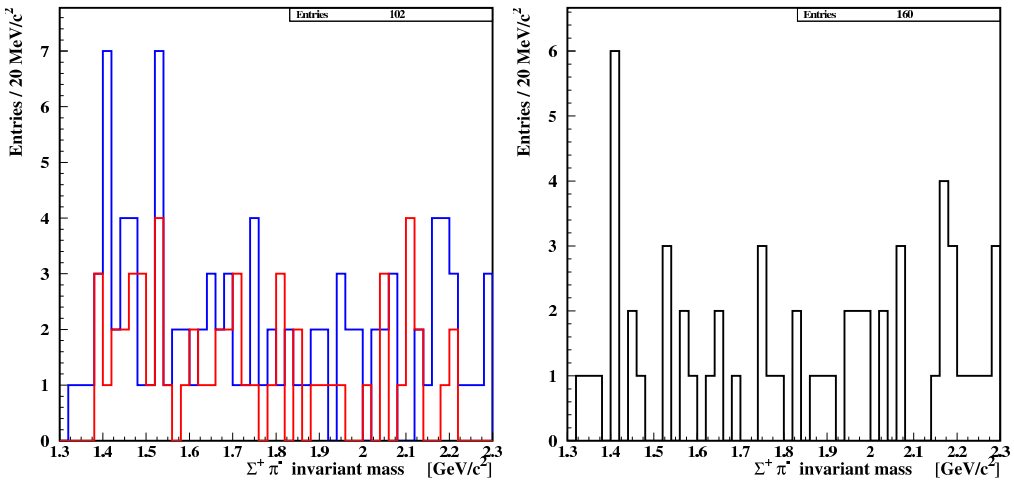

Figure 6.32: $\Sigma^+\pi^-$ invariant mass for the decay $\Xi_c^+ \to \Sigma^+\pi^-\pi^+$ (left), where the blue histogram corresponds to the signal region and the red histogram corresponds to the sideband region. Subtracted sideband is also shown (right).

sample and it is necessary to have a larger sample of events in order to get a value for that fraction.

The second decay mode analyzed is $\Xi_c^+ \to \Sigma^-\pi^+\pi^+$, where the first projection observed in Figure 6.33, corresponds to one $\Sigma^-\pi^+$ combination and the second projection observed in Figure 6.34 to the other $\Sigma^-\pi^+$ combination; as in the other decay, the distributions in blue correspond to the signal region, while distributions in red correspond to the left sideband region; besides, the sideband subtraction is also shown. There is not a doubly charged resonance for mesons, so the $\pi^+\pi^+$ projection is not shown.

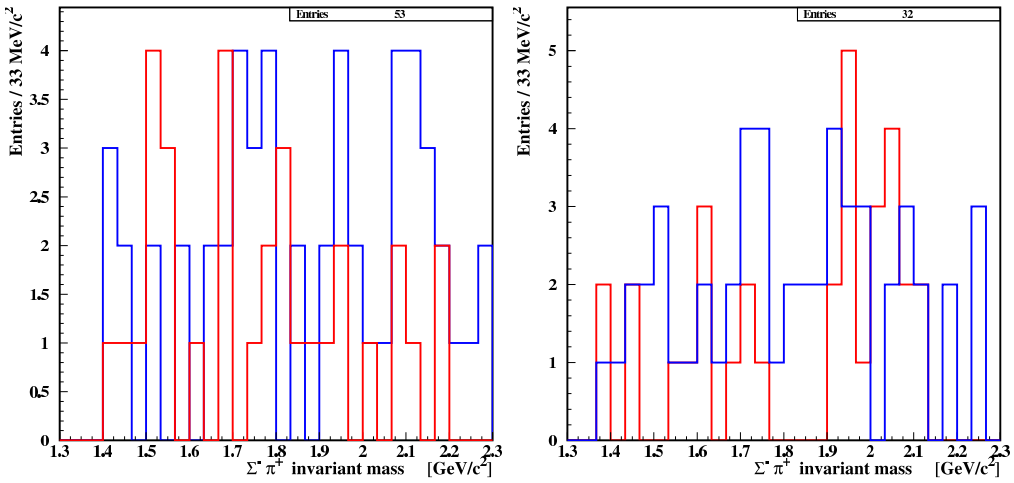

Figure 6.33: $\Sigma^-\pi^+$ invariant mass for the decay $\Xi_c^+ \to \Sigma^-\pi^+\pi^+$ (left), where the blue histogram corresponds to the signal region and the red histogram corresponds to the sideband region. Subtracted sideband is also shown (right).

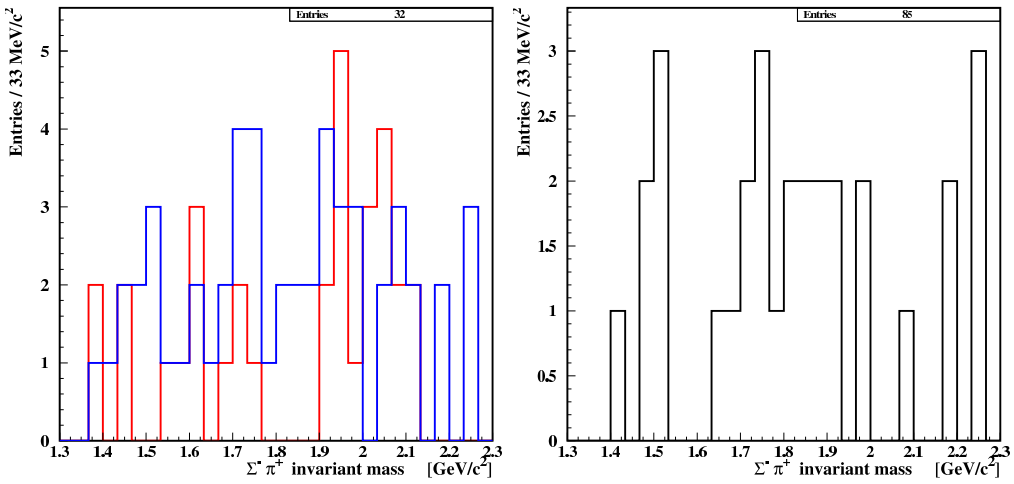

Figure 6.34: $\Sigma^-\pi^+$ invariant mass for the decay $\Xi_c^+ \to \Sigma^-\pi^+\pi^+$ (left), where the blue histogram corresponds to the signal region and the red histogram corresponds to the sideband region. Subtracted sideband is also shown (right).

There is no clear evidence for a resonance in this decay mode. As in the other decay, it is necessary to have a larger sample of events in order to get a fraction of Ξ_c^+ particles decaying via a resonance since this value is small.

The analysis for the presence of resonances in the sample of the new decay modes was performed for the distributions reported as evidence, but the same study was done for the distributions where the branching ratio is measured and the results did not change.

Finally, the $\Xi^-\pi^+\pi^+$ decay is also checked. Figure 6.35 shows the corresponding Dalitz plot and Figures 6.36 and 6.37 show the projections where there is a possibility to have a resonance.

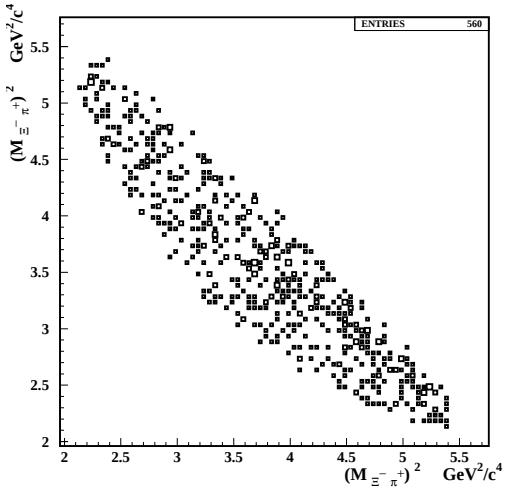

Figure 6.35: Dalitz plot for $\Xi_c^+ \to \Xi^-\pi^+\pi^+$ decay mode.

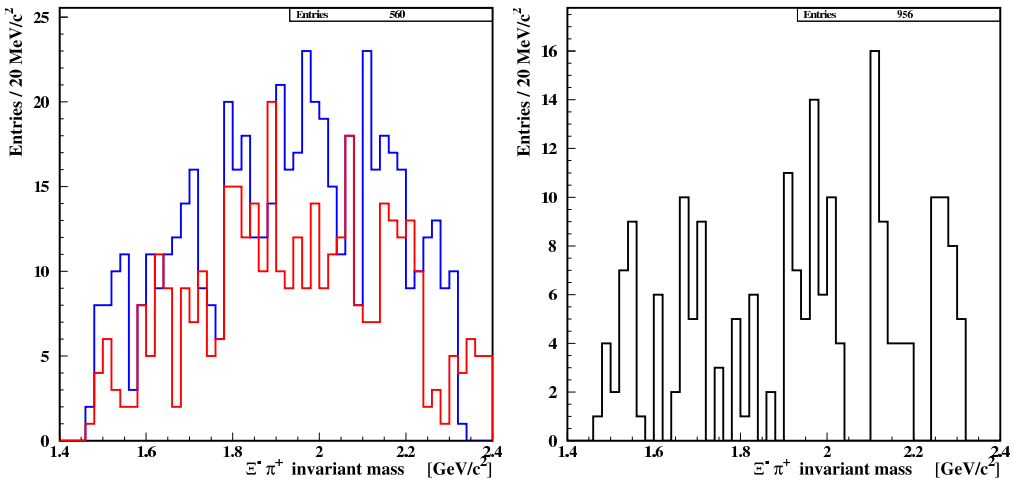

Figure 6.36: $\Xi^-\pi^+$ invariant mass for the decay $\Xi_c^+ \to \Xi^-\pi^+\pi^+$ (left), where the blue histogram corresponds to the signal region and the red histogram corresponds to the sideband region. Subtracted sideband is also shown (right).

The first projection observed in Figure 6.36, corresponds to one $\Xi^-\pi^+$ combination and the second projection observed in Figure 6.37, to the other $\Xi^-\pi^+$ combination. As in the other decays, the distributions in blue correspond to the signal region, while distributions in red correspond to the sideband region (left-right); besides, the sideband subtraction is also shown. For the reference mode, the sideband was taken from both sides of the signal in the invariant mass distribution since there is not a cutoff in this decay mode.

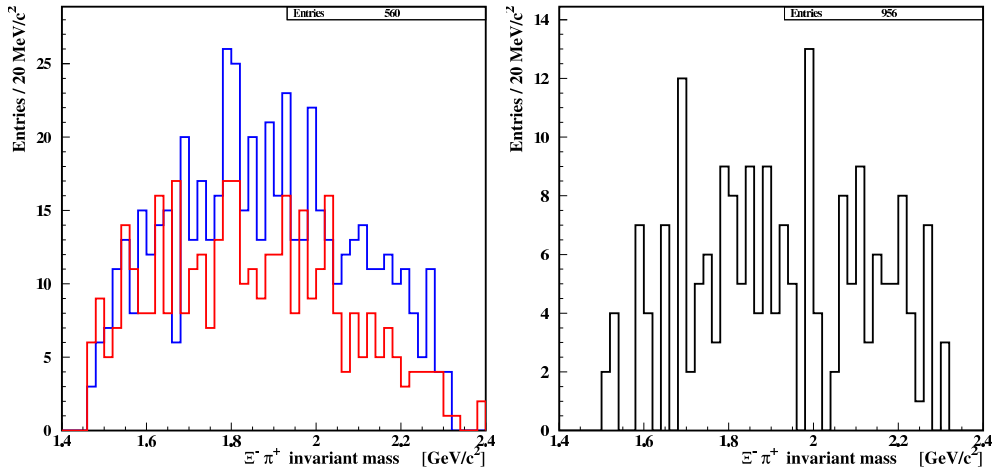

Figure 6.37: $\Xi^-\pi^+$ invariant mass for the decay $\Xi_c^+ \to \Xi^-\pi^+\pi^+$ (left), where the blue histogram corresponds to the signal region and the red histogram corresponds to the sideband region. Subtracted sideband is also shown (right).

There is not clear evidence for a resonant state neither in the Dalitz plot

nor in the projections, being the $\Xi^-\pi^+$ channel the only combination for a possible resonance. Undoubtedly, more studies are needed with a larger sample of events.

6.4 Branching Ratio Results

The results obtained for the branching ratio analysis performed are presented in this section; the absolute and relative efficiencies, the number of events found in SELEX data and the final branching ratios are included. It is important to note that the cuts applied to all the Ξ_c^+ and Λ_c^+ decay modes are very similar. Table 6.3 shows the applied cuts, that are different to the ones used in the evidence of the signals because in the determination of those peaks each decay mode was considered independently while in the branching ratio measurement two decay modes are divided, so the cuts are fixed to be the same between them in order to reduce and even to cancel some systematical dependence of the variables involved in the analysis. The main difference between the set of cuts for the evidence and the cuts for the branching ratio measurement is the requirement of having both pions in the RICH in this last case. This is necessary in order to keep the systematical error under control, so there are not fluctuations of the branching ratio as function of any variable.

Branching Ratio	Ξ_c^+ Modes	L/σ	$pvtx$	$\sum p_T^2$ [GeV$^2/c^2$]	χ^2_{sec}	scut	σ [cm]
BR_1	$\Sigma^+\pi^-\pi^+$ $\Xi^-\pi^+\pi^+$	> 13	< 13	> 0.35	< 8	> 8	< 0.10
BR_2	$\Sigma^-\pi^+\pi^+$ $\Xi^-\pi^+\pi^+$	> 13	< 10	> 0.35	< 8	> 8	< 0.10
BR_3	$\Sigma^-\pi^+\pi^+$ $\Sigma^+\pi^-\pi^+$	> 13	< 10	> 0.35	< 8	> 8	< 0.10
BR_4	$pK^-\pi^+$ $\Xi^-\pi^+\pi^+$	> 11	< 13	> 0.30	< 8	> 8	< 0.10

Table 6.3: Cuts applied for the different Ξ_c^+ decay modes.

Branching Ratio	Λ_c^+ Modes	L/σ	$pvtx$	$\sum p_T^2$ [GeV$^2/c^2$]	χ^2_{sec}	scut	σ [cm]
BR_5	$\Sigma^+\pi^-\pi^+$ $pK^-\pi^+$	> 11	< 7	> 0.35	< 4	> 8	< 0.10
BR_6	$\Sigma^-\pi^+\pi^+$ $\Sigma^+\pi^-\pi^+$	> 11	< 4	> 0.40	< 4	> 8	< 0.10
BR_7	$\Sigma^-\pi^+\pi^+$ $pK^-\pi^+$	> 11	< 4	> 0.40	< 4	> 8	< 0.10

Table 6.4: Cuts applied for the different Λ_c^+ decay modes.

6.4.1 Absolute Efficiency

Tables 6.5 and 6.6 show the efficiencies for each decay mode with $n = 2.5$ and $p_T = 1.0$, where 200,000 events were generated to each of them.

It can be noticed that the absolute efficiencies are smaller for the decay modes where a hyperon is produced ($\Sigma^{\pm}$, Ξ^{-}) than those for the decay mode $pK^{-}\pi^{+}$, due to the lifetime of the hyperons ($\sim 10^{-10}$ sec.), which is small compared to the other particles (p, K^{-} and π^{+}); so the hyperons do not live enough to reach some detectors such as the RICH, but at the same time this lifetime is large; so their decay can not be reconstructed in the vertex region. In fact the hyperon reconstruction code only finds hyperons that decay before reaching the M2 spectrometer, which considerably decreases the efficiency.

Branching Ratio	Ξ_c^+ Modes	Reconstructed Events	Efficiency [%]
BR_1	$\Sigma^+\pi^-\pi^+$	1173 ± 38	0.586
	$\Xi^-\pi^+\pi^+$	1649 ± 37	0.825
BR_2	$\Sigma^-\pi^+\pi^+$	1977 ± 46	0.988
	$\Xi^-\pi^+\pi^+$	1601 ± 38	0.800
BR_3	$\Sigma^-\pi^+\pi^+$	1977 ± 46	0.988
	$\Sigma^+\pi^-\pi^+$	1139 ± 37	0.570
BR_4	$pK^-\pi^+$	8328 ± 95	4.164
	$\Xi^-\pi^+\pi^+$	1831 ± 40	0.915

Table 6.5: Absolute efficiency for the different Ξ_c^+ decay modes.

Branching Ratio	Λ_c^+ Modes	Reconstructed Events	Efficiency [%]
BR_5	$\Sigma^+\pi^-\pi^+$	584 ± 26	0.292
	$pK^-\pi^+$	4734 ± 68	2.367
BR_6	$\Sigma^-\pi^+\pi^+$	868 ± 32	0.434
	$\Sigma^+\pi^-\pi^+$	482 ± 27	0.241
BR_7	$\Sigma^-\pi^+\pi^+$	868 ± 32	0.434
	$pK^-\pi^+$	3846 ± 62	1.923

Table 6.6: Absolute efficiency for the different Λ_c^+ decay modes.

6.4.2 Number of Events

Figures 6.38 and 6.39 show the invariant mass distributions to each decay mode with a Gaussian plus a linear fit. The decay modes are $\Sigma^+\pi^-\pi^+$, $\Sigma^-\pi^+\pi^+$, $pK^-\pi^+$, and $\Xi^-\pi^+\pi^+$.

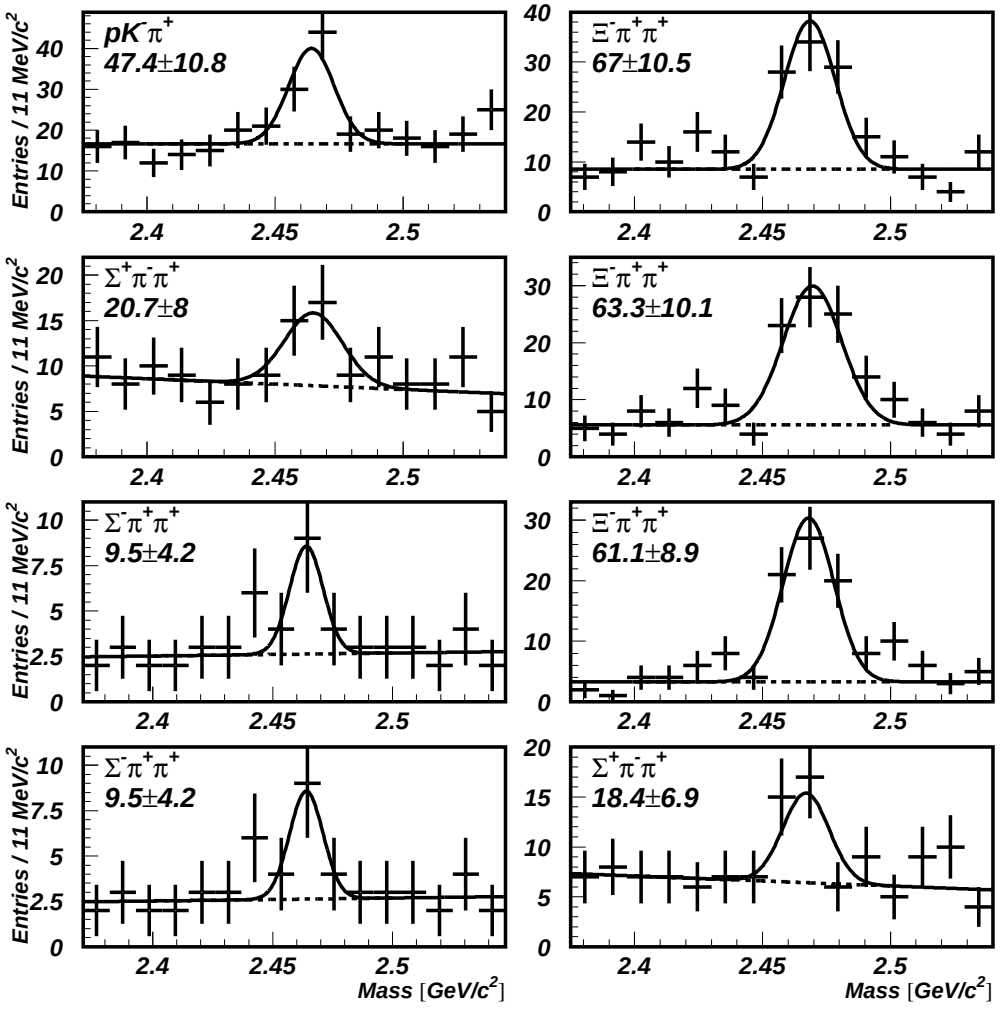

Figure 6.38: Invariant mass distribution of: $pK^-\pi^+$, $\Sigma^+\pi^-\pi^+$, $\Sigma^-\pi^+\pi^+$, $\Xi^-\pi^+\pi^+$, used to determine the relative branching ratios $\Gamma(\Xi_c^+ \to pK^-\pi^+)/\Gamma(\Xi_c^+ \to \Xi^-\pi^+\pi^+)$, $\Gamma(\Xi_c^+ \to \Sigma^+\pi^-\pi^+)/\Gamma(\Xi_c^+ \to \Xi^-\pi^+\pi^+)$, $\Gamma(\Xi_c^+ \to \Sigma^-\pi^+\pi^+)/\Gamma(\Xi_c^+ \to \Xi^-\pi^+\pi^+)$, and $\Gamma(\Xi_c^+ \to \Sigma^-\pi^+\pi^+)/\Gamma(\Xi_c^+ \to \Sigma^+\pi^-\pi^+)$, respectively. Gaussian fit (fixed width given by Monte Carlo) over a linear background to each of the distributions. The event yields are summarized in table 6.9.

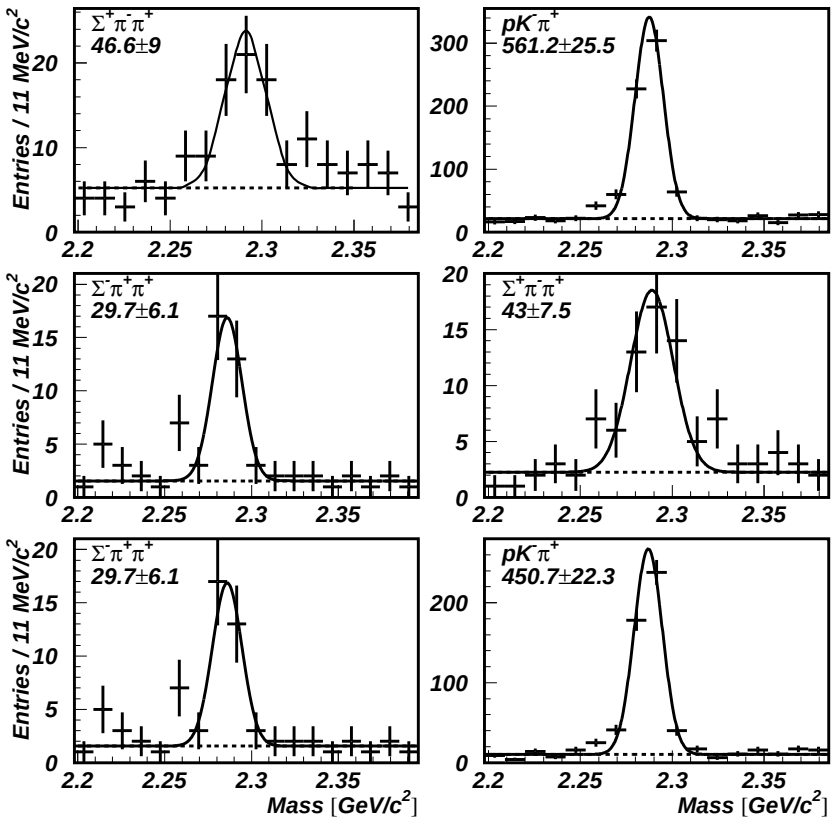

Figure 6.39: Invariant mass distribution of: $\Sigma^+\pi^-\pi^+$, $pK^-\pi^+$, $\Sigma^-\pi^+\pi^+$, used to determine the relative branching ratios $\Gamma(\Lambda_c^+ \to \Sigma^+\pi^-\pi^+)/\Gamma(\Lambda_c^+ \to pK^-\pi^+)$, $\Gamma(\Lambda_c^+ \to \Sigma^-\pi^+\pi^+)/\Gamma(\Lambda_c^+ \to \Sigma^+\pi^-\pi^+)$, and $\Gamma(\Lambda_c^+ \to \Sigma^-\pi^+\pi^+)/\Gamma(\Lambda_c^+ \to pK^-\pi^+)$ respectively. Gaussian fit (fixed width given by Monte Carlo) over a linear background to each of the distributions. The event yields are summarized in table 6.10.

6.4.2.1 Corrected Events

The number of corrected events for each of the modes is added to the number of events obtained from the Gaussian fit, where the methodology for the corrections performed is described in Section 5.3.1.2. A blind analysis was made in order to identify the reflections; some of them have a very small branching ratio, there is one Double Cabibbo-suppressed decay mode, and there is one mode that had not been observed ($\Lambda_c^+ \to p\pi^-\pi^+$, MSc thesis obtained from this work [57]); this is a clear indication that the new decay modes reported in this study are very rare. The removed reflections are listed next, while the number of corrected events for the Ξ_c^+ and Λ_c^+ channels for each reflection is summarized in Tables 6.7 and 6.8.

1. $D^+ \to K^-\pi^+\pi^+$

2. $D^+ \to K^+K^-\pi^+$
3. $D^+ \to K^+\pi^-\pi^+$
4. $D_s^+ \to K^+K^-\pi^+$
5. $D_s^+ \to K^+\pi^-\pi^+$
6. $\Lambda_c^+ \to p\pi^-\pi^+$
7. $\Lambda_c^+ \to \Sigma^-\pi^+\pi^+$
8. $\Lambda_c^+ \to pK^-\pi^+$
9. $\Xi_c^+ \to \Xi^-\pi^+\pi^+$
10. $\Xi_c^+ \to \Sigma^+K^-\pi^+$

BR	Ξ_c^+ Modes	Total	Removed Reflections and Corrected Events
BR_1	$\Sigma^+\pi^-\pi^+$	1.6	$\Xi_c^+ \to \Sigma^+K^-\pi^+$=1.6
	$\Xi^-\pi^+\pi^+$	2.0	$\Lambda_c^+ \to \Sigma^-\pi^+\pi^+$=2.0
BR_2	$\Sigma^-\pi^+\pi^+$	5.0	$D^+ \to K^-K^+\pi^+$=1.5 $D^+ \to \pi^-K^+\pi^+$=1.3 $D_s^+ \to \pi^-K^+\pi^+$=1.8 $\Xi_c^+ \to \Xi^-\pi^+\pi^+$=0.4
	$\Xi^-\pi^+\pi^+$	2.6	$\Lambda_c^+ \to \Sigma^-\pi^+\pi^+$=2.6
BR_3	$\Sigma^-\pi^+\pi^+$	5.0	$D^+ \to K^-K^+\pi^+$=1.5 $D^+ \to \pi^-K^+\pi^+$=1.3 $D_s^+ \to \pi^-K^+\pi^+$=1.8 $D_s^+ \to \pi^-\pi^+\pi^+$=0.4 $D_s^+ \to K^-K^+K^+$=0.9 $\Xi_c^+ \to \Xi^-\pi^+\pi^+$=0.7
	$\Sigma^+\pi^-\pi^+$	1.5	$\Xi_c^+ \to \Sigma^+K^-\pi^+$=1.5
BR_4	$pK^-\pi^+$	14.0	$D^+ \to \pi^+K^-\pi^+$=7.5 $D^+ \to K^+K^-\pi^+$=1.8 $D_s^+ \to K^+K^-\pi^+$=2.7 $\Lambda_c^+ \to p\pi^-\pi^+$=2.0
	$\Xi^-\pi^+\pi^+$	2.4	$\Lambda_c^+ \to \Sigma^-\pi^+\pi^+$=2.4

Table 6.7: Number of corrected events and removed reflections for Ξ_c^+ decay modes.

BR	Λ_c^+ Modes	Total	Removed Reflections and Corrected Events
BR_5	$\Sigma^+\pi^-\pi^+$	3.0	$\Lambda_c^+ \to pK^-\pi^+$=3.0
	$pK^-\pi^+$	0.0	—
BR_6	$\Sigma^-\pi^+\pi^+$	2.2	$\Xi_c^+ \to \Xi^-\pi^+\pi^+$=2.0 $D_s^+ \to \pi^-K^+\pi^+$=0.2
	$\Sigma^+\pi^-\pi^+$	3.4	$\Lambda_c^+ \to pK^-\pi^+$=3.4
BR_7	$\Sigma^-\pi^+\pi^+$	2.2	$\Xi_c^+ \to \Xi^-\pi^+\pi^+$=2.0 $D_s^+ \to \pi^-K^+\pi^+$=0.2
	$pK^-\pi^+$	0.0	—

Table 6.8: Number of corrected events and removed reflections for Λ_c^+ decay modes.

6.4.3 Relative Efficiency

Tables 6.9 and 6.10 summarizes the number of events that are obtained after corrections were performed due to the reflections eliminated from the distributions, and the relative efficiencies used for the measurement of the branching ratios for all the decay modes. The relative efficiency is of crucial importance because it is expected that all the dependences on kinematic variables cancel each other when taking the division. There is not associated error to the relative efficiency because it was arbitrarily reduced, running more events in the simulation, until it was smaller than the statistical error for the number of events, so it does not affect the quadrature sum of the total error. The systematical error is not either included since it is canceled as it will be demonstrated later (see Section 6.5).

Branching Ratio	Ξ_c^+ Modes	Number of Events	Relative Efficiency
BR_1	$\Sigma^+\pi^-\pi^+$	22.3 ± 8.6	1.406
	$\Xi^-\pi^+\pi^+$	65.3 ± 10.4	
BR_2	$\Sigma^-\pi^+\pi^+$	14.5 ± 6.4	0.810
	$\Xi^-\pi^+\pi^+$	63.7 ± 9.3	
BR_3	$\Sigma^-\pi^+\pi^+$	14.5 ± 6.4	0.576
	$\Sigma^+\pi^-\pi^+$	19.9 ± 7.5	
BR_4	$pK^-\pi^+$	61.4 ± 14.0	0.220
	$\Xi^-\pi^+\pi^+$	69.4 ± 10.9	

Table 6.9: Number of events and relative efficiency for Ξ_c^+ decay modes.

Branching Ratio	Λ_c^+ Modes	Number of Events	Relative Efficiency
BR_5	$\Sigma^+\pi^-\pi^+$	49.6 ± 9.6	8.106
	$pK^-\pi^+$	561.2 ± 25.5	
BR_6	$\Sigma^-\pi^+\pi^+$	31.9 ± 6.6	0.555
	$\Sigma^+\pi^-\pi^+$	46.4 ± 8.1	
BR_7	$\Sigma^-\pi^+\pi^+$	31.9 ± 6.6	4.431
	$pK^-\pi^+$	450.7 ± 22.3	

Table 6.10: Number of events and relative efficiency for Λ_c^+ decay modes.

6.4.4 Branching Ratio

As one of the main goals of this analysis: a branching ratio of 0.480±0.202 is reported for the Cabibbo-suppressed decay mode $\Xi_c^+ \to \Sigma^+\pi^-\pi^+$ and a branching ratio of 0.184 ± 0.086 is reported for the Cabibbo-suppressed decay mode $\Xi_c^+ \to \Sigma^-\pi^+\pi^+$, both calculated relative to the reference mode $\Xi^-\pi^+\pi^+$. It is the first measurement of these branching ratios:

$$BR_1 = \frac{\Gamma(\Xi_c^+ \to \Sigma^+\pi^-\pi^+)}{\Gamma(\Xi_c^+ \to \Xi^-\pi^+\pi^+)} = \frac{22.3 \pm 8.6}{65.3 \pm 10.4} \times 1.406 \tag{6.1}$$

$$= \mathbf{0.480 \pm 0.202}$$

$$BR_2 = \frac{\Gamma(\Xi_c^+ \to \Sigma^-\pi^+\pi^+)}{\Gamma(\Xi_c^+ \to \Xi^-\pi^+\pi^+)} = \frac{14.5 \pm 6.4}{63.7 \pm 9.3} \times 0.810 \tag{6.2}$$

$$= \mathbf{0.184 \pm 0.086}$$

The relative branching ratio between the new modes is also measured:

$$BR_3 = \frac{\Gamma(\Xi_c^+ \to \Sigma^-\pi^+\pi^+)}{\Gamma(\Xi_c^+ \to \Sigma^+\pi^-\pi^+)} = \frac{14.5 \pm 6.4}{19.9 \pm 7.5} \times 0.576 \tag{6.3}$$

$$= \mathbf{0.420 \pm 0.244}$$

The branching ratio obtained for the Ξ_c^+ in the $pK^-\pi^+$ decay mode relative to the $\Xi^-\pi^+\pi^+$ reference mode agrees with the previous SELEX measurement [7] and with the value averaged by the PDG [67]. The branching ratios for the control modes for the Λ_c^+ particle also agree with the value measured by CLEO2 [4] and the average from the PDG [67] in the $\Sigma^+\pi^-\pi^+$ channel; and with the value measured by E687 [6] in the $\Sigma^-\pi^+\pi^+$ channel:

$$BR_4 = \frac{\Gamma(\Xi_c^+ \to pK^-\pi^+)}{\Gamma(\Xi_c^+ \to \Xi^-\pi^+\pi^+)} = \frac{61.4 \pm 14.0}{69.4 \pm 10.9} \times 0.220 \tag{6.4}$$

$$= \mathbf{0.194 \pm 0.054}$$

$$BR_5 = \frac{\Gamma(\Lambda_c^+ \to \Sigma^+\pi^-\pi^+)}{\Gamma(\Lambda_c^+ \to pK^-\pi^+)} = \frac{49.6 \pm 9.6}{561.2 \pm 25.5} \times 8.106 \tag{6.5}$$

$$= \mathbf{0.716 \pm 0.144}$$

$$BR_6 = \frac{\Gamma(\Lambda_c^+ \to \Sigma^-\pi^+\pi^+)}{\Gamma(\Lambda_c^+ \to \Sigma^+\pi^-\pi^+)} = \frac{31.9 \pm 6.6}{46.4 \pm 8.1} \times 0.555 \tag{6.6}$$

$$= \mathbf{0.382 \pm 0.104}$$

Another branching ratio for Λ_c^+ is measured, in order to do some comparisons:

$$BR_7 = \frac{\Gamma(\Lambda_c^+ \to \Sigma^-\pi^+\pi^+)}{\Gamma(\Lambda_c^+ \to pK^-\pi^+)} = \frac{31.9 \pm 6.6}{450.7 \pm 22.3} \times 4.431 \tag{6.7}$$

$$= \mathbf{0.314 \pm 0.067}$$

Table 6.11 summarizes the branching ratios measured in this analysis (statistical errors are only calculated) and the α^2-parameter is calculated.

α^2 is defined as the branching ratio corrected for phase space differences and, in the case of comparing Cabibbo-favored and Cabibbo-suppressed modes, for the ratio of the CKM matrix elements ($V_{cd}/V_{cs} = 0.233 \pm 0.001$ [67]), as it was explained in Section 3.4.

Branching Ratio	This Analysis	Other Measurements
$\Gamma(\Xi_c^+ \to \Sigma^+\pi^-\pi^+)$ / $\Gamma(\Xi_c^+ \to \Xi^-\pi^+\pi^+)$	0.480 ± 0.202 $\alpha^2 = 6.38 \pm 2.68$	–
$\Gamma(\Xi_c^+ \to \Sigma^-\pi^+\pi^+)$ / $\Gamma(\Xi_c^+ \to \Xi^-\pi^+\pi^+)$	0.184 ± 0.086 $\alpha^2 = 2.49 \pm 1.16$	–
$\Gamma(\Xi_c^+ \to \Sigma^-\pi^+\pi^+)$ / $\Gamma(\Xi_c^+ \to \Sigma^+\pi^-\pi^+)$	0.420 ± 0.244 $\alpha^2 = 0.43 \pm 0.25$	–
$\Gamma(\Xi_c^+ \to pK^-\pi^+)$ / $\Gamma(\Xi_c^+ \to \Xi^-\pi^+\pi^+)$	0.194 ± 0.054 $\alpha^2 = 2.64 \pm 0.73$	$0.234 \pm 0.047 \pm 0.022$ [64] $0.20 \pm 0.04 \pm 0.02$ [7]
$\Gamma(\Lambda_c^+ \to \Sigma^-\pi^+\pi^+)$ / $\Gamma(\Lambda_c^+ \to pK^-\pi^+)$	0.314 ± 0.067 $\alpha^2 = 0.30 \pm 0.07$	–
$\Gamma(\Lambda_c^+ \to \Sigma^+\pi^-\pi^+)$ / $\Gamma(\Lambda_c^+ \to pK^-\pi^+)$	0.716 ± 0.144 $\alpha^2 = 0.68 \pm 0.14$	$0.74 \pm 0.07 \pm 0.09$ [4] $0.54^{+0.18}_{-0.15}$ [5]
$\Gamma(\Lambda_c^+ \to \Sigma^-\pi^+\pi^+)$ / $\Gamma(\Lambda_c^+ \to \Sigma^+\pi^-\pi^+)$	0.382 ± 0.104 $\alpha^2 = 0.39 \pm 0.11$	$0.53 \pm 0.15 \pm 0.07$ [6]

Table 6.11: Results of the different Branching Ratios measured in this analysis, and comparison to previously published results (if available). Also shown is the α^2-parameter for each branching ratio result.

6.5 Systematical Studies

The systematical studies performed are described in this section. The variables involved in the analysis were L/σ, $\chi^2_{\rm sec}$, pvtx, scut, p_T^2 and n (see Section 5.3.5).

6.5.1 $BR_1 = \frac{\Gamma(\Xi_c^+ \to \Sigma^+\pi^-\pi^+)}{\Gamma(\Xi_c^+ \to \Xi^-\pi^+\pi^+)}$

Results are shown for the branching ratio measured for the decay mode $\Xi_c^+ \to \Sigma^+\pi^-\pi^+$. The errors from one value of the variable (L/σ, $\chi^2_{\rm sec}$, pvtx, scut, p_T^2) to another are correlated (same data are used in the stability plots) so, in order to compare the relative errors between two branching ratio measurements it is important to note that they are smaller than they look.

The values taken for L/σ are 9, 10, 11, 12, 13, 14, 15 and 16, where it can be seen that the branching ratio is stable.

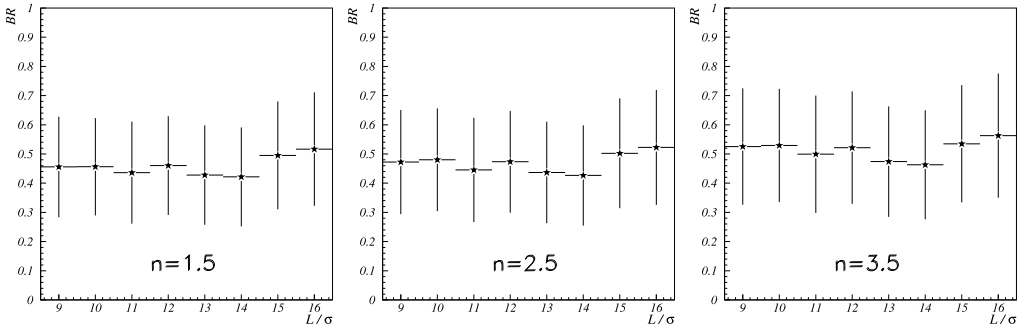

Figure 6.40: Branching ratio stability over L/σ for $\frac{\Gamma(\Xi_c^+ \to \Sigma^+\pi^-\pi^+)}{\Gamma(\Xi_c^+ \to \Xi^-\pi^+\pi^+)}$.

The values taken for $\chi^2_{\rm sec}$ are 3, 4, 5, 6, 7 and 8, where it can also be observed that the branching ratio is stable.

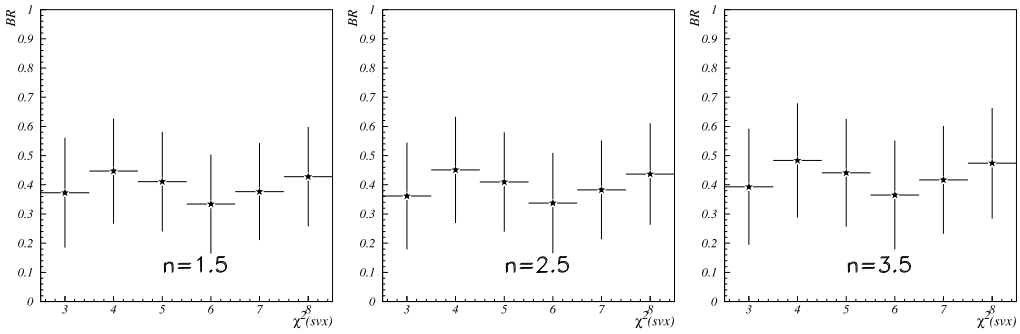

Figure 6.41: Branching ratio stability over $\chi^2_{\rm sec}$ for $\frac{\Gamma(\Xi_c^+ \to \Sigma^+\pi^-\pi^+)}{\Gamma(\Xi_c^+ \to \Xi^-\pi^+\pi^+)}$.

The values taken for pvtx are 10, 11, 12, 13, 14, 15, 16, 17, 18 and 19, where it can also be appreciated that the branching ratio is stable.

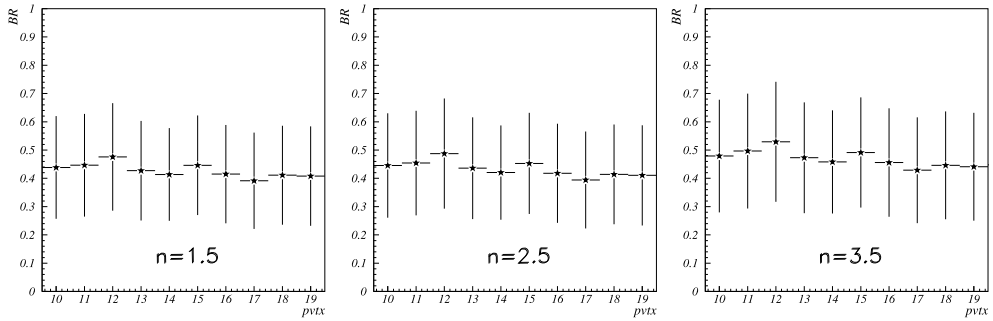

Figure 6.42: Branching ratio stability over pvtx for $\frac{\Gamma(\Xi_c^+ \to \Sigma^+ \pi^- \pi^+)}{\Gamma(\Xi_c^+ \to \Xi^- \pi^+ \pi^+)}$.

The values taken for scut are 3, 4, 5, 6, 7, 8, 9 ,10 and 11, where it can also be observed that the branching ratio is stable.

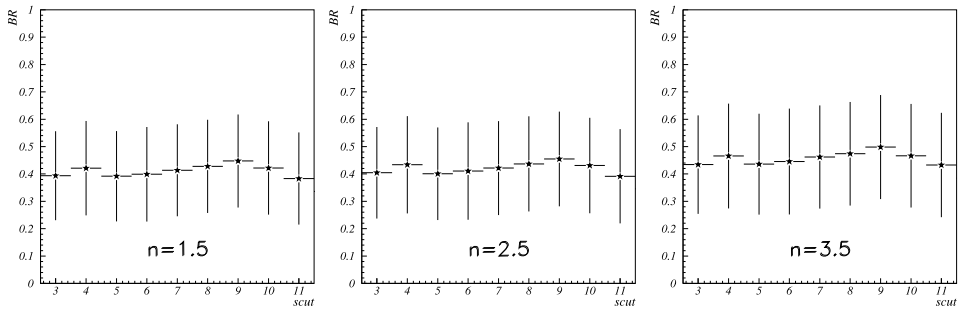

Figure 6.43: Branching ratio stability over scut for $\frac{\Gamma(\Xi_c^+ \to \Sigma^+ \pi^- \pi^+)}{\Gamma(\Xi_c^+ \to \Xi^- \pi^+ \pi^+)}$.

Finally, the values taken for p_T^2 are 0.25, 0.30, 0.35, 0.40, 0.45, 0.50, 0.55 and 0.6, where it can also be seen that the branching ratio is stable.

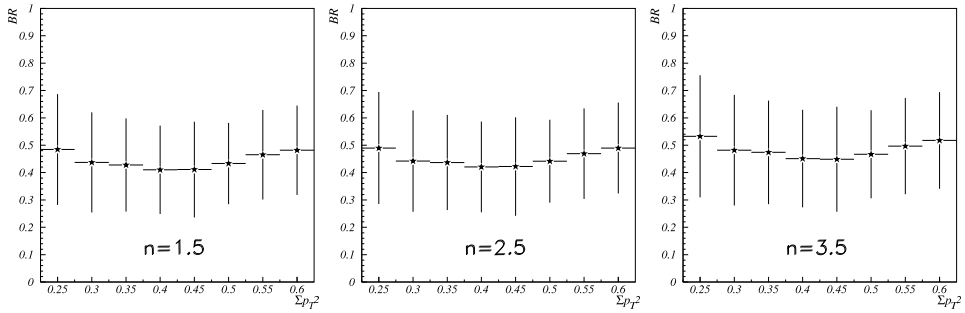

Figure 6.44: Branching ratio stability over p_T^2 for $\frac{\Gamma(\Xi_c^+ \to \Sigma^+ \pi^- \pi^+)}{\Gamma(\Xi_c^+ \to \Xi^- \pi^+ \pi^+)}$.

6.5.2 $BR_2 = \frac{\Gamma(\Xi_c^+ \to \Sigma^- \pi^+ \pi^+)}{\Gamma(\Xi_c^+ \to \Xi^- \pi^+ \pi^+)}$

Results are shown for the branching ratio measured for the decay mode $\Xi_c^+ \to \Sigma^- \pi^+ \pi^+$.

As it was explained in the previous decay mode, the errors from one value of the variable (L/σ, $\chi^2_{\rm sec}$, pvtx, scut, p_T^2) to another are correlated (same data are used in the stability plots) so, in order to compare the relative errors between two branching ratio measurements it is important to note that they are smaller than they look.

The values taken for L/σ are 9, 10, 11, 12, 13, 14, 15 and 16, where it can be seen that the branching ratio is stable.

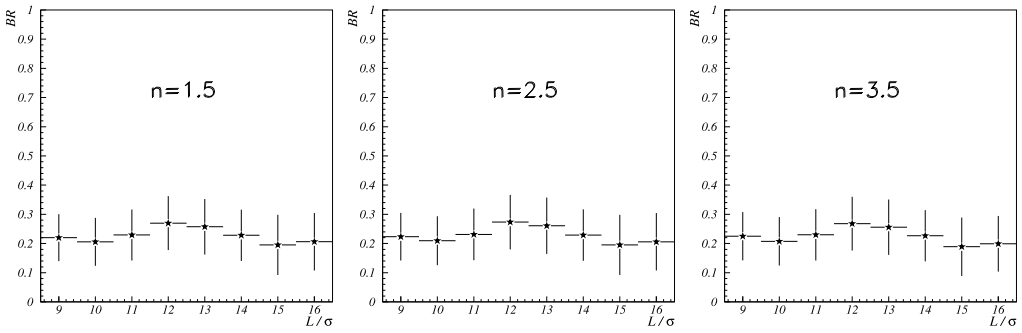

Figure 6.45: Branching ratio stability over L/σ for $\frac{\Gamma(\Xi_c^+ \to \Sigma^- \pi^+ \pi^+)}{\Gamma(\Xi_c^+ \to \Xi^- \pi^+ \pi^+)}$.

The values taken for $\chi^2_{\rm sec}$ are 3, 4, 5, 6, 7 and 8, where it can also be observed that the branching ratio is stable.

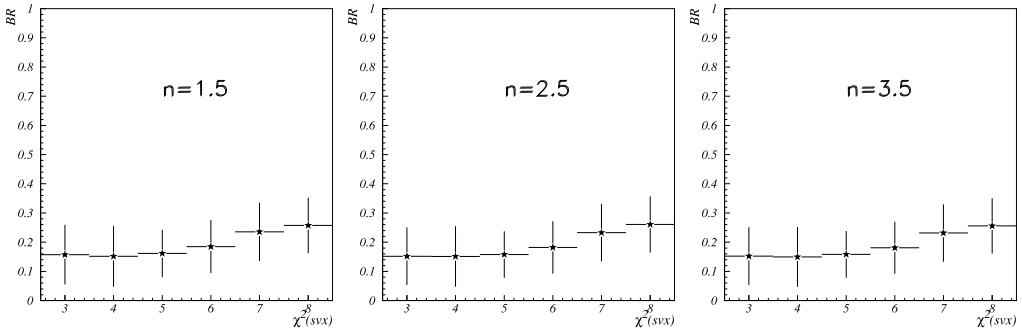

Figure 6.46: Branching ratio stability over $\chi^2_{\rm sec}$ for $\frac{\Gamma(\Xi_c^+ \to \Sigma^- \pi^+ \pi^+)}{\Gamma(\Xi_c^+ \to \Xi^- \pi^+ \pi^+)}$.

The values taken for pvtx are 7, 8, 9, 10, 11, 12, 13, 14, 15 and 16, where it can also be appreciated that the branching ratio is stable.

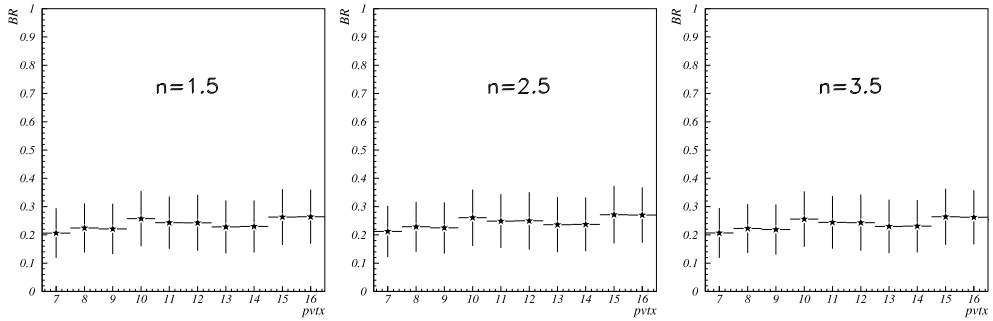

Figure 6.47: Branching ratio stability over pvtx for $\frac{\Gamma(\Xi_c^+ \to \Sigma^- \pi^+ \pi^+)}{\Gamma(\Xi_c^+ \to \Xi^- \pi^+ \pi^+)}$.

The values taken for scut are 3, 4, 5, 6, 7, 8, 9 ,10 and 11, where it can also be observed that the branching ratio is stable.

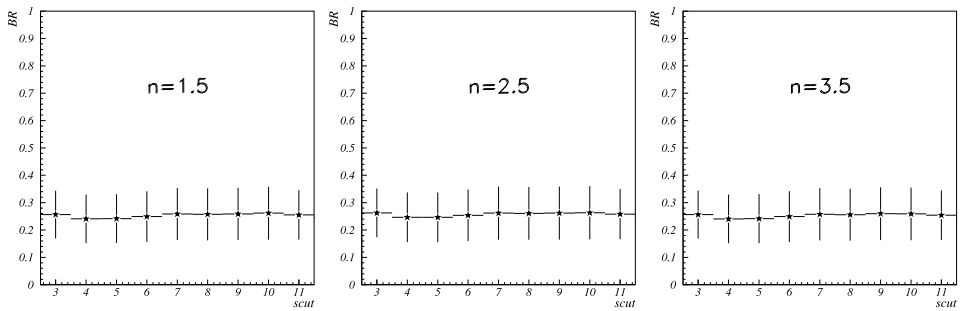

Figure 6.48: Branching ratio stability over scut for $\frac{\Gamma(\Xi_c^+ \to \Sigma^- \pi^+ \pi^+)}{\Gamma(\Xi_c^+ \to \Xi^- \pi^+ \pi^+)}$.

Finally, the values taken for p_T^2 are 0.10, 0.15, 0.20, 0.25, 0.30, 0.35, 0.40 and 0.45, where it can also be observed that the branching ratio is stable.

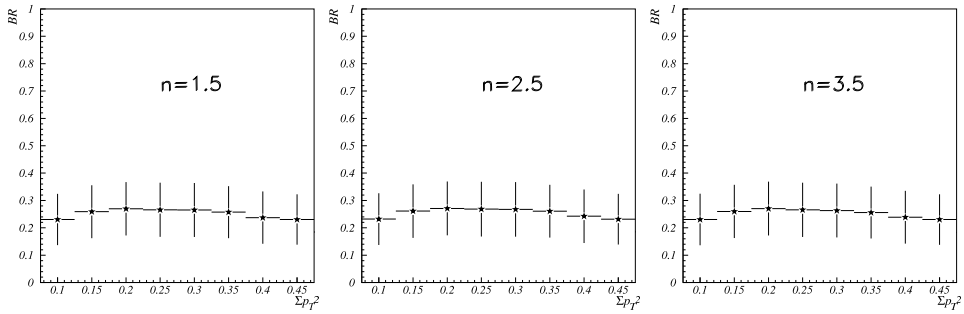

Figure 6.49: Branching ratio stability over p_T^2 for $\frac{\Gamma(\Xi_c^+ \to \Sigma^- \pi^+ \pi^+)}{\Gamma(\Xi_c^+ \to \Xi^- \pi^+ \pi^+)}$.

6.5.3 Control modes

The systematical study is also performed for the control modes. One decay mode for cascade charm and two for lambda charm are shown. The yellow bands indicate previous measurements from SELEX and other experiments.

6.5.3.1 Ξ_c^+ control mode: $BR_4 = \frac{\Gamma(\Xi_c^+ \to pK^-\pi^+)}{\Gamma(\Xi_c^+ \to \Xi^-\pi^+\pi^+)}$

As it can be observed, the measurement of the branching ratio is independent from most of the variables described above, where the yellow band indicates the previous SELEX measurement [7]. The values obtained do not only agree with SELEX results but also with the FOCUS collaboration results [64].

The values taken for L/σ are 10, 11, 12, 13, 14 and 15, where it can be observed that the branching ratio is stable.

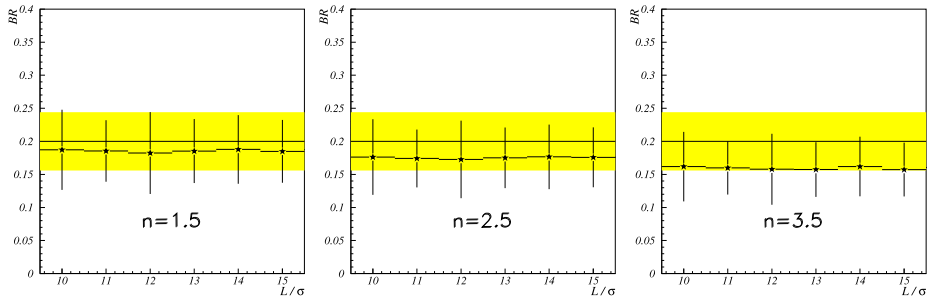

Figure 6.50: Branching ratio stability over L/σ for $\frac{\Gamma(\Xi_c^+ \to pK^-\pi^+)}{\Gamma(\Xi_c^+ \to \Xi^-\pi^+\pi^+)}$; the yellow band indicates the previous SELEX measurement [7].

The values taken for χ^2_{sec} are 3, 4, 5, 6, 7 and 8, where it can be seen that the branching ratio is stable.

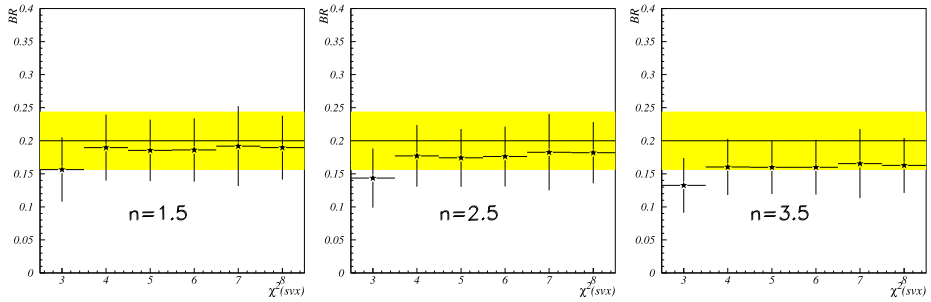

Figure 6.51: Branching ratio stability over χ^2_{sec} for $\frac{\Gamma(\Xi_c^+ \to pK^-\pi^+)}{\Gamma(\Xi_c^+ \to \Xi^-\pi^+\pi^+)}$; the yellow band indicates the previous SELEX measurement [7].

The values taken for pvtx are 8, 9, 10, 11, 12, 13, 14, 15, 16 and 17, where it can also be appreciated that the branching ratio is stable.

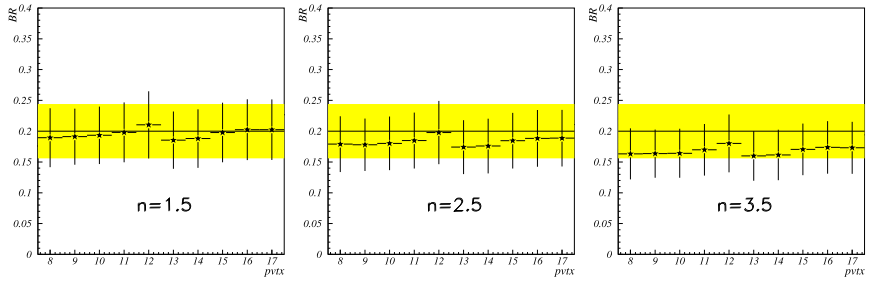

Figure 6.52: Branching ratio stability over pvtx for $\frac{\Gamma(\Xi_c^+ \to pK^-\pi^+)}{\Gamma(\Xi_c^+ \to \Xi^-\pi^+\pi^+)}$; the yellow band indicates the previous SELEX measurement [7].

The values taken for scut are 3, 4, 5, 6, 7, 8, 9, 10 and 11, where it can also be noticed that the branching ratio is stable.

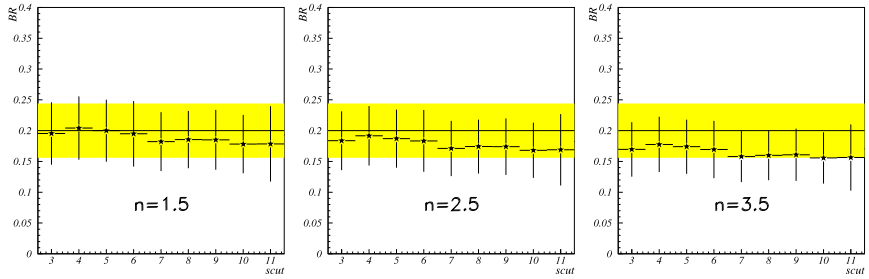

Figure 6.53: Branching ratio stability over scut for $\frac{\Gamma(\Xi_c^+ \to pK^-\pi^+)}{\Gamma(\Xi_c^+ \to \Xi^-\pi^+\pi^+)}$; the yellow band indicates the previous SELEX measurement [7].

Finally, the values taken for p_T^2 are 0.25, 0.30, 0.35, 0.40, 0.45, 0.50 and 0.55, where it can also be observed that the branching ratio is stable.

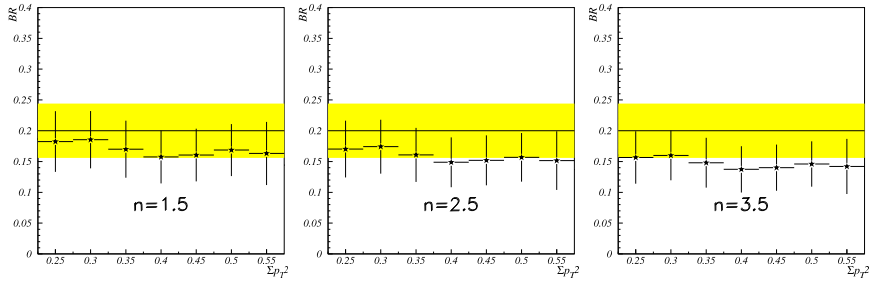

Figure 6.54: Branching ratio stability over p_T^2 for $\frac{\Gamma(\Xi_c^+ \to pK^-\pi^+)}{\Gamma(\Xi_c^+ \to \Xi^-\pi^+\pi^+)}$; the yellow band indicates the previous SELEX measurement [7].

6.5.3.2 Λ_c^+ control mode: $BR_5 = \frac{\Gamma(\Lambda_c^+ \to \Sigma^+\pi^-\pi^+)}{\Gamma(\Lambda_c^+ \to pK^-\pi^+)}$

For this control mode, there is not dependence on any of the variables mentioned above. The yellow band indicates the previous CLEO2 measurement [4]. It is important to note that the L/σ range has changed due to the lifetime difference between the Λ_c^+ and the Ξ_c^+, and in this case, $n = 2.45 \pm 0.18$ for Λ_c^+ production [62].

The values taken for L/σ are 8, 9, 10, 11, 12 and 13, where it can be seen that the branching ratio is stable.

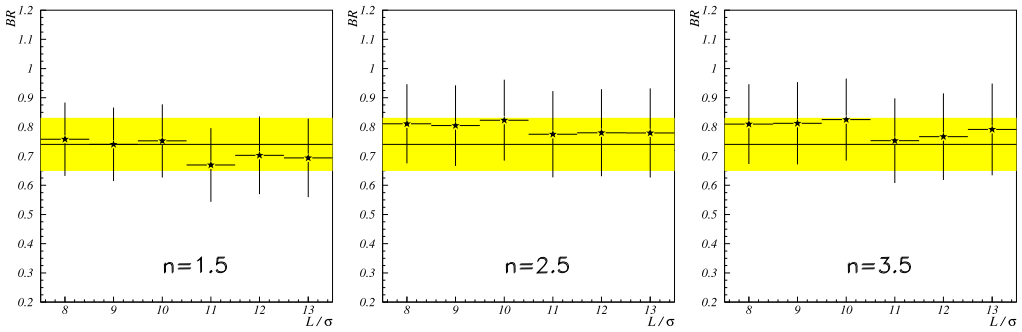

Figure 6.55: Branching ratio stability over L/σ for $\frac{\Gamma(\Lambda_c^+ \to \Sigma^+\pi^-\pi^+)}{\Gamma(\Lambda_c^+ \to pK^-\pi^+)}$; the yellow band indicates the CLEO2 measurement [4] (the most significant one performed up to now).

The values taken for χ^2_{sec} are 3, 4, 5, 6, 7 and 8, where it can also be appreciated that the branching ratio is stable.

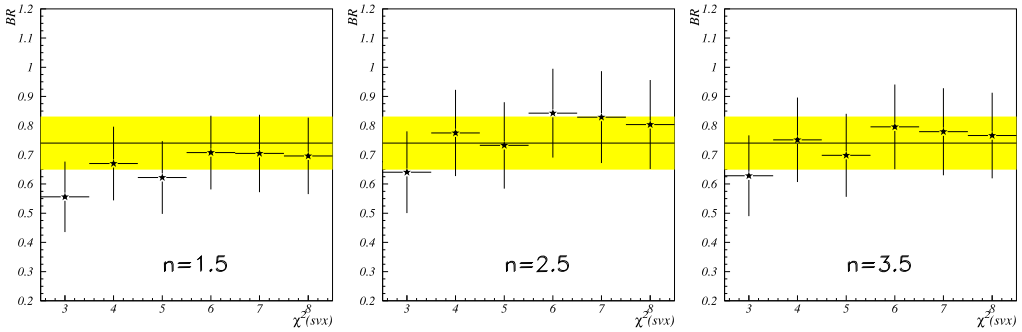

Figure 6.56: Branching ratio stability over χ^2_{sec} for $\frac{\Gamma(\Lambda_c^+ \to \Sigma^+\pi^-\pi^+)}{\Gamma(\Lambda_c^+ \to pK^-\pi^+)}$; the yellow band indicates the CLEO2 measurement [4] (the most significant one performed up to now).

The values taken for pvtx are 4, 5, 6, 7, 8, 9, 10 and 11, where it can also be observed that the branching ratio is stable.

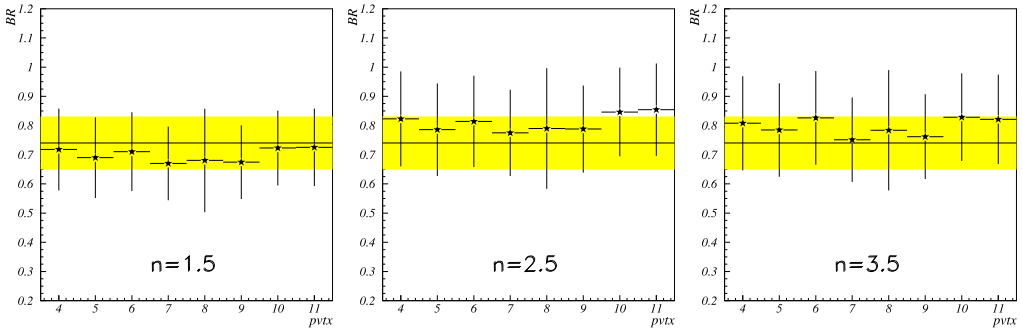

Figure 6.57: Branching ratio stability over pvtx for $\frac{\Gamma(\Lambda_c^+ \to \Sigma^+ \pi^- \pi^+)}{\Gamma(\Lambda_c^+ \to pK^- \pi^+)}$; the yellow band indicates the CLEO2 measurement [4] (the most significant one performed up to now).

The values taken for scut are 3, 4, 5, 6, 7, 8, 9, 10 and 11, where it can also be seen that the branching ratio is stable.

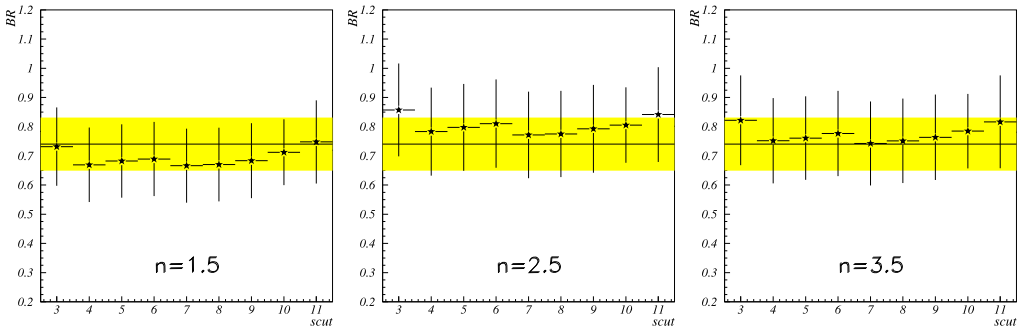

Figure 6.58: Branching ratio stability over scut for $\frac{\Gamma(\Lambda_c^+ \to \Sigma^+ \pi^- \pi^+)}{\Gamma(\Lambda_c^+ \to pK^- \pi^+)}$; the yellow band indicates the CLEO2 measurement [4] (the most significant one performed up to now).

Finally, the values taken for p_T^2 are 0.25, 0.30, 0.35, 0.40, 0.45, 0.50 and 0.55, where it can also be observed that the branching ratio is stable.

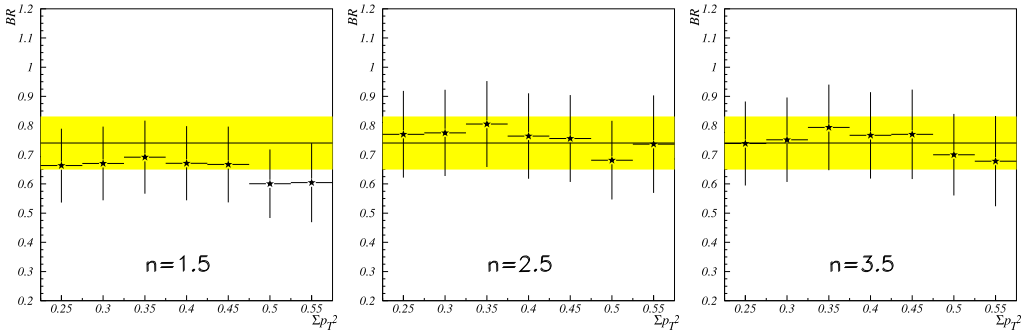

Figure 6.59: Branching ratio stability over p_T^2 for $\frac{\Gamma(\Lambda_c^+ \to \Sigma^+\pi^-\pi^+)}{\Gamma(\Lambda_c^+ \to pK^-\pi^+)}$; the yellow band indicates the CLEO2 measurement [4] (the most significant one performed up to now).

6.5.3.3 Λ_c^+ control mode: $BR_6 = \frac{\Gamma(\Lambda_c^+ \to \Sigma^-\pi^+\pi^+)}{\Gamma(\Lambda_c^+ \to \Sigma^+\pi^-\pi^+)}$

For this control mode, there is no dependence on any of the variables mentioned above. The yellow band indicates the previous E687 measurement [6], the only one performed up to now. It is important to note that the background in the invariant mass distributions for the decay modes reported by the E687 Collaboration does not look as smooth as the ones presented in this study, so it can be appreciated a difference between both measurements, but they are still consistent within errors.

As in the case of the other Λ_c^+ control mode, the L/σ range has changed due to the lifetime difference between the Λ_c^+ and the Ξ_c^+ and, $n = 2.45 \pm 0.18$ for Λ_c^+ production [62].

The values taken for L/σ are 8, 9, 10, 11, 12 and 13, where it can be seen that the branching ratio is stable.

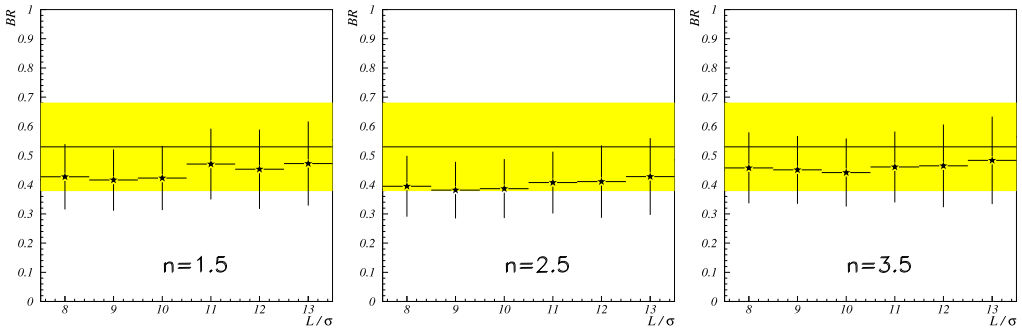

Figure 6.60: Branching ratio stability over L/σ for $\frac{\Gamma(\Lambda_c^+ \to \Sigma^-\pi^+\pi^+)}{\Gamma(\Lambda_c^+ \to \Sigma^+\pi^-\pi^+)}$; the yellow band indicates the E687 measurement [4] (the only one performed up to now).

The values taken for $\chi^2_{\rm sec}$ are 3, 4, 5, 6, 7 and 8, where it can also be appreciated that the branching ratio is stable.

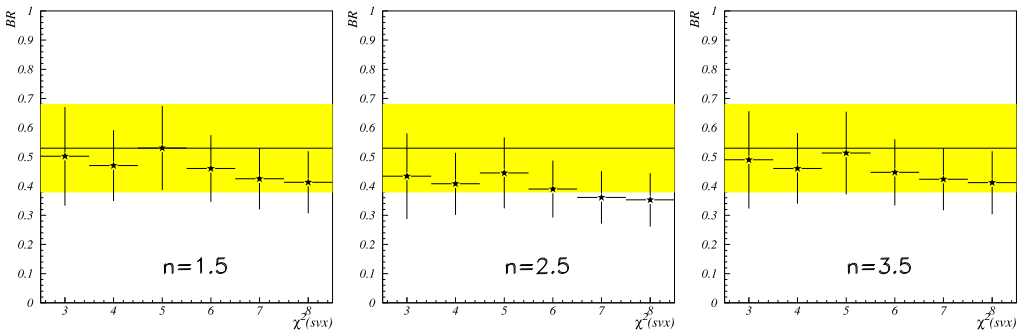

Figure 6.61: Branching ratio stability over $\chi^2_{\rm sec}$ for $\frac{\Gamma(\Lambda_c^+\to\Sigma^-\pi^+\pi^+)}{\Gamma(\Lambda_c^+\to\Sigma^+\pi^-\pi^+)}$; the yellow band indicates the E687 measurement [4] (the only one performed up to now).

The values taken for pvtx are 4, 5, 6, 7, 8, 9, 10 and 11, where it can also be observed that the branching ratio is stable.

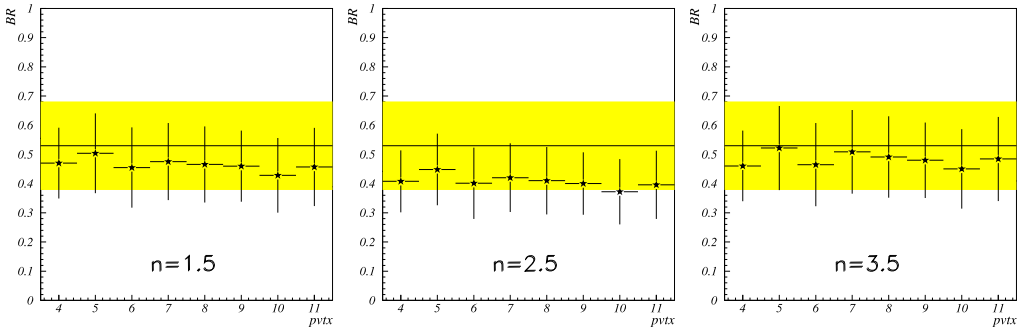

Figure 6.62: Branching ratio stability over pvtx for $\frac{\Gamma(\Lambda_c^+\to\Sigma^-\pi^+\pi^+)}{\Gamma(\Lambda_c^+\to\Sigma^+\pi^-\pi^+)}$; the yellow band indicates the E687 measurement [4] (the only one performed up to now).

The values taken for scut are 3, 4, 5, 6, 7, 8, 9, 10 and 11, where it can also be seen that the branching ratio is stable.

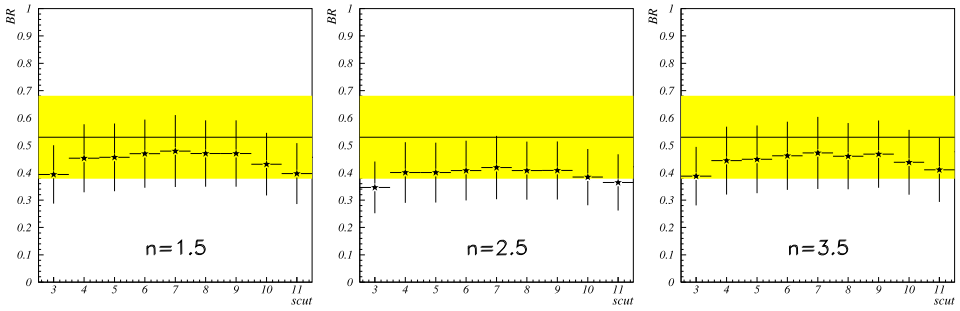

Figure 6.63: Branching ratio stability over scut for $\frac{\Gamma(\Lambda_c^+ \to \Sigma^- \pi^+ \pi^+)}{\Gamma(\Lambda_c^+ \to \Sigma^+ \pi^- \pi^+)}$; the yellow band indicates the E687 measurement [4] (the only one performed up to now).

Finally, the values taken for p_T^2 are 0.25, 0.30, 0.35, 0.40, 0.45, 0.50 and 0.55, where it can also be observed that the branching ratio is stable.

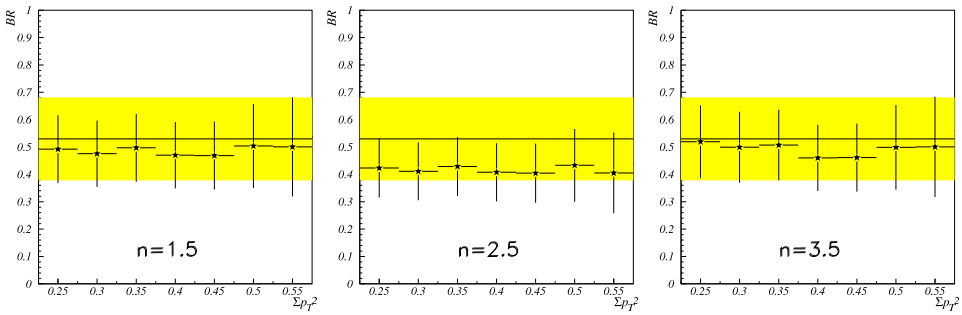

Figure 6.64: Branching ratio stability over p_T^2 for $\frac{\Gamma(\Lambda_c^+ \to \Sigma^- \pi^+ \pi^+)}{\Gamma(\Lambda_c^+ \to \Sigma^+ \pi^- \pi^+)}$; the yellow band indicates the E687 measurement [4] (the only one performed up to now).

Summary

It is important to consider that the values obtained for the analysis performed in this work are consistent with the previous measurements obtained by other experiments over a wide interval for all the important variables taken into account, besides, the branching ratios are also stable; however, a dependence is observed on n for the Ξ_c^+ production in the $pK^-\pi^+$ channel; nevertheless, the values are still inside the band of the previous measurement and as it was seen $n = 2.06 \pm 0.77$ (chapter 5, section 5.3.5) for Ξ_c^+ so, it does not make sense to take values outside the interval [1.5,3.5], because the n-dependence barely affects the branching ratio.

Summarizing, any single cut value was varied for the systematic studies (L/σ, χ^2_{sec}, pvtx, scut, p_T^2), as well as the parameter n for the x_F distribution in the Monte Carlo production, within some range and the branching

ratio for every set of parameters did not show evidence of any trend since all systematic variations are small compared to the statistical error, so the quadrature sum of the total error is not affected and the final results include only statistical errors measurements.

Chapter 7

Conclusions

This analysis reports the observation of two new Cabibbo-suppressed Ξ_c^+ decay modes. The first one:

$$\Xi_c^+ \to \Sigma^+\pi^-\pi^+$$

with 59 ± 14 events observed, where the number of events is determined with two methods (Gaussian fit and counting) which are totally consistent, and the background under the signal region is 87 ± 7. The Poisson probability for the signal to be a background fluctuation is 6.2×10^{-7}.

The second one:

$$\Xi_c^+ \to \Sigma^-\pi^+\pi^+$$

with 22 ± 8 events observed, where the number of events is also determined with two methods (Gaussian fit and counting) which are totally consistent, and the background under the signal region is 13 ± 3. The Poisson probability for the signal to be a background fluctuation is 2.3×10^{-5}.

The branching ratios of the decay modes relative to the well known mode $\Xi_c^+ \to \Xi^-\pi^+\pi^+$ are:

$$\frac{\Gamma(\Xi_c^+ \to \Sigma^+\pi^-\pi^+)}{\Gamma(\Xi_c^+ \to \Xi^-\pi^+\pi^+)} =$$

$$0.480 \pm 0.202$$

and

$$\frac{\Gamma(\Xi_c^+ \to \Sigma^-\pi^+\pi^+)}{\Gamma(\Xi_c^+ \to \Xi^-\pi^+\pi^+)} =$$

$$0.184 \pm 0.086$$

It has been proven that the results do not depend on the n for the x_F distribution in the Monte Carlo production nor on the most critical cuts applied (L/σ, pvtx, χ^2, scut and p_T^2), and since the statistical error is considerably larger than the systematical one, only the first one is computed in the final results.

The analysis performed has been tested with one Ξ_c^+ and two Λ_c^+ already reported decay modes, which are similar to the ones reported here.

The Ξ_c^+ control mode measurement is:

$$\frac{\Gamma(\Xi_c^+ \to pK^-\pi^+)}{\Gamma(\Xi_c^+ \to \Xi^-\pi^+\pi^+)} = 0.194 \pm 0.054$$

and the branching ratio obtained agrees with the previous SELEX[7] and FOCUS[15] measurements. In Figure 7.1 the comparison is sketched.

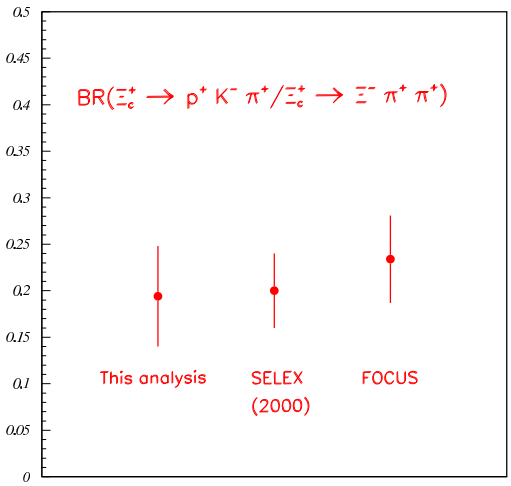

Figure 7.1: Branching ratio comparison for $\Xi_c^+ \to pK^-\pi^+$ control mode.

The branching ratios for the Λ_c^+ control modes also agree with the values measured. First, the branching ratio:

$$\frac{\Gamma(\Lambda_c^+ \to \Sigma^+\pi^-\pi^+)}{\Gamma(\Lambda_c^+ \to pK^-\pi^+)} = 0.716 \pm 0.144$$

which agrees with the previous result from CLEO2 [4]. Figure 7.2 compares the result with others measurements. Second, the branching ratio:

$$\frac{\Gamma(\Lambda_c^+ \to \Sigma^-\pi^+\pi^+)}{\Gamma(\Lambda_c^+ \to \Sigma^+\pi^-\pi^+)} = 0.382 \pm 0.104$$

which also agrees with the previous result from E687 [6]. The comparison is

sketched in Figure 7.2.

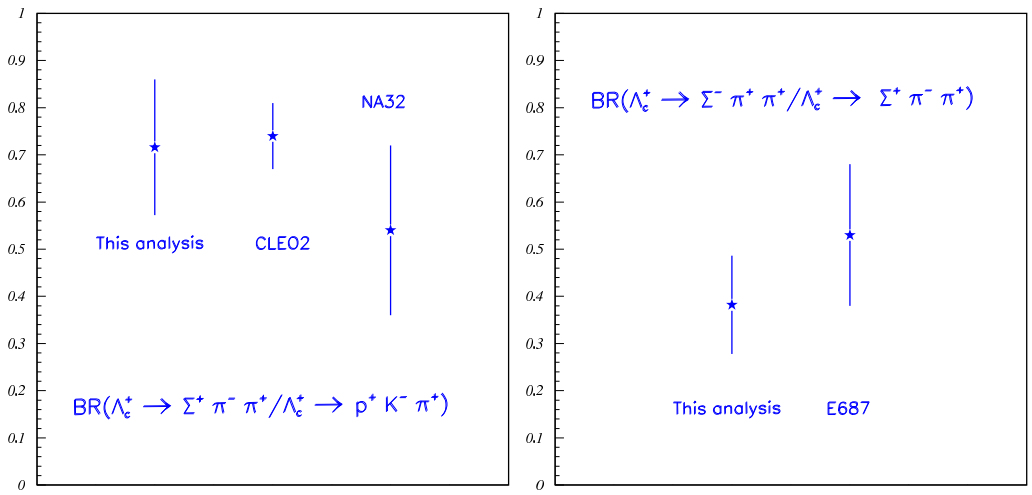

Figure 7.2: Branching ratio comparison for $\Lambda_c^+ \to \Sigma^+\pi^-\pi^+$(left) and for $\Lambda_c^+ \to \Sigma^-\pi^+\pi^+$(right) control modes.

The central values for the relative branching ratio of the new decays are nearly consistent for Ξ_c^+ and Λ_c^+, but the error for the Ξ_c^+ measurement is huge, so this conclusion needs to be carefully studied with a larger sample of events in order to reduce the statistical error.

The values obtained for the branching ratios are:

$$\frac{\Gamma(\Xi_c^+ \to \Sigma^-\pi^+\pi^+)}{\Gamma(\Xi_c^+ \to \Sigma^+\pi^-\pi^+)} =$$

$$0.420 \pm 0.244$$

and

$$\frac{\Gamma(\Lambda_c^+ \to \Sigma^-\pi^+\pi^+)}{\Gamma(\Lambda_c^+ \to \Sigma^+\pi^-\pi^+)} =$$

$$0.382 \pm 0.104$$

Figure 7.3 resumes what it was described above.

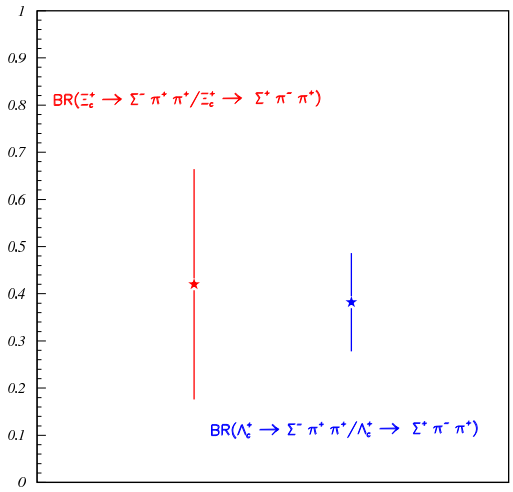

Figure 7.3: Branching ratios for Ξ_c^+ and Λ_c^+ decay modes measured in this analysis.

The α-parameter calculated from the branching ratios may describe some important points about the decay mechanism. They are sketched in Figure 7.4, where it can be observed that the values for Ξ_c^+ are nearly consistent with each other and the Λ_c^+ ones too, but at a different range.

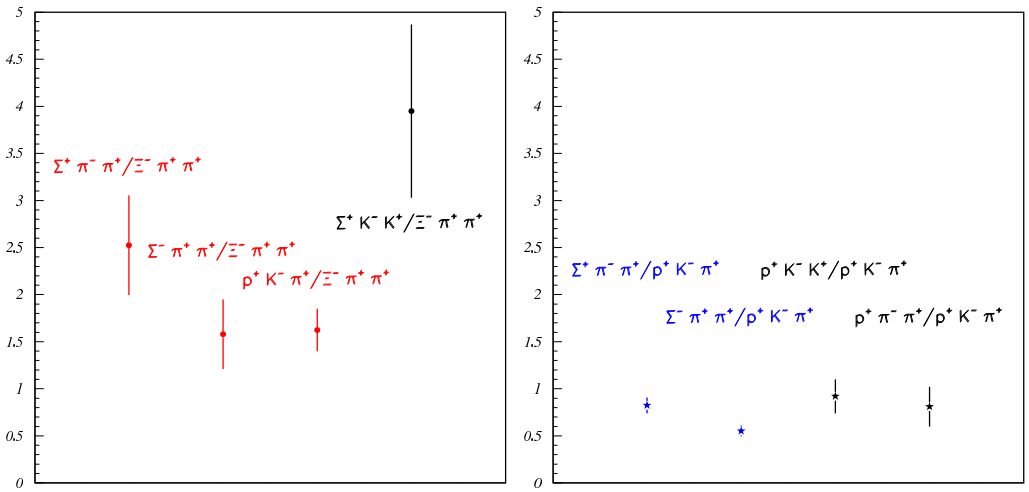

Figure 7.4: α-parameters for Ξ_c^+(left) and Λ_c^+(right) decay modes, where it has been included one extra value for other Ξ_c^+ Cabibbo-suppressed decay ($\Sigma^+K^-K^+/\Xi^-\pi^+\pi^+$) and two extra values for Λ_c^+ ($pK^-K^+/pK^-\pi^+$ and $p\pi^-\pi^+/pK^-\pi^+$); their branching ratios were obtained from the PDG [67].

It is observed that the reference mode for Ξ_c^+ has a different matrix element than for Λ_c^+, where the first one is smaller than the second one; moreover two α-parameters for Λ_c^+ decay modes have been added to this comparison;

one of them is $\Lambda_c^+ \to pK^-K^+$ and the other one is $\Lambda_c^+ \to p\pi^-\pi^+$, both obtained from the PDG and another α-parameter for other Ξ_c^+ Cabibbo-suppressed decay has also been added, $\Xi_c^+ \to \Sigma^+K^-K^+$, obtained from the PDG [67] as well.

Comparing the spectator diagrams and the branching ratios for the decay modes $\Sigma^+\pi^-\pi^+$ and $\Sigma^-\pi^+\pi^+$, it can be appreciated that the source of the s-quark in the final states (in the Ξ_c^+ case from the decay of the c-quark, in the Λ_c^+ case as spectator) does not affect the results and that in all cases a $u\overline{u}$ or $d\overline{d}$ quark pair from the sea is needed; besides after the different elements of the CKM matrix and phase space contributions are factorized, the quark diagrams are identical when viewed by the strong interaction since all the quark flavor labels vanish, and this is reflected by the branching ratio results.

The development of the theory of charm baryon decays has been excused due to the insufficient experimental data. Now, two more Cabibbo-suppressed decays of the Ξ_c^+ have been reported, and they contribute to the information about charm-strange baryons; besides, two more modes are on the way, $\Xi_c^+ \to \Xi^-K^+\pi^+$ (also a Cabibbo-suppressed decay) and $\Xi_c^+ \to \Sigma^+K^+\pi^-$ (a Doubly Cabibbo-suppressed decay).

There are still some important issues such as the close difference between the branching ratio for Cabibbo-suppressed and Cabibbo-favored decays, observed in this analysis, and the testing of models from Heavy Quark Expansion, which are left opened to theorists.

Appendix A

Vee and Kink Package

The package that led to the discovery of the new Ξ_c^+ decay modes is described in this appendix, at this time some bugs were corrected for the package but additional fixes are needed, specially when Monte Carlo simulation is performed due to the ambiguities obtained from the reconstructed events as it was explained in Section 4.7.

A.1 Tracking

The main ds-kink package starts at vertex routine, where vertices are found for this kind of reconstructions. First of all, it calls the *"kink_makeclones_ds"*; routine that creates clones from parts of existing tracks to improve kink finding and it is based on three subroutines:

1. *"kink_clone_single"*: It is called twice, one for the vertex spectrometer and another for the m2 spectrometer; it loops through all existing segments in the spectrometer and makes tracks (1-segment) out of them, later vx's can be added on as kinks. It calls *"seg_add_trk"* to create the single segment tracks.

2. *"kink_find_pairs"*: It finds pairs of segments (vx-m1 and m1-m2, so, it is called twice too) as candidates to add as new tracks in order to improve kink finding. The routine takes in a starting spectrometer for an event and then flags all existing 2-segment tracks (so they will not be duplicated). Then, it loops through all segments in that event and applies cut parameters on:

   (a) maximum and minimum momentum

   (b) intersection of segments in z-position

   (c) maximum difference in y-angle between segments

   (d) minimum difference in x-angle between segments

(e) maximum difference in y-intercept between segments

Finally, it links 2-segment tracks that do not already exist matching some parameters.

3. *"kink_clone_pairs"*: It creates 2-tseg tracks out of links. Links are taken from pairs found in *"kink_find_pairs"*. The subroutine calls *"seg_add_trk"* to create the single segment track and *"seg_link_trk"* to link the second segment to the new track (a cut on chi2 of the track is applied).

It is important to remember that when cloning is done, a set of new tracks is added to the tracking list. Also and not less important is that some of the tracks have unknown momentum, so when kink vertex is done later (add end of one track to the beginning of another track), it is possible to have a vertex with one of the tracks with unknown momentum.

A.2 Vertex

After *"kink_makeclones_ds"* is called, the main kink finder code starts: *"kink_ds"*, by getting an **approximate vertex**; for the case in which the curvatures of both tracks are known, it uses information in the xz plane, to get an initial vertex, it iterates using distance-of-closest-approach (DCA) (of course, a good fitting is not always accomplished); and for the case in which one of the curvatures is missing or it was not possible to fit with the two curvatures, it does a field free fit in the yz plane to get this **approximate vertex**.

Then, it checks to see if either there is any B field between the vertex and either track; or if there is no field, a 3d field-free fit is done as a result.

Important to remember is that when the curvature of both tracks is known and the **approximate vertex** is in a field-free region, a better fit to a vertex is done with vtx2 package.

In case one curvature is missing and the **approximate vertex** (information gotten from the yz plane) is in a field free region, the subroutine *"vee_pfind_ds"* is used to find the curvature of the track. This curvature is obtained with an iterative method (taking two initial values, c1=0.10 plus c2=0.09, and then using the function *"trajectory"*). Finally, a better vertex fitting is done with the subroutine *"seg_xyfind_ds"*.

On the other hand, in case one curvature is missing and the **approximate vertex** (information gotten from the yz plane) is in a field region, the subroutine *"vee_xfind_ds"* is used. Firstly to find the x-coordinate of the track with the known curvature at the **approximate vertex** (x-position that will be used later in the subroutine *"vee_pfind_ds"* to find the missing curvature). Secondly, to do a better vertex fitting with the subroutine *"seg_xyfind_ds"*.

In both cases (field free and not free region), the function *"trajectory"*

Field	Parent Momentum	Daughter Momentum	Status	Mass Calculation?
no	no	no	0	no
no	no	yes	1	no
no	yes	no	2	no
no	yes	yes	3	yes
yes	no	no	4	no
yes	yes	no	5	yes
yes	no	yes	6	yes
yes	yes	yes	7	yes

Table A.1: Status Info

is used for calculations. An important aspect is that in this function the parabolic trajectory is switched on.

At the end of all these calculations a status is set, table 1 shows the possible values.

Also done in *"kink_ds"* is the kink candidate multiplicity reduction code, that checks if vertices have two z values, in order to eliminate duplicate events that may appear, since two tracks are used for, sometimes two z values are gotten.

The methods used are χ^2 comparison of both tracks, which takes that one with the minimum χ^2 and total number of planes comparison, which takes that one with the maximum number of planes on.

A.3 Recon

At the end of the process, kinks vertices are found under geometrical considerations and the reconstruction process begins:

First, important to state is that in the *"recdf.ocs"* (E781 Open Constant System) the kink search is done with a defined *id* number that CAN NOT be changed. The fixed *recdf id* numbers are shown in the *recdf.ocs* file below. The main recon file is *"recon_kinks_ds"*, where several cuts are applied for the kink reconstruction:

1. minimum and maximum decay angle
2. likelihood on charged daughter (absolute and ratio)
3. photon calorimeter: 1 and 2 gammas for energy (min and max) and for angle

```
! recdf for kink search
```

```
id  name   from  pr q  pid ls_min ls_max mass_min mass_max out
!
20 kshort   vk1  2  0  i-i+   0.  9999.   0.30   0.70   $0008
21 lambda   vk1  2  0  p+i-   0.  9999.   1.00   2.00   $0008
22 alambda  vk1  2  0  p-i+   0.  9999.   1.00   2.00   $0008
23 signpi-  vk1  2 -1  s-i-   0.  9999.   1.00   2.00   $0008
24 asignpi+ vk1  2 +1  s+i+   0.  9999.   1.00   2.00   $0008
25 sigppi0  vk1  2  0  s+p+   0.  9999.   1.00   2.00   $0008
26 asigppi0 vk1  2  0  s-p-   0.  9999.   1.00   2.00   $0008
27 caslpi-  vk1  2 -1  x-i-   0.  9999.   1.10   2.10   $0008
28 acaslpi+ vk1  2 +1  x+i+   0.  9999.   1.10   2.10   $0008
29 olamk-   vk1  2 -1  o-k-   0.  9999.   1.30   2.30   $0008
30 aolamk+  vk1  2 +1  o+k+   0.  9999.   1.30   2.30   $0008
31 ocaspi-  vk1  2 -1  o-i-   0.  9999.   1.30   2.30   $0008
32 aocaspi+ vk1  2 +1  o+i+   0.  9999.   1.30   2.30   $0008
33 ocaspi0  vk1  2 -1  o-x-   0.  9999.   1.30   2.30   $0008
34 ocaspi0  vk1  2 +1  o+x+   0.  9999.   1.30   2.30   $0008
```

A loop over all existing kinks gotten from *"kink_ds"* is done. First of all, values of x, tx, y and ty for the tracks (parent and daughter) that are part of the vertex are obtained from their curvatures. The momentum (p=1/curvature) is also calculated for this parent and daughter tracks, momentum of the neutral track is calculated from momentum conservation, decay angle is calculated from tx and ty differences in both tracks; actually the square root of their differences squared.

The key point in this reconstruction is a loop over all possibilities in the hyperon decays. In case a particular decay is asked for, calculations for the invariant mass of the parent particle are accomplished with mass constraint on the products of the decay using the momenta obtained before. These calculations depend on the hyperon decay asked for in the *recdf.ocs* file.

For example, if a $\Sigma^- \rightarrow n\pi^-$ decay is asked for, the momenta gotten from the vertex tracks and the neutral particle momentum are combined with neutron and pion constrained masses to calculate the invariant mass of the Σ^- particle, but, if a $\Xi^- \rightarrow \Lambda\pi^-$ decay is asked for, the same vertex info (momenta vertex tracks and neutral particle momentum) is combined with Λ and π constrained masses to calculate the invariant mass of the Ξ^- particle; and so on for similar hyperon decays asked, in fact, the ones with a negative charged hyperon.

At the end of the calculations it is possible to get invariant masses for the same vertex, for as many as hyperon decays required in the *recdf.ocs* file.

Appendix B

Reading Vtuples with Fortran

B.1 Codes to use vtuples

Once the structure of the vtuples is understood, the use of the FORTRAN codes to work with them is described. It needs the include file "reconvtup.inc", the subroutines "readvtuple.F" and "fillvtuple.F, and the c subroutine "tuple.c".

The file used to analyze data and fill histograms (like anal.F in the case of ftuples) is called "vtuple.F".

- The c subroutine "tuple.c" is used to open the vtup file and to get the size of each object of the vtuple. Its form is shown below.
- "reconvtup.inc" file contains the variables definition used when data are analyzed, having the format of variable size tuple written by the recon package. Its form is also shown below.
- "readvtuple.F" and "fillvtuple.F" fill the tuple, event per event, with the information to be analyzed by vtuple.F

B.2 Compiling

To compile this program, it is necessary to compile the c subroutine; the instruction is (this has to be done just once):

cc -c tuple.c -o tuple.o

Next, in order to compile the FORTRAN program "vtuple.F":

f77 vtuple.F readvtuple.F fillvtuple.F tuple.o libraries -o executable

The libraries used are:*-I$OFF781_INC /usr /people /ehep /LINUX /off781 /devel /lib /libutility.a* and */usr /people /ehep /LINUX+2.2 /cern /2000 /lib /libpacklib.a -lnsl -lcrypt -ldl*.

Finally; run the executable with the vtuple files:

./executable vtuple(s)

B.3 Vtuple blocks and Fortran codes

Vtups blocks are structured in this order:
(take in consideration that -tuple → real and -tupli → integer)

1. Header: Recon information (important info about reconstruction); it is called rtuple.
   (a) rtupli(1): run → run number.
   (b) rtupli(2): event → 100000*processor + event.
   (c) rtupli(3): bitsor → event recon, ored bits.
   (d) rtupli(4): id → id of recon definition, used in recdf.ocs.
   (e) rtupli(5): status → 100* # recons + # this recon
   (f) rtupli(6): tgt → target number assigned to primary vertex.
   (g) rtuple(7): l → z distance from primary vertex [cm].
   (h) rtuple(8): sigma → l uncertainty [cm].
   (i) rtuple(9): pvtx → point-back reduced chi-squared.
   (j) rtuple(10): chi2 → tgt-prim_vtx reduced chi-squared.
   (k) rtupli(11): ndof → tgt-prim_vtx degrees of freedom.
   (l) rtuple(12): chi2m → vtx2 Chi2(best nprong-1 vertex).
   (m) rtuple(13): chi2p → vtx2 Chi2(best nprong+1 vertex).
   (n) rtupli(14): nentity
   This number is very important because it tells how many blocks of every object we have, its meaning is presented here;

nentity	= nbeamtracks	+ nprimvert*2
	+ nsecvert*10	+ nsvkinks*100
	+ nds*1000	+ ngammarecon*10000
	+ nverttrk*1000000	+ nuserbox*100000000

2. Primary vertex: Data about primary vertex; it is called ptuple.
   (a) ptuple(1): x → x vertex coordinate [cm].
   (b) ptuple(2): y → y vertex coordinate [cm].

(c) ptuple(3): z → z vertex coordinate [cm].

(d) ptuple(4): sx → x coordinate error [cm].

(e) ptuple(5): sy → y coordinate error [cm].

(f) ptuple(6): sz → z coordinate error [cm].

(g) ptuple(7): chi2 → chi2 of the vertex fit.

(h) ptupli(8): ndof → tracks in fit.

(i) ptupli(9): nt → number of tracks in the vertex.

3. Beam: Beam track data; it is called btuple.

(a) btuple(1): x0 → x track coordinate at z=0 [cm].

(b) btuple(2): y0 → y track coordinate at z=0 [cm].

(c) btuple(3): px → x track momenta component [GeV/c].

(d) btuple(4): py → y track momenta component [GeV/c].

(e) btuple(5): pz → z track momenta component [GeV/c].

(f) btupli(6): pid → pid word of the particle as in RICH.

(g) btuple(7): chi2 → segmented reduced chi2.

(h) btupli(8): type → track type q*[1000*nplanes + track_type].

4. Secondary vertex: Secondary vertices and/or subreconstruction data; it is called stuple.

(a) stupli(1): id → recon ID.

(b) stuple(2): x → x vertex coordinate [cm].

(c) stuple(3): y → y vertex coordinate [cm].

(d) stuple(4): z → z vertex coordinate [cm].

(e) stuple(5): sx → x coordinate error [cm].

(f) stuple(6): sy → y coordinate error [cm].

(g) stuple(7): sz → z coordinate error [cm].

(h) stuple(8): chi2 → vertex reduced chi2.

(i) stuple(9): isol → vertex isolation distance.

(j) stupli(10): status → status of the vertex.

(k) stuple(11): e → energy [GeV/c^2].

(l) stuple(12): px → px momentum [GeV/c].

(m) stuple(13): py → py momentum [GeV/c].

(n) stuple(14): pz → pz momentum [GeV/c].

(o) stuple(15): mass → effective mass [GeV].

(p) stuple(16): dmass → effective mass uncertainty [GeV].

5. Tracking: Data about tracks participated from sec. vertices; it is called ttuple.

   (a) ttuple(1): x0 → x track coordinate at z=0 [cm].

   (b) ttuple(2): y0 → y track coordinate at z=0 [cm].

   (c) ttuple(3): px → x component of the track momenta [GeV/c].

   (d) ttuple(4): py → y component of the track momenta [GeV/c].

   (e) ttuple(5): pz → z component of the track momenta [GeV/c].

   (f) ttupli(6): pid1 → ric hyp : e m i k p s x o

   (g) ttupli(7): pid2 → ric ID, etr hit & prob, phot ID + mama

   (h) ttuple(8): chi2 → chi2 of track fit.

   (i) ttupli(9): type → track type q*[1000*nplanes + track_type].

   (j) ttupli(10): pmtrk → word containing suggested pid and mass.

6. Data about kinks used in recon_sv; it is called ktuple.
   It has 14 variables.

7. Vees-Kinks: Data about reconstructions made by recon_vk1; it is called dstuple.

   (a) dstupli(1): status → type of the ds.

   (b) dstuple(2): x0 → x of the branch at decay point [cm].

   (c) dstuple(3): y0 → y of the branch at decay point [cm].

   (d) dstuple(4): px → x component of the momenta or zero [GeV/c].

   (e) dstuple(5): py → y component of the momenta or zero [GeV/c].

   (f) dstuple(6): pz → z component of the momenta or zero [GeV/c].

   (g) dstupli(7): pid → pid.

   (h) dstuple(8): qp → curvature.

   (i) dstuple(9): x0 → x of the second branch [cm].

   (j) dstuple(10): y0 → y of the second branch [cm].

   (k) dstuple(11): px → x momentum component for branch 2 [GeV/c].

   (l) dstuple(12): py → y momentum component for branch 2 [GeV/c].

   (m) dstuple(13): pz → z momentum component for branch 2 [GeV/c].

   (n) dstupli(14): pid → pid for branch 2.

(o) dstuple(15): qp → curvature for branch 2.

8. Gamma: Data about gammas, pi0, eta; it is called gtuple.

   (a) gtuple(1): x0 → x coordinate of the glass blocks.
   (b) gtuple(2): y0 → y coordinate of the glass blocks.
   (c) gtuple(3): px → x momentum component.
   (d) gtuple(4): py → y momentum component.
   (e) gtuple(5): pz → z momentum component.
   (f) gtupli(6): pid → ID.
   (g) gtuple(7): chi2 → chi2 of the track.
   (h) gtupli(8): type → track type.

9. User: Reserved for something, e.g. Monte Carlo and it is called utuple. It has 8 variables.

B.3.1 tuple.c

```
#include <fcntl.h>
#include <stdio.h>
#include <unistd.h>
#include <math.h>

#ifndef TRUE
#define TRUE 1
#endif
#ifndef FALSE
#define FALSE 0
#endif

/* C subroutine to open and read vtuples. It is called by
 * vtuple.F and by the subroutine readvtuple.F.
 * It also works with gzipped vtuples.
 * This programs assumes that gzip is somewhere in your path.
 */

int tuple_(int io_vtuple[], char fname[])
{
  static FILE *infile;
  char cmd[256];
  int size,lwc,twc,j;
  char zed[4];
```

```
  char gi[4];
  char point[4];
  static int do_pipe;

  strcpy(zed, "z");
  strcpy(gi, "g");
  strcpy(point, ".");

  if (infile==NULL) {
    strcpy(cmd, "gzip -dc ");
    strncat(cmd, fname, sizeof(cmd)-strlen(cmd));

    if (cmd[strlen(cmd)-1] != zed[0]){
      if (cmd[strlen(cmd)-2] != gi[0]){
if (cmd[strlen(cmd)-3] != point[0]){
  do_pipe = FALSE;
  infile = fopen(fname, "rb");
  if(infile == NULL) {
    fprintf(stderr, "fopen failed \n");
    return 2;
  }
}
      }
    }

    if (cmd[strlen(cmd)-1] == zed[0]){
      if (cmd[strlen(cmd)-2] == gi[0]){
if (cmd[strlen(cmd)-3] == point[0]){
  do_pipe = TRUE;
  if ((infile = popen(cmd, "r"))== NULL) {
    fprintf(stderr, "popen failed\n");
    return 2;
  }
}
      }
    }

  }

  /*printf("feof= %d\n",feof(infile));*/

  if ( fread( &lwc, 4, 1, infile ) != 1 ) {
    if(feof(infile)!=0) goto do_close;
```

```
    printf("wrong feof (corrupted file)= %d\n",feof(infile));
    /*printf("wrong reading lwc=  %d\n",lwc);*/
    infile=NULL;
    return 2;
  }

  /*printf("reading lwc=  %d\n",lwc);*/
  size = lwc/4;

  /*printf("size=  %d\n",size);*/

  if ( fread( io_vtuple, 4, size, infile ) != size ) {
    /*printf("wrong size=  %d\n",size);*/
    infile=NULL;
    return 2;
  }

  if ( fread( &twc, 4, 1, infile ) != 1 ) {
    /*printf("wrong reading twc=  %d\n",twc);*/
    infile=NULL;
    return 2;
  }

  /*  printf("reading1 twc=  %d\n",twc);*/

  if ( lwc != twc ) {
    /*printf("twc not equal lwc\n");*/
    infile=NULL;
    return 2;
  }

  if ( lwc != (io_vtuple[0]+1)*4 ) {
    /*printf("bad reading\n");*/
    infile=NULL;
    return 2;
  }

  if (infile!=0) {
    return size;
  }

do_close:
```

```
  if(do_pipe==TRUE) {
    /*printf("pclosing\n");*/
    if (pclose(infile) != 0) {
      fprintf(stderr, "pclose failed\n");
      return 555;
    }
    infile=NULL;
    return 2;
  }
  else {
    /*    printf("fclosing\n");*/
    if (fclose(infile) != 0) {
      fprintf(stderr,"fclose failed\n");
      return 666;
    }
    infile=NULL;
    return 2;
  }

  return 0; /* just to make compiler happy */
}
```

B.3.2 reconvtuple.inc

```
c include file for vtuple.F program

integer head,prim,beam
Parameter (head=1,prim=1,beam=1)
       integer objs,tra,gam
Parameter (objs=9,tra=50,gam=50)

Integer
  &   llrtuple,  !recon info
  &   llptuple,  !prim vtx info
  &   llbtuple,  !beam track info
  &   llstuple,  !sec vertex info
  &   llttuple,  !track info
  &   llktuple,  !sv-kink info
  &   lldstuple, !ds-field
  &   llgtuple,  !gamma info
  &   llutuple   !user info (mc)

Parameter
  &   (llrtuple=14,llptuple=9,
  &   llbtuple=8,llstuple=16,
  &   llttuple=10,llktuple=14,
  &   lldstuple=15,llgtuple=8,
  &   llutuple=8)

c **********************
c header info

integer*4
     &  run(llrtuple,head),
     & event(llrtuple,head),
     & bitsor(llrtuple,head),
     & id(llrtuple,head),
     & status(llrtuple,head),
     & tgt(llrtuple,head)
real*4
     & l(llrtuple,head),
     & sigma(llrtuple,head),
     & pvtx(llrtuple,head),
     & chi2(llrtuple,head)
integer*4
     & ndof(llrtuple,head)
real*4
     & chi2m(llrtuple,head),
     & chi2p(llrtuple,head)
integer*4
     & nentity(llrtuple,head)

c *************************
c primary vertex

real*4
     & pvx_x(llptuple,prim),
     & pvx_y(llptuple,prim),
     & pvx_z(llptuple,prim),
     & pvx_sx(llptuple,prim),
     & pvx_sy(llptuple,prim),
     & pvx_sz(llptuple,prim),
     & pvx_chi2(llptuple,prim)
integer*4
     & pvx_nf(llptuple,prim),
     & pvx_nt(llptuple,prim)

c *************************
c  beam track

real*4
     & btk_x0(llbtuple,beam),
     & btk_y0(llbtuple,beam),
     & btk_px(llbtuple,beam),
     & btk_py(llbtuple,beam),
     & btk_pz(llbtuple,beam)
integer*4
     & btk_pid(llbtuple,beam)
real*4
     & btk_chi2(llbtuple,beam)
integer*4
     & btk_type(llbtuple,beam)

c *************************
c secondary vertex

integer*4
     & svx_id(llstuple,objs)
real*4
     & svx_x(llstuple,objs),
     & svx_y(llstuple,objs),
     & svx_z(llstuple,objs),
     & svx_sx(llstuple,objs),
     & svx_sy(llstuple,objs),
```

```
     & svx_sz(llstuple,objs),
     & svx_chi2(llstuple,objs),
     & svx_isol(llstuple,objs)
integer*4
     &  svx_status(llstuple,objs)
real*4
     & e(llstuple,objs),
     & px(llstuple,objs),
     & py(llstuple,objs),
     & pz(llstuple,objs),
     &  mass(llstuple,objs),
     & dmass(llstuple,objs)


c ************************
c vertex track

real*4
     & tk_x0(llttuple,tra),
     & tk_y0(llttuple,tra),
     & tk_px(llttuple,tra),
     & tk_py(llttuple,tra),
     & tk_pz(llttuple,tra)
integer*4
     & tk_pid1(llttuple,tra),
     & tk_pid2(llttuple,tra)
real*4
     & tk_chi2(llttuple,tra)
integer*4
     & tk_type(llttuple,tra),
     & tk_pmtrk(llttuple,tra)

c ************************
c sv-kink

c ************************
c ds-object

integer*4
     & ds_status(lldstuple,objs)
real*4
     & ds_x01(lldstuple,objs),
     & ds_y01(lldstuple,objs),
     & ds_px1(lldstuple,objs),
     & ds_py1(lldstuple,objs),
     & ds_pz1(lldstuple,objs)
integer*4
     & ds_pid1(lldstuple,objs)
real*4
     & ds_qp1(lldstuple,objs),
     & ds_x02(lldstuple,objs),
     & ds_y02(lldstuple,objs),
     & ds_px2(lldstuple,objs),
     & ds_py2(lldstuple,objs),
     & ds_pz2(lldstuple,objs)
integer*4
     & ds_pid2(lldstuple,objs)
real*4
     & ds_qp2(lldstuple,objs)

c ************************
c gamma

real*4
     & g_x0(llgtuple,gam),
     & g_y0(llgtuple,gam),
     & g_px(llgtuple,gam),
     & g_py(llgtuple,gam),
     & g_pz(llgtuple,gam)
integer*4
     & g_pid(llgtuple,gam)
real*4
     & g_chi2(llgtuple,gam)
integer*4
     & g_type(llgtuple,gam)

c ************************
c user

real*4
     &  u_start_spec(llutuple,objs),
     &  u_ang_y(llutuple,objs),
     &  u_y(llutuple,objs),
     &  u_ang_x(llutuple,objs),
     &  u_zmag(llutuple,objs),
     &  u_zmag_dev(llutuple,objs),
     &  u_p(llutuple,objs),
     &  u_chi2(llutuple,objs),
     &  u_ang_y_err(llutuple,objs),
     &  u_y_err(llutuple,objs),
     &  u_ang_x_err(llutuple,objs),
     &  u_zmag_dev_err(llutuple,objs),
```

```
     &  u_p_err(llutuple,objs)

c ****************************
c ****************************

     Integer nv,np,nb,ns,nsv,nsd,ng,nu

c ****************************
c ****************************
c ****************************

       Real                              &         rtuple(llrtuple,head)
       Integer                           &         rtupli(llrtuple,head)
       Equivalence                       &        (rtuple,rtupli)

       Real                              &         ptuple(llptuple,prim)
       Integer                           &         ptupli(llptuple,prim)
       Equivalence                       &        (ptuple,ptupli)

       Real                              &         btuple(llbtuple,beam)
       Integer                           &         btupli(llbtuple,beam)
       Equivalence                       &        (btuple,btupli)

       Real                              &         stuple(llstuple,objs)
       Integer                           &         stupli(llstuple,objs)
       Equivalence                       &        (stuple,stupli)

       Real                              &         ttuple(llttuple,tra)
       Integer                           &         ttupli(llttuple,tra)
       Equivalence                       &        (ttuple,ttupli)

                                           Real
                                         &         ktuple(llktuple,objs)
                                           Integer
                                         &         ktupli(llktuple,objs)
                                           Equivalence
                                         &        (ktuple,ktupli)

                                           Real
                                         &         dstuple(lldstuple,objs)
                                           Integer
                                         &         dstupli(lldstuple,objs)
                                           Equivalence
                                         &        (dstuple,dstupli)

                                           Real
                                         &         gtuple(llgtuple,gam)
                                           Integer
                                         &         gtupli(llgtuple,gam)
                                           Equivalence
                                         &        (gtuple,gtupli)

                                           Real
                                         &         utuple(llutuple,objs)
                                           Integer
                                         &         utupli(llutuple,objs)
                                           Equivalence
                                         &        (utuple,utupli)

                                       c ****************************
                                       c ****************************

                                       equivalence
                                            &  (run,rtupli(1,1)),
                                            &  (event,rtupli(2,1)),
                                            &  (bitsor,rtupli(3,1)),
                                            &  (id,rtupli(4,1)),
                                            &  (status,rtupli(5,1)),
                                            &  (tgt,rtupli(6,1)),
                                            &  (l,rtuple(7,1)),
                                            &  (sigma,rtuple(8,1)),
                                            & (pvtx,rtuple(9,1)),
                                            & (chi2,rtuple(10,1)),
                                            & (ndof,rtupli(11,1)),
                                            & (chi2m,rtuple(12,1)),
```

```
     & (chi2p,rtuple(13,1)),
     & (nentity,rtupli(14,1))

equivalence
     & (pvx_x,ptuple(1,1)),
     & (pvx_y,ptuple(2,1)),
     & (pvx_z,ptuple(3,1)),
     & (pvx_sx,ptuple(4,1)),
     & (pvx_sy,ptuple(5,1)),
     & (pvx_sz,ptuple(6,1)),
     & (pvx_chi2,ptuple(7,1)),
     & (pvx_nf,ptupli(8,1)),
     & (pvx_nt,ptupli(9,1))

equivalence
     & (btk_x0,btuple(1,1)),
     & (btk_y0,btuple(2,1)),
     & (btk_px,btuple(3,1)),
     & (btk_py,btuple(4,1)),
     & (btk_pz,btuple(5,1)),
     & (btk_pid,btupli(6,1)),
     & (btk_chi2,btuple(7,1)),
     & (btk_type,btupli(8,1))

equivalence
     & (svx_id,stupli(1,1)),
     & (svx_x,stuple(2,1)),
     & (svx_y,stuple(3,1)),
     & (svx_z,stuple(4,1)),
     & (svx_sx,stuple(5,1)),
     & (svx_sy,stuple(6,1)),
     & (svx_sz,stuple(7,1)),
     & (svx_chi2,stuple(8,1)),
     & (svx_isol,stuple(9,1)),
     &  (svx_status,stupli(10,1)),
     & (e,stuple(11,1)),
     & (px,stuple(12,1)),
     & (py,stuple(13,1)),
     & (pz,stuple(14,1)),
     &  (mass,stuple(15,1)),
     & (dmass,stuple(16,1))

equivalence
     & (tk_x0,ttuple(1,1)),
     & (tk_y0,ttuple(2,1)),
     & (tk_px,ttuple(3,1)),
     & (tk_py,ttuple(4,1)),
     & (tk_pz,ttuple(5,1)),
     & (tk_pid1,ttupli(6,1)),
     & (tk_pid2,ttupli(7,1)),
     & (tk_chi2,ttuple(8,1)),
     & (tk_type,ttupli(9,1)),
     & (tk_pmtrk,ttupli(10,1))

equivalence
     & (ds_status,dstupli(1,1)),
     & (ds_x01,dstuple(2,1)),
     & (ds_y01,dstuple(3,1)),
     & (ds_px1,dstuple(4,1)),
     & (ds_py1,dstuple(5,1)),
     & (ds_pz1,dstuple(6,1)),
     & (ds_pid1,dstupli(7,1)),
     & (ds_qp1,dstuple(8,1)),
     & (ds_x02,dstuple(9,1)),
     & (ds_y02,dstuple(10,1)),
     & (ds_px2,dstuple(11,1)),
     & (ds_py2,dstuple(12,1)),
     & (ds_pz2,dstuple(13,1)),
     & (ds_pid2,dstupli(14,1)),
     & (ds_qp2,dstuple(15,1))

equivalence
     & (g_x0,gtuple(1,1)),
     & (g_y0,gtuple(2,1)),
     & (g_px,gtuple(3,1)),
     & (g_py,gtuple(4,1)),
     & (g_pz,gtuple(5,1)),
     & (g_pid,gtupli(6,1)),
     & (g_chi2,gtuple(7,1)),
     & (g_type,gtupli(8,1))

equivalence
     &  (u_start_spec,utuple(1,1)),
     &  (u_ang_y,utuple(2,1)),
     &  (u_y,utuple(3,1)),
     &  (u_ang_x,utuple(4,1)),
     &  (u_zmag,utuple(5,1)),
     &  (u_zmag_dev,utuple(6,1)),
     &  (u_p,utuple(7,1)),
     &  (u_chi2,utuple(8,1)),
     &  (u_ang_y_err,utuple(2,2)),
     &  (u_y_err,utuple(3,2)),
```

```
     &  (u_ang_x_err,utuple(4,2)),
     &  (u_zmag_dev_err,utuple(6,2)),
     &  (u_p_err,utuple(7,2))

common /vtuples/ rtuple,ptuple,btuple,stuple,
     & ttuple,ktuple,dstuple,gtuple,utuple,
     & nv,np,nb,ns,nsv,nsd,ng,nu
```

B.3.3 readvtuple.F

```
      subroutine readvtuple(ret,u,vtupfile2)

      implicit none

      Character*256 vtupfile
      Integer u
      integer*1 vtupfile2(256)
      integer*4 mio_vtuple
      parameter (mio_vtuple=999)
      Integer tuple_integer(mio_vtuple)
      Real tuple_real(mio_vtuple)
      equivalence (tuple_integer,tuple_real)
      integer lltuple(mio_vtuple)
      real rrtuple(mio_vtuple)
      Integer ret
      integer tuple


c      Call vzero(tuple_real,mio_vtuple)
c      call vzero(rrtuple,ret)

*****************************************
*     ret is a c function invoked to open  *
*     and get info from the vtuples        *
*****************************************

      ret = tuple(tuple_integer,vtupfile2)
      if (ret.eq.2) goto 555
      call ucopy (tuple_integer,lltuple,ret)
      call ucopy (tuple_real,rrtuple,ret)

*************************************************
*     Subroutine that fills the known tuple blocks *
*************************************************

      call fillvtuple(lltuple,rrtuple,u)

 555  continue
      return
      end
```

B.3.4 fillvtuple.F

```
      subroutine fillvtuple(lltuple,rrtuple,u)

      implicit none

#include "reconvtup.inc"
#include "part_cbk.inc"

      Integer i,j,k,ll,u
      integer nv1,nv2,nv3
      integer ng1,ng2,ng3
      integer nsd1,en,a
      integer nsv1,ns1,nb1
      real aa
      integer lltuple(*)
      real rrtuple(*)

      en = lltuple(15)

      nu   = en / 100000000
      nv1  = en - ( nu * 100000000 )
      nv2  = nv1 / 10000000
      nv3  = nv1 - ( nv2 * 10000000 )
      nv   = nv3 / 1000000
      ng1  = nv3 - ( nv * 1000000 )
      ng2  = ng1 / 100000
      ng3  = ng1 - ( ng2 * 100000 )
      ng   = ng3 / 10000
      nsd1 = ng3 - ( ng * 10000 )
      nsd  = nsd1 / 1000
      nsv1 = nsd1 - ( nsd * 1000 )
      nsv  = nsv1 / 100
      ns1  = nsv1 - ( nsv * 100 )
      ns   = ns1 / 10
      a    = (nu*100000000)+(nv*1000000)+(ng*10000)+
     &     (nsd*1000)+(nsv*100)+(ns*10)
      a    = en - a

      if (a.eq.0) then
        np=0
        nb=0
      else
        if (a.eq.1) then
```

```
      np=0
      nb=1
    else
      if (a.eq.2) then
        np=1
        nb=0
      else
        if (a.eq.3) then
          np=1
          nb=1
        endif
      endif
    endif
  endif

  call ucopy (lltuple(2),rtupli(1,head),6)
  call ucopy (rrtuple(8),rtuple(7,head),4)
  call ucopy (lltuple(12),rtupli(11,head),1)
  call ucopy (rrtuple(13),rtuple(12,head),3)

  j = 0
  do i=1,np
    call ucopy (rrtuple(16+j),ptuple(1,i),7)
    call ucopy (lltuple(23+j),ptupli(8,i),2)
    j = j + 9
  enddo

  do i=1,nb
    u = u + 1
    call ucopy (rrtuple(16+j),btuple(1,i),5)
    call ucopy (lltuple(21+j),btupli(6,i),1)
    call ucopy (rrtuple(22+j),btuple(7,i),1)
    call ucopy (lltuple(23+j),btupli(8,i),1)
    j = j + 8
  enddo

  do i=1,ns
    call ucopy (lltuple(16+j),stupli(1,i),1)
    call ucopy (rrtuple(17+j),stuple(2,i),8)
    call ucopy (lltuple(25+j),stupli(10,i),1)
    call ucopy (rrtuple(26+j),stuple(11,i),6)
    j = j + 16
  enddo
```

```
do i=1,nv
  call ucopy (rrtuple(16+j),ttuple(1,i),5)
  call ucopy (lltuple(21+j),ttupli(6,i),2)
  call ucopy (rrtuple(23+j),ttuple(8,i),1)
  call ucopy (lltuple(24+j),ttupli(9,i),2)
  j = j + 10
enddo

do i=1,nsv
  call ucopy (rrtuple(16+j),ktuple(1,i),14)
  j = j + 14
enddo

do i=1,nsd
  call ucopy (lltuple(16+j),dstupli(1,i),1)
  call ucopy (rrtuple(17+j),dstuple(2,i),5)
  call ucopy (lltuple(22+j),dstupli(7,i),1)
  call ucopy (rrtuple(23+j),dstuple(8,i),6)
  call ucopy (lltuple(29+j),dstupli(14,i),1)
  call ucopy (rrtuple(30+j),dstuple(15,i),1)
  j = j + 15
enddo

do i=1,ng
  call ucopy (rrtuple(16+j),gtuple(1,i),5)
  call ucopy (lltuple(21+j),gtupli(6,i),1)
  call ucopy (rrtuple(22+j),gtuple(7,i),1)
  call ucopy (lltuple(23+j),gtupli(8,i),1)
  j = j + 8
enddo

do i=1,nu
  call ucopy (rrtuple(16+j),utuple(1,i),8)
  j = j + 8
enddo

return
end
```

Appendix C

The SELEX Collaboration

G.P. Thomas
Ball State University, Muncie, IN 47306, U.S.A.

E. Gülmez
Bogazici University, Bebek 80815 Istanbul, Turkey

R. Edelstein, S.Y. Jun, A.I. Kulyavtsev[1], A. Kushnirenko, D. Mao[1], P. Mathew[2], M. Mattson, M. Procario[3], J. Russ, J. You[4]
Carnegie-Mellon University, Pittsburgh, PA 15213, U.S.A.

A.M.F. Endler
Centro Brasiliero de Pesquisas Físicas, Rio de Janeiro, Brazil

P.S. Cooper, J. Kilmer, S. Kwan, J. Lach, E. Ramberg, D. Skow, L. Stutte
Fermilab, Batavia, IL 60510, U.S.A.

V.P. Kubarovsky, V.F. Kurshetsov, A.P. Kozhevnikov, L.G. Landsberg, V.V. Molchanov, S.B. Nurushev, S.I. Petrenko, A.N. Vasiliev, D.V. Vavilov, V.A. Victorov
Institute for High Energy Physics, Protvino, Russia

Li Yunshan, Mao Chensheng, Zhao Wenheng, He Kangling, Zheng Shuchen, Mao Zhenlin
Institute of High Energy Physics, Beijing, P.R. China

M.Y. Balatz[5], G.V. Davidenko, A.G. Dolgolenko, G.B. Dzyubenko, A.V. Evdokimov, M.A. Kubantsev, I. Larin, V. Matveev, A.P. Nilov, V.A. Prutskoi, A.I. Sitnikov, V.S. Verebryusov, V.E. Vishnyakov
Institute of Theoretical and Experimental Physics, Moscow, Russia

U. Dersch[6], I. Eschrich[7], I. Konorov[8], H. Krüger[9], J. Simon[10], K. Vorwalter[11]
Max-Planck-Institut für Kernphysik, 69117 Heidelberg, Germany

I.S. Filimonov[5], E.M. Leikin, A.V. Nemitkin, V.I. Rud
Moscow State University, Moscow, Russia

A.G. Atamantchouk, G. Alkhazov, N.F. Bondar, V.L. Golovtsov, V.T. Kim, L.M. Kochenda, A.G. Krivshich, N.P. Kuropatkin, V.P. Maleev, P.V. Neoustroev, B.V. Razmyslovich, V. Stepanov, M. Svoiski, N.K. Terentyev[12], L.N. Uvarov, A.A. Vorobyov
Petersburg Nuclear Physics Institute, St. Petersburg, Russia

I. Giller, M.A. Moinester, A. Ocherashvili, V. Steiner
Tel Aviv University, 69978 Ramat Aviv, Israel

J. Amaro, E. A. Blanco C., J. Engelfried[4], N. P. Estrada, A. Flores, G. Hinojosa, A. Morelos, J. L. Sánchez, I. Torres, E. Vázquez-Jáuregui
Universidad Autónoma de San Luis Potosí, San Luis Potosí, Mexico

M. Luksys
Universidade Federal da Paraíba, Paraíba, Brazil

V.J. Smith
University of Bristol, Bristol BS8 1TL, United Kingdom

M. Kaya, E. McCliment, K.D. Nelson[13], C. Newsom, Y. Onel, E. Ozel, S. Ozkorucuklu, P. Pogodin
University of Iowa, Iowa City, IA 52242, U.S.A.

L.J. Dauwe
University of Michigan-Flint, Flint, MI 48502, U.S.A.

M. Gaspero, M. Iori
University of Rome "La Sapienza" and INFN, Rome, Italy

L. Emediato, C.O. Escobar[14], F.G. Garcia[4], P. Gouffon, T. Lungov[15], M. Srivastava, R. Zukanovich-Funchal
University of São Paulo, São Paulo, Brazil

A. Lamberto, A. Penzo, G.F. Rappazzo, P. Schiavon
University of Trieste and INFN, Trieste, Italy

Bibliography

[1] E.G. Cazzoli, *et al.*, "Evidence for $\Delta S = -\Delta Q$ Currents for Charmed-Baryon Production by Neutrinos",
Phys. Rev. Lett. **34** (1975) 1125-1128.

[2] B. Knapp, *et al.*,
Phys. Rev. Lett. **37** (1976) 882.

[3] S.F. Biagi, *et al.*,"Observation of a narrow state at $2.46\,\mathrm{GeV}/c^2$ - A candidate for the charmed strange baryon A^+",
Phys. Lett. **B122** (1983) 455.

[4] Y. Kubota *et al.*, CLEO Collab., "Measurement of exclusive Λ_c Decays with a Σ^+ in the final state",
Phys. Rev. Lett. **71** (1993) 3255-3258.

[5] S. Barlag *et al.*, ACCMOR Collab., "An observation of exclusive Λ_c decays into Σ^+ and mesons",
Phys. Lett. **B283** (1992) 465.

[6] P.L. Frabetti, *et al.*,FNAL E687 Collab., "First observation of the $\Sigma^-\pi^+\pi^+$ decay mode of the Λ_c baryon and its branching ratio relative to the $\Sigma^+\pi^-\pi^+$ mode",
Phys. Lett. **B328** (1994) 193.

[7] S.Y. Jun *et al.*, SELEX Collab., "Observation of the Cabibbo-Suppressed Decay $\Xi_c^+ \to pK^-\pi^+$",
Phys. Rev. Lett. **84** (2000) 1857-1861.

[8] A proposal to construct SELEX,
SELEX documentation, November, 1987.

[9] H. Albrecht, *et al.*,
Phys. Lett. **B207** (1988) 109.

[10] G. D. Crawford, *et al.*,"Measurement of baryon production in B-meson decay"
Phys. Rev. **D45** (1992) 752.

[11] H. Albrecht, *et al.*,
Phys. Lett. **B269** (1991) 234.

[12] T. Bergfeld, *et al.*,
Phys. Lett. **B323** (1994) 219.

[13] D.E. Jaffe, *et al.*," Measurement of $\Gamma(\Lambda_c^+ \to pK^-\pi^+)$ "
Phys. Rev. **D62** (2000) 072005.

[14] F.E. Close and H.J. Lipkin,
Phys. Lett. **B551** (2003) 337.

[15] J. M. Link *et al.*, FOCUS Collab., "Measurements of Ξ_c^+ branching ratios",
Phys. Lett. **B571** (2003) 139.

[16] B. Guberina, H. Stefancic,"Cabibbo suppressed decays and the Ξ_c^+ lifetime "
Phys. Rev. **D65** (2002) 114004.

[17] E. Eichten, B. Hill,
Phys. Lett. **B234** (1990) 511.

[18] H. Georgi,
Phys. Lett. **B240** (1990) 447.

[19] B. Povh, K. Rith, C. Scholz and F. Zetsche, Particles and nuclei,
Springer, 1995.

[20] A. Paschos, U. Türke,
Phys. Rep. **178** (1989) 145.

[21] G. Dissertori, I. Knowles and M. Schmelling, "Quantum Chromodynamics, High Energy Experiments and Theory",
Oxford Science Publications, 2003.

[22] Lewis H. Ryder, "Quantum Field Theory",
Cambridge University Press, 1999.

[23] J. J. Aubert, *et al.*, "Experimental Observation of a Heavy Particle J",
Phys. Rev. Lett. **33** (1974) 1404.

[24] J. E. Augustin, *et al.*, "Discovery of a Narrow Resonance in e^+e^- Annihilation",
Phys. Rev. Lett. **33** (1974) 1406.

[25] S.F. Biagi, *et al.*,"Observation of a narrow state at $2.46\,\mathrm{GeV}/c^2$ - A candidate for the charmed strange baryon A^+",
Phys. Lett. **B122** (1983) 455.

[26] S. L. Glashow, J. Iliopoulos, and L. Maiani, "Weak Interactions with Lepton-Hadron Symmetry",
Phys. Rev. **D2** (1970) 1285.

[27] S. Glashow, Experimental Meson Spectroscopy -1974 (EMS-74), A. Garelick (ed.), AIP, New York, 1974, p.387.

[28] K. Niu, E. Mikumo, Y. Maeda,
Prog. Theor. Phys. **46** (1971) 1644.

[29] C. Bacci, *et al.*, "Preliminary result of Frascati (ADONE) on the Nature of a New $3.1-$GeV Particle Produced in e^+e^- Annihilation",
Phys. Rev. Lett. **33** (1974) 1408.

[30] A. de Rújula, H. Georgi and S.L. Glashow,
Phys. Rev. **D12** (1975) 147.

[31] S.F. Biagi, *et al.*,"Measurement of the lifetime of the charmed strange baryon A^+",
Phys. Lett. **B150** (1985) 230.

[32] T. Bergfeld, *et al.*, CLEO Collab.
Phys. Lett. **B365** (1996) 431.

[33] P. Avery, *et al.*, CLEO Collab.
Phys. Rev. Lett. **75** (1995) 4364.

[34] P. L. Frabetti, *et al.*, FNAL E687 Collab.
Phys. Rev. Lett. **70** (1993) 1381.

[35] H. Albrecht, *et al.*, ARGUS Collab.
Phys. Lett. **B247** (1990) 121.

[36] M. S. Alam, *et al.*, CLEO Collab.
Phys. Lett. **B226** (1989) 401.

[37] S. Bianco, F. L. Fabbri, D. Benson and I. Bigi,
A Cicerone for the Physics of Charm, arXiv:0309021v1, 2003.

[38] U. Dersch, *et al.*,"Total cross section measurements with π^-, Σ^- and protons on nuclei and nucleons around $600\,GeV/c$",
Nucl. Phys. **B579** (2000) 277.

[39] The Beam Group, "Status of E781 Beam Physcis",
H-Note 784, SELEX internal report, 1997.

[40] Joe Lach, "Charged Hyperon Beam Flux Measurements - A Chronology",
H-Note 821, SELEX internal report, 1999.

[41] N. Bondar, *et al.*,"E781 beam transition radiation detector",
H-Note 746, SELEX internal report, 1995.

[42] M.Y. Balatz, *et al.*,"The lead-glass electromagnetic calorimeter for the SELEX experiment",
Nucl. Instrum. Meth. **A545** (2005) 114-138.

[43] V. Matveev, *et al.*,"Description and test results for DPWC and TRD in E781",
H-Note 747, SELEX internal report, 1995.

[44] J. Amaro-Reyes, J. Engelfried,"Efficiency of the eTRD in SELEX"
H-Note 878, SELEX internal report, 2007.

[45] J. Engelfried, *et al.*,"The E781 (SELEX) RICH detector",
Nucl. Instrum. Meth. **A409** (1998) 439-442.

[46] J. Engelfried, *et al.*,"The SELEX Phototube RICH Detector",
Nucl. Instrum. Meth. **A431** (1999) 53-69.

[47] J. Engelfried,"Summary of SELEX RICH Efficiency Measurements",
H-Note 825, SELEX internal report, 2000.

[48] I.E.T. Lungov," Vector Drift Chambers Database",
H-Note 779, SELEX internal report, 1997.

[49] J. Engelfried, P. Cooper, and D. Mao, " The E781 Trigger and DAQ System",
H-Note 643, SELEX internal report, 1995.

[50] A. Kulyatsev, P. Cooper, A. Kozhevnikov, J. Russ, " E781 Hardware Trigger Preliminary Design",
H-Note 676, SELEX internal report, 1994.

[51] P.S. Cooper, SELEX Charged Particle Tracking,
SELEX documentation, V2.1 February 28, 1996.

[52] Peter S. Cooper, Primary and close secondary vertexing code
SELEX documentation, August, 1997.

[53] Mark Edward Mattson, "Search for baryons with two charm quarks",
Carnegie Mellon University, PhD Thesis, 2002.

[54] M.A. Olivo Gómez, "Producción inclusiva de Λ, $\overline{\Lambda}$ y K_s mediante las colisiones Σ^-, $\pi^\pm$ y p-Nucleón",
Universidad Autónoma de San Luis Potosí, MSc Thesis, 2004.

[55] A. Flores, "Búsqueda de resonancias bariónicas en el experimento SELEX E781",
Universidad Autónoma de San Luis Potosí, MSc Thesis, 2006.

[56] J.L. Sánchez, "Polarización de Λ^0 y $\overline{\Lambda}^0$ en colisiones Σ^- y p - Nucleón",
Universidad Autónoma de San Luis Potosí, MSc Thesis, 2006.

[57] G. López Hinojosa, "Determinación de la razón de decaimiento de $\Lambda_c^+ \to p\pi^+\pi^-$",
Universidad Autónoma de San Luis Potosí, MSc Thesis, 2008.

[58] M. Procario and S. Kushnirenko, "EDG-Embedded Data Generator for SELEX",
SELEX documentation, Research note, SELEX collaboration, 1998.

[59] CLEO collaboration, "Comprehensive QQ documentation",
Research note.

[60] R. Blankenbecler and S. J. Brodsky, "Unified description of inclusive and exclusive reactions at all momentum transfers",
Phys. Rev. **D10** (1974) 2973-2992.

[61] J. You, "Event Embedding in SELEX",
H-Note 815, SELEX internal report, 1998.

[62] Fernanda Gallinucci Garcia, "Hadroprodução do Bárion Charmoso Λ_c no Experimento SELEX - E781",
Universidade de São, Paulo PhD Thesis, 2000.

[63] E.A. Blanco-Covarrubias,
(Private communication with A. Blanco-Covarrubias)
Universidad Autónoma de San Luis Potosí, PhD Thesis, in prep.

[64] J. M. Link *et al.*, FOCUS Collab.,
Phys. Lett. **B512** (2001) 277-282.

[65] Kenneth Day Nelson, "Polarization of Λ^0 inclusively produced by a $610\,GeV/c$ Σ^- beam",
University of Iowa, SELEX PhD Thesis, 1999.

[66] Aneesh V. Manohar and Mark B. Wise, Heavy Quark Physics,
Cambridge University Press, 2000.

[67] Particle Data Group, Review of Particle Physics,
W-M Yao *et al.*, J. Phys. G: Nucl. Part. Phys. **33** (2006) 1.

[68] E. Vázquez-Jáuregui, J. Engelfried *et al.*, SELEX Collab., "First Observation of the Cabibbo-suppressed Decays $\Xi_c^+ \to \Sigma^+\pi^-\pi^+$ and $\Xi_c^+ \to \Sigma^-\pi^+\pi^+$ and Measurement of their Branching Ratios", Physics Letters B 666 (2008) 299-304.
Preprint: Fermilab-Pub-08-084-E, arXiv:0804.2298.